

University of Alberta

The Effect of Fine Flocculating Particles and Fine Inerts on Carrier Fluid
Viscosity

by

Azadeh Asadi Shahmirzadi

A thesis submitted to the Faculty of Graduate Studies and Research
in partial fulfillment of the requirements for the degree of

Master of Science
in
Chemical Engineering

Department of Chemical and Materials Engineering

©Azadeh Asadi Shahmirzadi
Fall 2012
Edmonton, Alberta

Permission is hereby granted to the University of Alberta Libraries to reproduce single copies of this thesis and to lend or sell such copies for private, scholarly or scientific research purposes only. Where the thesis is converted to, or otherwise made available in digital form, the University of Alberta will advise potential users of the thesis of these terms.

The author reserves all other publication and other rights in association with the copyright in the thesis and, except as herein before provided, neither the thesis nor any substantial portion thereof may be printed or otherwise reproduced in any material form whatsoever without the author's prior written permission.

Abstract

Design and maintenance of coarse-particle Newtonian slurries pipeline requires the knowledge of carrier fluid viscosity. Since measurements of carrier fluid viscosity are difficult, numerous empirical correlations are typically used to predict this value. The main deficiency of available correlations arises from the fact that the viscosity is predicted from the volume fraction of total fines. This approach neglects the different effects of various fines present in the suspensions (e.g., flocculating versus inert fines). In this study, idealized aqueous slurries consisting of inert silica ($d \sim 20 \mu\text{m}$) and flocculating kaolinite clay were tested. A novel optical-based particle size analysis technique (FPIA) was commissioned to study flocculating and inert fines and estimate volume fraction of aggregates. Experimental data suggest that viscosity correlations are improved significantly if the volume fraction of aggregates is used as the primary correlating parameter, rather than the more conventional use of total fine solids volume fraction.

Acknowledgement

First and foremost, I would like to thank my family and friends, my dearest Azar, Arash, Vahid, Sepideh and Morvarid. Endless gratitude and love to the strongest woman I know, my Maman Mahvash, to my Amoo Mansoor, who is as dear as a father to me, and to my beloved Baba, Alireza Asadi Shahmirzadi, whom I still and forever acknowledge in any achievements of my life.

A Persian proverb says you are forever indebted to whoever taught you a single word. I am forever grateful to my supervisor, Dr. Sean Sanders, who was also my first professor at University of Alberta. I have benefited not only from his excellent teaching, but also his guidance and support. I am proud to say that I made great advances in both the scientific and personal aspects during my life as a graduate student under the supervision of Dr. Sanders.

Many thanks go to my group members at the University of Alberta Pipeline Transport Processes research group: Mahshad Pazouki, Maedeh Marefatallah, Ardalan Sadighian, Reza Hashemi, Hafizur Rahman, Jean Sebastien Kroll-Rabotin, Sayeed Rushd and Kofi Adane for their friendship and support. Thank you my dear Terry Runyon for your help. I also wish to express my deepest gratitude to my yoga teachers Andre, Rene Johnson, Henri Ferguson and Afsheen Peyrow who helped me cultivate balance and space in myself.

I would like to thank NSERC Industrial Research Chair in Pipeline Transport Processes, the CONRAD group, Mr. Peter Cleyle from Suncor and Mr. Jason Schaan from Shell for providing financial support. I would also like to thank the staff of Chemical and Materials Engineering department for their support. I feel grateful to Dr. Zhenghe Xu for giving me permission to work with the rheometer in his laboratory. Thank you beautiful Lily Laser for your endless help.

Table of Contents

1.	Background and Literature Review	1
1.1.	Introduction: Importance of Slurry Flows in the Oil Sands Industry	1
1.2.	Operation of Slurry Pipelines in Oil Sands Industry.....	2
1.3.	Carrier Fluid Viscosity.....	4
1.4.	Overall Objectives of the Research Project	8
1.4.1.	Model Components.....	10
1.4.2.	Anticipated Contribution to the Oil Sands Industry	11
1.5.	Governing Factors in the Carrier Fluid Viscosity.....	12
1.6.	Aggregate Structures in Flocculating Kaolinite Suspensions.....	14
1.7.	Modeling of Carrier Fluid Viscosity.....	19
1.8.	Characterization of Particle Suspensions by FPIA	23
1.8.1.	Applications of FPIA in Literature	24
1.8.2.	Advantages of FPIA over Conventional Sizing Techniques	25
1.8.3.	Limitations of FPIA	28
2.	Project Objectives	30
2.1.	Activities.....	32
3.	Experimental Methods.....	34
3.1.	Materials	34
3.1.1.	De-ionized Water	34
3.1.2.	Kaolinite.....	34

3.1.3.	Silica Flour	35
3.2.	Apparatus	35
3.2.1.	Mixer	35
3.2.2.	Scale	37
3.2.3.	Vacuum system	37
3.2.4.	Sysmex Flow Particle Image Analyzer-3000 (FPIA)	37
3.2.5.	TA Instrument AR-G2 Rheometer	41
3.3.	Procedures	46
3.3.1.	Mixture Preparation	46
3.3.2.	FPIA Tests	47
3.3.3.	Concentric Cylinders Viscometer Tests	49
4.	FPIA Performance Tests Using Suspensions Containing Kaolinite or Sand	52
4.1.	Repeatability of FPIA Measurements	54
4.2.	Effect of FPIA on Particle Size Distribution	59
4.2.1.	Effect of Mixing Unit	59
4.2.2.	Effect of Sample Dilution	59
4.3.	Particle Size Distributions of Sand-Kaolinite Suspensions	62
4.4.	Summary	65
5.	Results and Discussion	67
5.1.	Effect of Water Chemistry on PSD of Kaolinite Suspensions	68
5.2.	Determination of Aggregates Volume Fractions Using FPIA Measurements	72

5.3.	Rheological Characterization of Kaolinite Suspensions.....	77
5.3.1.	Repeatability of AR-G2 Measurements.....	77
5.3.2.	Rheological Behaviour of Kaolinite Suspensions at pH 4 and pH 9	77
5.4.	Prediction of Relative Viscosity Using FPIA Measurements.....	89
5.5.	Rheological Characterization of Sand-Kaolinite Suspensions.....	90
5.6.	Summary.....	98
6.	Conclusions and Future Work.....	100
6.1.	Conclusions.....	100
6.2.	Future Work.....	103
	References.....	105
	Appendices.....	111
	Appendix 1: Rheological Measurements of De-ionized Water.....	112
	Newtonian viscosity (mPa.s).....	113
	Appendix 2: Rheological Measurements of Kaolinite-Water Mixtures at pH 9...	115
	Concentration: $C_k = 2\%$	116
	Concentration: $C_k = 3.5\%$	120
	Concentration: $C_k = 5\%$	124
	Concentration: $C_k = 7\%$	128
	Concentration: $C_k = 10\%$	131

Appendix 3: Rheological Measurements of Kaolin-Water Mixtures at pH 4. 135

Concentration: $C_k = 1\%$	136
Concentration: $C_k = 2\%$	138
Concentration: $C_k = 3.5\%$	142
Concentration: $C_k = 5\%$	144
Concentration: $C_k = 7\%$	146
Concentration: $C_k = 10\%$	150

Appendix 4: Rheological Measurements of Sand-Kaolin-Water Mixtures 155

Concentration: $C_s = 10\%$	156
Concentration: $C_s = 15\%$	158
Concentration: $C_s = 20\%$	160
Concentration: $C_s = 25\%$	162

List of Tables

Table 2.1 Compositions of idealized carrier fluid for particle size and shape measurements by FPIA.	33
Table 2.2 Compositions of idealized carrier fluid for rheology measurements....	33
Table 3.1 De-ionized water specifications.	34
Table 3.2 Physical properties of Pioneer kaolinite.	35
Table 3.3 Physical properties of Sil 325 fine silica sand.	35
Table 3.4 FPIA-3000 particle size measuring ranges for 10x, 20x and 5x lens units in High power field (HPF) and Low power field (LPF).	38
Table 3.5 Particle number density measured by FPIA for different kaolinite mixtures using 10x standard lens unit in HPF mode. Mean (N) D_{CE} is the number-based mean circular equivalent diameter of particles.	39
Table 3.6 Specifications of AR-G2 rheometer for concentric cylinders measuring system in controlled rate mode (CR).	43
Table 3.7 Viscosity values of standard oil (S6) and de-ionized water provided by the manufacturer, and the calculated value from AR-G2 measurements.	46
Table 3.8 Testing parameters for AR-G2 viscosity measurements.	50
Table 3.9 Required conditioning time for different mixtures prior to rheological measurements.	51
Table 5.1 Compositions of mixtures for FPIA measurements on the effect of water chemistry for kaolinite suspensions.	69

Table 5.2 Results of FPIA measurements on the effect of water chemistry for kaolinite suspensions.	69
Table 5.3 Volume calculations for aggregates using FPIA results for kaolinite-water mixtures.....	76
Table 5.4 Error value for the Newtonian model fitting and calculated viscosity values for kaolinite-water mixtures at pH 9.....	83
Table 5.5 Error value for the Bingham model fitting and calculated viscosity values for kaolinite-water mixtures at pH 4.....	87
Table 5.6 Error value for the Bingham model fitting and calculated viscosity values for sand-kaolinite-water mixtures.....	95

List of Figures

Figure 1.1 Schematic of a slurry pipeline cross section showing carrier fluid and coarse sand particles.....	2
Figure 1.2 The relative contributions of fine silica particles and clay flocs to carrier fluid viscosity. The dashed line is from Shook et al. (2002) and the solid line is from Schaan et al. (2000).	6
Figure 1.3 Slurry pipeline hydraulics predicted by two commonly-found carrier fluid viscosity correlations: $D= 0.69$ m, $d_{\text{coarse particles}} = 0.2$ mm, $C_{\text{coarse particles}} = 0.275$, $C_{\text{fines}} = 0.055$	7
Figure 1.4 Compositions of clay minerals in oil sands fine tailing stream adopted from Kaminsky et al. (2009).	11
Figure 1.5 SEM micrograph of kaolinite particles obtained from Zbik et al. (2008).	15
Figure 1.6 Atomic structure of kaolinite clay showing T and O faces. (Modified from Tombacz and Szekeres, 2006).	15
Figure 1.7 Illustration of card-house flocculation structure for kaolinite particles at low pH.	16
Figure 1.8 Illustration of de-flocculated kaolinite particles.	16
Figure 1.9 Illustration of card-pack flocculation structure for kaolinite particles at high pH in presence of strong electrolytes.	17

Figure 1.10 SEM micrograph of kaolinite aggregates obtained from Zbik et al. (2008).....	17
Figure 1.11 Illustration of highly flocculated structure for kaolinite particles.	18
Figure 1.12 Particle structures in a flocculating suspension flowing at low shear rates (right) and high shear rates (left), modified from Michaels and Bolger (1962) (b).....	21
Figure 1.13 Illustration of the effect of particle interactions on volume fraction. Aggregate size and void fraction increases from left to right: $C_{\text{primary particles}} \sim 1/10$, $C_A \sim 1/4$, and $C_A \sim 1/2$	23
Figure 3.1 Schematics of sample flow inside FPIA (Sysmex FPIA-3000 Operator's Manual, 2006).....	39
Figure 3.2 PSD results for 2 mixtures of monodisperse latex spheres ($d = 2.00 \mu\text{m}$) in de-ionized water from the FPIA.....	40
Figure 3.3 Particle shape distribution results for 2 mixtures of monodisperse latex spheres ($d = 2.00 \mu\text{m}$) in de-ionized water from the FPIA.	41
Figure 3.4 The AR-G2 rheometer (AR-G2 Operator's Manual, 2006).	42
Figure 3.5 Schematic of concentric cylinder system. $R_1 = 14.00 \text{ mm}$; $R_2 = 15.00 \text{ mm}$; $L = 42.00 \text{ mm}$	42
Figure 3.6 Plot of torque divided by α from rheological results for de-ionized water and standard oil (S6).	45

Figure 4.1 Image of a kaolinite aggregate in a kaolinite-water mixture from the FPIA.....	54
Figure 4.2 PSD results for 5 samples of a highly flocculated kaolinite-water mixture (mixture 1) alongside a PSD curve for a moderately flocculated kaolinite-water mixture (mixture 2) from the FPIA. Mixture 1: $C_k = 0.25\%$; 0.007 M CaCl_2 . Mixture 2: $C_k = 0.25\%$	56
Figure 4.3 Particle size cumulative distribution results for 5 samples of a highly flocculated kaolinite-water mixture (mixture 1) alongside a cumulative distribution curve for a moderately flocculated kaolinite-water mixture (mixture 2) from the FPIA. Mixture 1: $C_k = 0.25\%$; 0.007 M CaCl_2 . Mixture 2: $C_k = 0.25\%$	56
Figure 4.4 Particle shape distribution results for 5 samples of a flocculated kaolinite-water mixture from the FPIA. $C_k = 0.25\%$; 0.007 M CaCl_2	57
Figure 4.5 PSD results for 2 identical batches of a flocculated kaolinite-water mixture from the FPIA. $C_k = 0.25\%$; 0.007 M CaCl_2	58
Figure 4.6 Particle shape distribution results for 2 identical batches of a flocculated kaolinite-water mixture from the FPIA. $C_k = 0.25\%$; 0.007 M CaCl_2	58
Figure 4.7 PSD results by FPIA for samples of a kaolinite-water mixture from the FPIA. $C_k = 0.25\%$; pH 11; 0.007 M CaCl_2	60
Figure 4.8 PSD results for a dispersed kaolinite-water mixture from FPIA. $C_k = 5\%$;	61

Figure 4.9 PSD results for a kaolinite-water mixture. The mixture was diluted 50, 100, 200 and 500 times. CE mean (N) diameter for each dilution is 11.35, 7.90, 4.66 and 2.57 μm , respectively. $C_k = 5\%$; pH 4.	62
Figure 4.10 FPIA Image of a Silica sand particle in a sand-water mixture.	63
Figure 4.11 Particle shape distribution results for a sand-water mixture from the FPIA.	63
Figure 4.12 PSD results for a kaolinite-water mixture ($C_k = 1.7\%$) and a sand-kaolinite-water mixture ($C_k = 1.7\%$; $C_s = 1.7\%$) from FPIA.	64
Figure 5.1 PSD results for 4 kaolinite-water mixtures from FPIA at different water chemistries. $C_k = 0.25\%$	70
Figure 5.2 FPIA Images of a kaolinite-water mixture from the FPIA. $C_k = 0.25\%$; pH 11; TSPP = 0.02 wt/wt kaolinite.	70
Figure 5.3 FPIA Images of small kaolinite aggregates in a kaolinite-water mixture from the FPIA. $C_k = 0.25\%$; pH 6.	70
Figure 5.4 FPIA Images of kaolinite aggregates in a kaolinite-water mixture from the FPIA. $C_k = 0.25\%$; pH 5.	71
Figure 5.5 FPIA Images of large kaolinite aggregates in a kaolinite-water mixture from the FPIA. $C_k = 0.25\%$; pH 11; 0.007 M CaCl_2	71
Figure 5.6 Loose bricks and two possible assemblies of the bricks.	72
Figure 5.7 PSD results for kaolinite-water mixtures from the FPIA at different water chemistries.	73

Figure 5.8 Particle shape distribution results for kaolinite-water mixtures at different water chemistries.....	74
Figure 5.9 Torque response data for two samples of a kaolinite-water mixture. $C_k = 3.5\%$; pH 4.....	78
Figure 5.10 Torque response data for 4 identical batches of a kaolinite-water mixture. $C_k = 7\%$; pH 4.....	78
Figure 5.11 Torque response data for conditioning a kaolinite-water mixture. $C_k = 10\%$;	79
Figure 5.12 Torque response data for the recording of 5 data for a kaolinite-water mixture. $C_k = 10\%$; pH 9.....	80
Figure 5.13 Torque response data for ramp up and ramp down steps performed on a kaolinite-water mixture. $C_k = 10\%$; pH 9.....	80
Figure 5.14 Plot of torque divided by α obtained from rheological results for a kaolinite-water mixture. $C_k = 10\%$; pH 9.	82
Figure 5.15 Torque response data for kaolinite-water mixtures at pH 9.	83
Figure 5.16 Torque response data for conditioning a kaolinite-water mixture. $\omega = 40$ rad/s; $C_k = 10\%$; pH 4.....	84
Figure 5.17 Torque response data for the recording of 5 data points for a kaolinite-water mixture. $C_k = 10\%$; pH 4.....	85
Figure 5.18 Torque response data for ramp up and ramp down steps performed on a kaolinite-water mixture. $C_k = 10\%$; pH 4.....	85

Figure 5.19 Plot of torque divided by α from rheological results for a kaolinite-water mixture. $C_k = 10\%$; pH 4..... 86

Figure 5.20 Torque response data for kaolinite-water mixtures at pH 4. 87

Figure 5.21 Plot of calculated relative viscosity values versus solid volume fraction for kaolinite-water mixtures at pH 4 and 9..... 88

Figure 5.22 Plot of calculated relative viscosity values versus volume fraction of aggregates using value of 3.11 for λ for kaolinite-water mixtures at pH 4 and 9. 90

Figure 5.23 Torque response data for conditioning a sand-kaolinite-water mixture. $\omega = 25$ rad/s; $C_s = 20\%$; $C_k = 7\%$ 92

Figure 5.24 Torque response data for 2 samples of a sand-kaolinite-water mixture. $C_s = 20\%$; $C_k = 7\%$ 93

Figure 5.25 Torque response data for the recording of 3 data points for a sand-kaolinite-water mixture. $C_s = 25\%$; $C_k = 7\%$ 93

Figure 5.26 Torque response data for sand-kaolinite-water mixtures. $C_k = 7\%$... 94

Figure 5.27 Plot of calculated relative viscosity values versus solid volume fraction for sand-kaolinite-water mixtures fitted with Equation 1.5 by Gillies et al. (1999)..... 96

Figure 5.28 Plot of calculated relative viscosity values versus solid volume fraction for kaolinite-water mixtures at pH 4 and 9 and for sand-kaolinite-water mixtures..... 96

Figure 5.29 Plot of calculated relative viscosity values versus volume fraction of aggregates for kaolinite-water mixtures at pH 4 and 9, and for sand-kaolinite-water mixtures which are fitted with Equation 1.5 by Gillies et al. (1999). A value of 3.11 and 1.00 was used for λ to convert mixture concentration from solid volume fraction to volume fraction of aggregates for kaolinite-water mixtures at pH 4 and 9, respectively..... 97

List of Symbols

Symbols

C	Volume fraction
d	Particle diameter (m)
D_{CE}	Circular Equivalent Diameter (μm)
g	Gravity acceleration, (m/s^2)
L	Cylinder immersed height (m)
Mean (N)	Number-based mean
R_1, R_2	Radius of spindle and cup (m)
T	Torque (N.m)
T_0	Bingham yield stress (Pa)
u_T	Terminal Velocity (m/s)
α	Viscosity measuring system geometry factor (m^3)
$\dot{\gamma}$	Shear rate (1/s)
μ	Viscosity (Pa.s)
ρ	Density (kg/m^3)
τ	Shear stress (Pa)
ω	Spindle speed (rad/s)

Subscripts

k	Kaolinite
L	Suspending medium
f	Fluid
r	Relative
p	Particle
s	Sand
solid	Solid
w	Water

1. Background and Literature Review

1.1. Introduction: Importance of Slurry Flows in the Oil Sands Industry

The Alberta oil sands industry represents an intensive application of slurry pipeline technology. An estimated amount of 152 billion barrels of bitumen are recoverable from reserves located in northern Alberta by surface mining operations (Wallwork et al., 2008). Oil sands ores are fluidized by addition of water and enter the production units in slurry pipelines. Slurry pipelines are also used to transport the discharged solids from the production units (Sanders et al., 2004).

At the start of the bitumen production process, oil sands ores are mined by the shovels and carried by large trucks to crushers. Here, the oil sands lumps are broken down and are mixed with warm process water. Next, the mixture of process water and oil sands is pumped into a slurry pipeline, referred to as the hydrotransport pipeline. Surface layers of each oil sands lump are sheared away in the hydrotransport pipeline. This process is called ablation. Ablation liberates the bitumen from the solids. Liberated bitumen droplets attach to the air bubbles in the slurry in the hydrotransport pipeline. Therefore, the hydrotransport pipeline provides an environment for conditioning the oil sands before the main separation processes. The slurry of solids and liberated bitumen is then transported to a gravity-separation vessel. The aerated bitumen is collected in the form of froth at the top of the separation vessel and is sent to bitumen recovery units. A slurry of water, sand, fine clays and some un-recovered bitumen exit from the bottom of the separation vessel. Slurry pipelines are used to transport the underflow stream to tailings ponds or water recovery units (Masliyah et al., 2009). Hence, slurry pipelines serve another important purpose in oil sands industry: slurry transport to and from the process plants (Masliyah et al., 2009). The application of slurry pipelines offers an economic and efficient method of transporting solids over long distances in the oil sands industry. An approximate amount of 0.5 million tonnes

per day of solids flows in the form of slurry in the oil sands industry (Sanders et al., 2004).

Oil sands ores are extracted from the open pit mines. A typical oil sands deposit contains 9-13% bitumen, 3-7% water, and 80-85% mineral solids (Masliyah et al., 2009). Mineral solids contain 85-70% coarse large silica particles and 15-30% “fines”. Fines are comprised of sand and clay-type particles less than 44 μm in sieve type diameter (Masliyah et al., 2009). Mixing the oil sands ores with process water produces heterogeneous slurry (Wallwork et al., 2008). Oil sands slurry is comprised of the suspending medium, referred to as “carrier fluid”, and large coarse particles suspended by the carrier fluid. Carrier fluid is a stable suspension of process water and fines. Figure 1.1 depicts the carrier fluid and coarse particles in a slurry pipeline cross section.

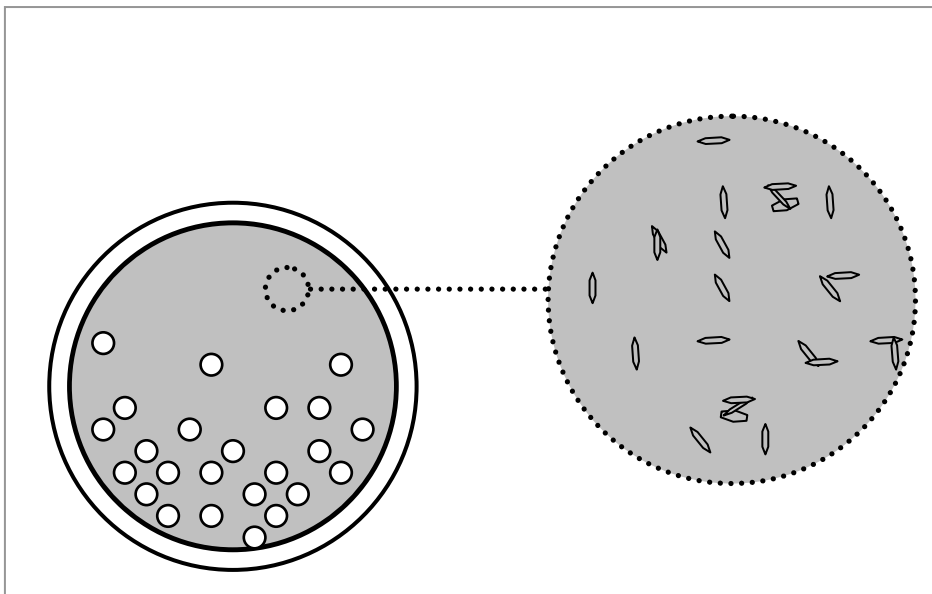


Figure 1.1 Schematic of a slurry pipeline cross section showing carrier fluid and coarse sand particles.

1.2. Operation of Slurry Pipelines in Oil Sands Industry

There are numerous challenges associated with the handling of fluid-particle mixtures in slurry pipelines in oil sands industry. Unexpected pipeline failures are

a major problem on the operation of mining and extraction plants. A common issue resulting in pipeline operation challenges include the sedimentation of slurry solid components. Solid particles suspended in the slurry accumulate in the pipeline when it is operated below a critical (minimum) velocity known as the deposition velocity, V_c . These particles sediment and form a dense bed when turbulent dispersion forces are not strong enough to balance the immersed particle weight (Shook et al., 2002). In such situations, the operation is shut down and water is pumped through the clogged pipeline to remove the deposits (Sanders et al., 2004). Consequently, operating costs are substantially increased. Therefore, pipelines must be operated at sufficient velocities in order to provide adequate turbulence in the fluid and prevent the sedimentation of solid particles. Under-prediction of the value of the deposition velocity in the pipeline design could lead to shut down and line blockage. On the other hand, operating at high velocities causes high frictional energy loss and substantially increases pipeline wear rates (Wilson et al., 2006). Hence, it is crucial to predict the deposition velocity accurately to avoid both the formation of stationary beds and unnecessary pressure drop (energy consumption).

Pressure drop is another important parameter required for pipeline design and maintenance. Unreliable pressure drop calculations would lead to downtime and loss of production. In the oil sands industry, the SRC (Saskatchewan Research Council) Two-Layer Model (Shook et al., 2002) is primarily used to predict pressure drop for coarse particle slurry pipelines. The SRC Two-Layer Model has been used to design almost every oil sands hydrotransport and coarse tailings pipeline in the oil sands industry since the early 1990's. This model is also used to assess the operation of existing pipelines (Sanders et al., 2004). One of the important features of this model is that the solids contained in a slurry are classified according to the type of friction they contribute: 'fine' particles that are part of the carrier fluid contribute viscous or "fluid-like" friction while the coarser solids suspended by the carrier fluid contribute to the overall friction loss through wall collisions and other, more complex mechanisms (Shook et al., 2002; Wilson

et al., 2006). Concentration profiles of solid particles over the cross section of a slurry pipeline are not uniform. The SRC Two-Layer model divides the fluid flow into two layers: an upper layer that comprises solely of carrier fluid and coarse particles effectively suspended by fluid turbulence, and a layer around the bottom wall of the pipeline where coarse large particles are not suspended by the carrier fluid (Shook et al., 2002). Therefore, successful application of SRC Two-Layer Model to the operation of slurry pipelines requires the knowledge of carrier fluid properties. The density of the carrier fluid can be calculated from the volume concentration of fines in the carrier fluid. However, the determination of the viscosity of the carrier fluid is challenging.

1.3. Carrier Fluid Viscosity

Carrier fluid viscosity is an important parameter in calculations of minimum pipeline operating velocity (deposition velocity), pipeline friction loss predictions (SRC Two-Layer Model), analysis of oil sands conditioning, and prediction of hydrocyclone and separation cell performance. Carrier fluid viscosity depends on the volume concentration of fines, fines mineralogy, and water chemistry (Masliyah et al., 2011).

Clearly, on-site measurement for each slurry is the best recommendation to evaluate the viscosity; unfortunately, this is impractical due to numerous measurement difficulties. Online sampling is expensive and time consuming. Moreover, samples must usually be transported to another facility for measurements. Another issue is that settling of coarser particles may occur in the viscometer. However, it is still best to make measurements instead of using correlations.

Challenges associated with viscosity measurements leave us to resort to the application of correlations. Numerous empirical correlations are in use in the oil sands industry to predict the value of carrier fluid viscosity. The applicability of

any empirical correlation is limited to the specific conditions at which the experimental data were obtained. For example, if the assessment of fines concentration in a slurry is based on a light scattering particle size analysis technique to derive a certain empirical viscosity correlation, using fines concentration data from a sieve analysis in such correlation can produce substantial errors. Another example which causes even more significant errors is applying a certain correlation at a water chemistry different from which the correlation was obtained for.

Another source of error in existing correlations relates to the different behaviour of the variety of fine types in the carrier fluid. X-ray powder diffraction results (Omotoso et al., 2006; Mercier et al., 2008; Kaminsky et al., 2009; Adeyinka et al., 2009) show that the mineral composition of fines in oil sands industry includes clay-type and sand particles. Clay particles have a strong tendency to flocculate while sands are relatively inert. Rheological data (Adeyinka et al., 2009) clearly indicate that viscosity of carrier fluids containing fines with largest amount of clays was the highest for the same total solids concentration. Figure 1.2 shows the contribution each particle type is expected to make toward increasing the carrier fluid viscosity. Figure 1.2 demonstrates that compared with clay particles, fine silica particles provide a rather mild increase in carrier fluid viscosity. Note that for a given solid volume fraction, the carrier fluid viscosity can be 3.5 times greater for clay suspensions compared to fine silica suspensions. This behaviour was verified through measurements by Gillies (2012) and Sumner et al. (2000). The mixture of clay fines and water provided a carrier fluid viscosity that was highly dependent on clay volume concentration. As Figure 1.2 suggests, flocculating and inert particle types have distinct effects on the carrier fluid viscosity. However, current industry standards consider all types of fines (particles less than 44 μm in diameter) to contribute equally to an augmented carrier fluid viscosity. Errors in the estimation of carrier fluid viscosity can lead to suboptimal process design or misdiagnosis of operating difficulties.

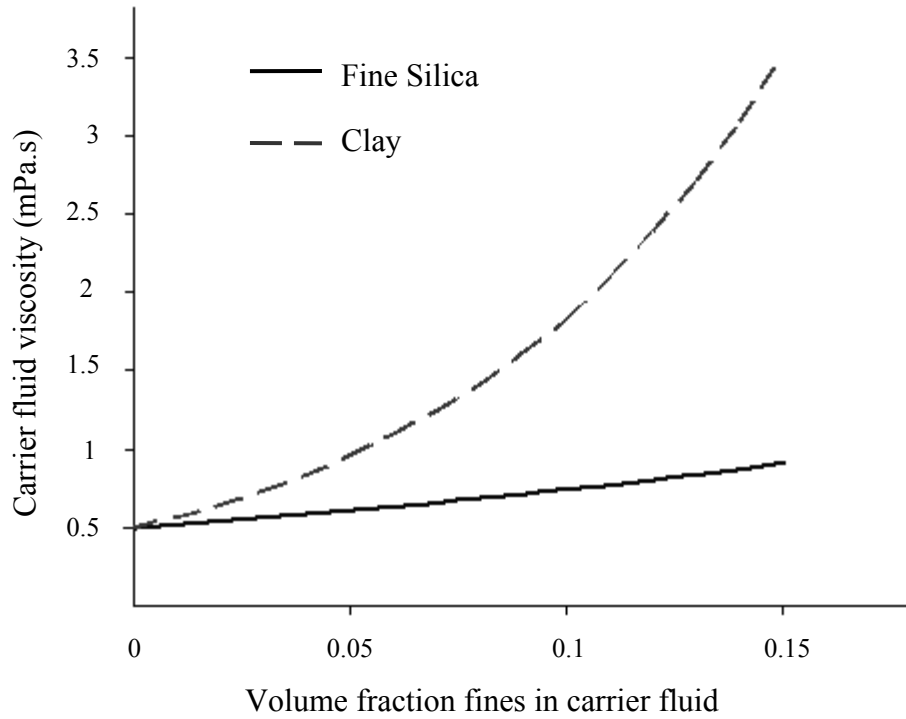


Figure 1.2 The relative contributions of fine silica particles and clay flocs to carrier fluid viscosity. The dashed line is from Shook et al. (2002) and the solid line is from Schaan et al. (2000).

Figure 1.3 demonstrates significant uncertainty in the operational analysis of a slurry pipeline produced by utilization of empirical correlations. Figure 1.3 illustrates the effect of the carrier fluid viscosity on the slurry deposition velocity. The low-velocity terminal point on each line indicates the slurry deposition velocity. Figure 1.3 shows slurry hydraulics predictions made with the SRC Two-Layer Model (Shook et al., 2002) for the flow of a sand-clay mixture in a 0.69 m (diameter) pipeline. The sand particles have a diameter of 0.2 mm and the volume fraction of fines in the carrier fluid is 0.055. The carrier fluid viscosity is predicted using two different correlations, Correlation A (Sanders et al., 2004) and Correlation B (Shook et al., 2002), presented in Equation 1.1 and 1.2, respectively:

$$\mu_r = \frac{\mu_f}{\mu_w} = 1 + 15C_f \quad \mathbf{1.1}$$

$$\mu_r = \frac{\mu_f}{\mu_w} = \exp(12.5C_f) \quad 1.2$$

where μ_r is the relative viscosity. Both correlations A and B have been used by Canadian firms to design existing slurry pipelines. In any given situation, there is no way to know if either correlation is accurate. Figure 1.3 shows that the predicted deposition velocity decreases by a factor of 2, from 4.8 m/s using Correlation A to 2.3 m/s using Correlation B. New correlations should be developed to allow for more accurate prediction of carrier fluid viscosity. It is necessary to distinguish between the effect of flocculating clay-like fine particles and inert fine particles to improve the quality of carrier fluid viscosity correlations.

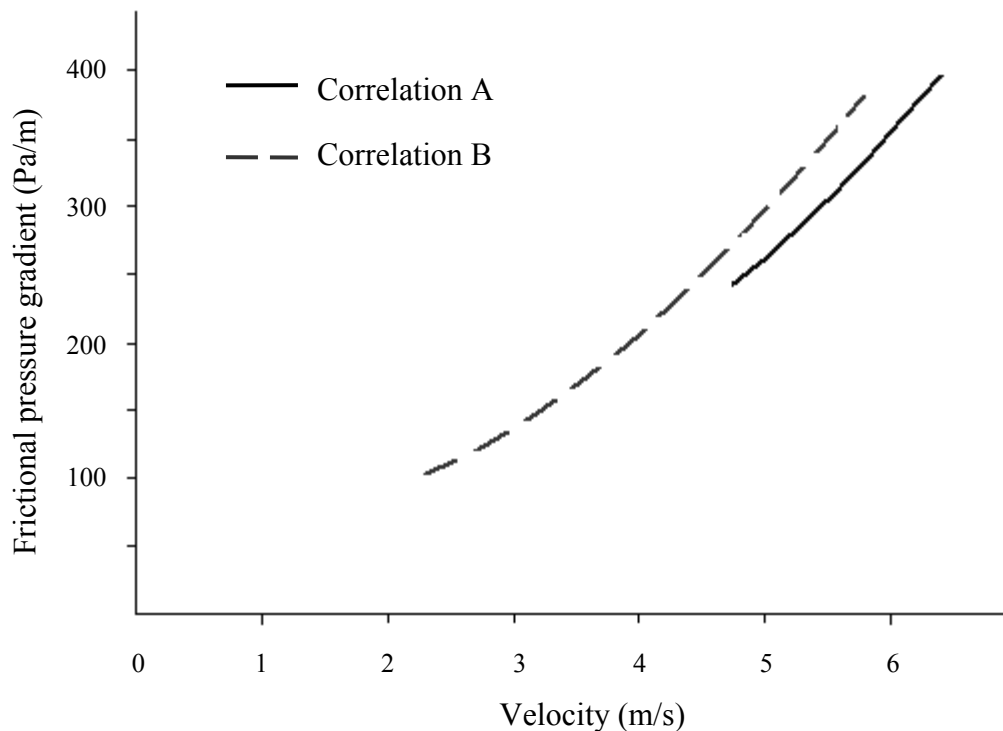


Figure 1.3 Slurry pipeline hydraulics predicted by two commonly-found carrier fluid viscosity correlations: $D= 0.69$ m, $d_{\text{coarse particles}} = 0.2$ mm, $C_{\text{coarse particles}} = 0.275$, $C_{\text{fines}} = 0.055$.

1.4. Overall Objectives of the Research Project

Difficulties associated with the measurement of carrier fluid viscosity leave us to resort to correlations to evaluate this important pipeline parameter. In the oil sands industry, numerous empirical correlations are used to predict carrier fluid viscosity but their applicability and accuracy are suspect. The main deficiency of existing correlations relates to the fact that the viscosity is predicted using the volume fraction of total fines as the primary correlating parameter. This approach neglects the different effects of the variety of fines present in the suspensions. In this project, a more accurate method of predicting carrier fluid viscosity is provided. In this work, particles are classified as “inert fines” and “flocculating fines” as they play different roles in affecting the carrier fluid viscosity. Flocculating particles in the carrier fluid form aggregate structures. It is proposed that the aggregate structures are the building blocks of a flocculating mixture, and it is the concentration of aggregate structures that govern the viscosity of the mixture (Michaels and Bolger, 1962 (a, b)). The main focus of this study is to demonstrate that viscosity correlations are improved significantly if the concentration of aggregates is used as the primary correlating parameter, rather than the more conventional use of total fine solids concentration in the (fines + water) carrier fluid.

In this work, volume fraction and Particle Size Distributions (PSD) of flocculating fines are determined in the state in which they exist in a slurry without being broken down into their primary particle sizes. A novel PSD measurement technique is introduced to the industry that does not appear to break the aggregated structure down into deflocculated particles. The Sysmex Flow Particle Image Analyzer (FPIA-3000) is utilized in this project for PSD measurements of fine particles. This size measurement technique is based on automated image capture of particles in the mixture. This method allows one to view the aggregate structures in the sample in their natural state. Viscosity measurements are conducted on mixtures containing flocculating and inert fines. The effect of each

fine particle type on carrier fluid viscosity is studied. In the second stage of the project, samples will be obtained from actual hydrotransport and tailings streams. Samples from oil sands industry contain coarse fractions and finite concentrations of bitumen. Therefore, special procedures should be developed for testing these complex samples. Improved carrier fluid viscosity correlations will be developed for oil sands industry. The second stage of the project is not covered in the present study.

In the present study, idealized aqueous slurries consisting of kaolinite clay and sand flour ($d \sim 20 \mu\text{m}$) are studied. The PSD of the idealized slurries is determined with the FPIA. The FPIA is a novel technology and there has not been any research reported in literature on the application of the FPIA in clay suspension analysis. Therefore, the initial objective of this work is to investigate the capabilities of the device and develop a standard testing procedure for kaolinite clay and sand suspensions.

The effect of each fine particle type on the PSD of the mixture is studied using the FPIA. The water chemistry and the volume concentrations of each fines component are varied. Kaolinite clay particles flocculate in the mixture and the resulting aggregate structures dictate the viscosity of the mixture. The FPIA is used to measure the size of kaolinite clay aggregates rather than the fully dispersed particle size of the clay in the mixture, which is the current practice in the oil sands industry. The FPIA takes images of clay aggregates without breaking the aggregates down to primary sizes. Concentration of clay aggregates is estimated from analysis of these images. Hence, volume fraction of aggregates, instead of volume fraction of solids, could be measured and used in viscosity correlations. The variability of aggregate concentration with changes in water chemistry and component volume fraction is analyzed. The viscosities of the idealized slurries are determined at varying mixture chemistry and component volume fraction. Experimental data are presented to demonstrate the distinct effects of flocculating and inert fines on the viscosity of the mixtures. The effect

of water chemistry on the mixture viscosity is investigated as well. Rheological data are presented to show that aggregate concentration can be used to represent the effect of both flocculating solid concentration and mixture chemistry on the mixture viscosity. The main objective of this work is to show how mixture viscosity could be reasonably predicted when aggregate concentration is used as the primary correlating parameter.

1.4.1. Model Components

In this study, the treatment and testing of samples from the oil sands industry is avoided due to three main complications: such samples will contain coarse fractions that must be separated from the carrier fluid; the variability of the clay fines and inert fines fraction is uncontrolled; and the samples are likely to contain finite concentrations of bitumen, which could foul and disable the FPIA. Therefore, experiments are done using idealized suspensions. De-ionized water is used as the dispersing medium in the idealized suspension. Kaolinite clay and silica flour ($d \sim 20 \mu\text{m}$) are used to represent flocculating clay-type particles and small sand particles, respectively.

Kaolinite clay occurs abundantly in soil and is thus expected to make up a large portion of any clay slurry. Kaminsky et al. (2009) measured the composition of clay minerals in oil sands process streams using the X-ray powder diffraction technique. The composition of clay minerals in an oil sands fine tailings stream is presented in Figure 1.4. Kaolinite is shown to make up the major component of clay sized minerals in oil sands fines (Kaminsky et al., 2008 and 2009). Numerous studies of kaolinite surface chemistry and factors controlling particle interaction forces have been conducted (Van Olphen (1963); Schroth and Sposito (1997); Zbik et al. (1999); Tombacz and Szekeres (2006)). kaolinite is chosen to represent clay-type fines in this work because of the substantial body of work available in the literature on kaolinite properties, as well as the dominant presence of kaolinite among clay minerals in the oil sands industry.

1.4.2. Anticipated Contribution to the Oil Sands Industry

This project is anticipated to have a significant impact on the oil sand industry. The major contribution of the two stages of this project includes the development of accurate correlations relating carrier fluid viscosity to fines concentration. Accurate viscosity correlations are important for the design of new hydrotransport and tailings pipeline systems as well as the trouble shooting of the existing slurry handling equipment. Miscalculation of carrier fluid viscosity leads to errors in prediction of the deposition velocity and pipeline frictional energy loss.

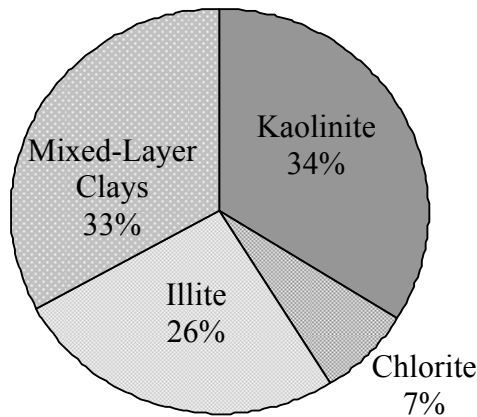


Figure 1.4 Compositions of clay minerals in oil sands fine tailing stream adopted from Kaminsky et al. (2009).

In the oil sands industry, carrier fluid viscosity is conventionally predicted using the volume fraction of total fines, neglecting the different effects of the variety of fine types present in the suspensions (e.g., flocculating versus inert fines). This study demonstrates the necessity of discrimination between clay aggregates and inert sands as they have distinct effects on the carrier fluid viscosity. This project introduces a novel PSD measurement technique to the oil sands industry that does not break the aggregated structure down into deflocculated particles. Sysmex FPIA-3000 is a powerful new instrument that will provide both size and shape analysis information of particles (Sysmex FPIA-3000/FPIA-3000S operator's

manual, 2006). This instrument provides images of each analyzed particle that allows one to view the aggregate structures in the sample in their natural state.

1.5. Governing Factors in the Carrier Fluid Viscosity

Carrier fluid is a suspension of fine sand and clay-type particles in the process water (Masliyah et al., 2009). The dependence of suspension viscosity on the volume concentration of fines has been the subject of extensive research since its introduction by Einstein in 1905 (Thomas, 1965). Einstein published a theoretical analysis on the effect of solid particles on the viscosity of dilute suspensions in 1905. His approach included relating the suspensions viscosity to the energy dissipation in the bulk of the fluid. He calculated the viscosity of extremely dilute suspensions of solid spheres as a function of the solids volume fraction:

$$\mu_r = \frac{\mu}{\mu_L} = 1 + 2.5C \quad 1.3$$

where μ_r is the relative viscosity. Equation 1.3 holds for rigid non-interacting uniform spheres in purely laminar flow with maximum solid volume fraction of 1% (Thomas, 1965). At higher concentrations, it is necessary to account for complexities such as hydrodynamic particle interactions, particle rotation, collision and agglomerate formation (Thomas, 1965). Hence, deriving a theoretical correlation for concentrated suspensions has been one of the most challenging rheological problems. Thomas (1965) studied concentrated suspensions of uniform spherical particles in a Newtonian fluid. He analyzed extensive experimental data on materials including polystyrene, latex, glass, and methyl methacrylate. The data were obtained by rotational and capillary viscometers for closely sized non-interacting spheres with a range of diameters from 0.099 to 435 μm . Thomas (1965) employed both theoretical analysis and experimental data to propose an equation relating suspension viscosity and solid volume fraction:

$$\mu_r = \frac{\mu}{\mu_L} = 1 + 2.5C + 10C^2 + 0.00273 \exp(16.6C) \quad \mathbf{1.4}$$

where C is the solids volume fraction. Non-spherical particles produce a higher viscosity than spherical particles. Numerous empirical correlations exist for non-spherical particles (many in the form of Equation 1.4 with adjusted experimental constants). Gillies et al. (1999) integrated the effect of non-spherical particle shape into Equation 1.4 for non-interacting sand grains with maximum packing concentration of 0.63:

$$\mu_r = \frac{\mu}{\mu_L} = 1 + 2.5C + 10C^2 + 0.0019 \exp(20C) \quad \mathbf{1.5}$$

However, the aforementioned equations are not applicable to interacting particles, such as clays. Particle interactions should be considered in the calculation of the viscosity of such flocculating suspensions. Hao (2008) conducted a theoretical study on the viscosity of colloidal suspensions of interacting polydispersed particles of different shapes. Hao (2008) shows that when particles are charged, it is necessary to account for the viscosity contribution due to the electrostatic interactions between particles. Hao (2008) explains that particle interaction causes aggregate structures to form inside the suspension. A fraction of the dispersing medium is trapped inside the aggregate structures. Hence, compared with dispersed systems, coagulated systems have a reduced free volume for the same mass fraction of solids. Viscosity increases as the free volume is reduced due to the formation of large and void aggregate structures. Therefore, particle interactions affect the suspension viscosity. Kaolinite particle interactions include electrostatic interactions as kaolinite particles assume charges in an aqueous suspension (Tombacz and Szekeres, 2006). Electrostatic interactions depend on the surface charge of kaolinite particles. The surface chemistry of clay minerals was originally presented by Van Olphen (1963) and further elaborated in many

subsequent investigations (e.g. Schroth and Sposito (1997), Zbik et al. (1999), and Tombacz and Szekeres (2006)).

In summary, carrier fluid viscosity depends on the volume concentration of fines, fines mineralogy, and water chemistry. Kaolinite mineralogy and aggregate structures are further explained in the following section in order to clarify the effect of kaolinite mineral structure and suspension chemistry on carrier fluid structure.

1.6. Aggregate Structures in Flocculating Kaolinite Suspensions

Kaolinite minerals represent the clay-type solid components of carrier fluid in this work. Kaolinite is a clay mineral with the composition $\text{Al}_2\text{Si}_2\text{O}_5(\text{OH})_4$ (Tombacz and Szekeres, 2006). Kaolinite occurs in nature in the form of thin, roughly hexagonal platelets with face to edge area ratio of almost 10. According to SEM measurements, kaolinite particles are in the colloidal range of 100 nm in size (Zbik et al., 2008). The kaolinite lattice is built of Alumina octahedral (O) and silica tetrahedral (T) sheets. Layers of kaolinite are bound together strongly by hydrogen bonds between hydroxyl groups of O faces and oxygens of the T faces (Tombacz and Szekeres, 2006). The basal planes of the particles, so called the “faces”, are permanently negatively charged due to isomorphic substitutions of lower valence metals for Al^{3+} and Si^{4+} .

Tombacz and Szekeres (2006) conducted a review on the effect of solution chemistry on kaolinite particle interactions. It is shown in their work that when kaolinite particles are dispersed in aqueous suspensions, the amphoteric Si-O and Al-OH polar sites at the edges and O faces are hydrolyzed. Positive charges are formed on these sites at pH below 6-6.5 because of the protonation reaction. Under these conditions, the overall particle charge remains negative on the faces, and positive on the edges. “Card-house” structures are formed due to the electrostatic attraction between edges and faces of kaolinite particles (Zbik et al.,

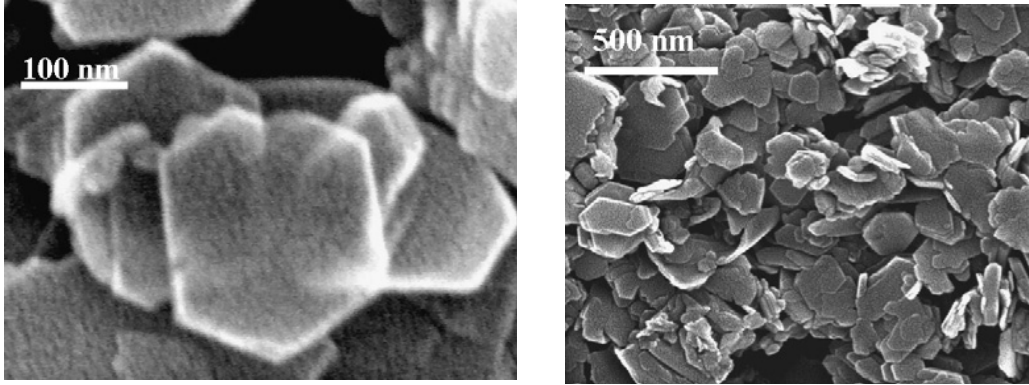


Figure 1.5 SEM micrograph of kaolinite particles obtained from Zbik et al. (2008).

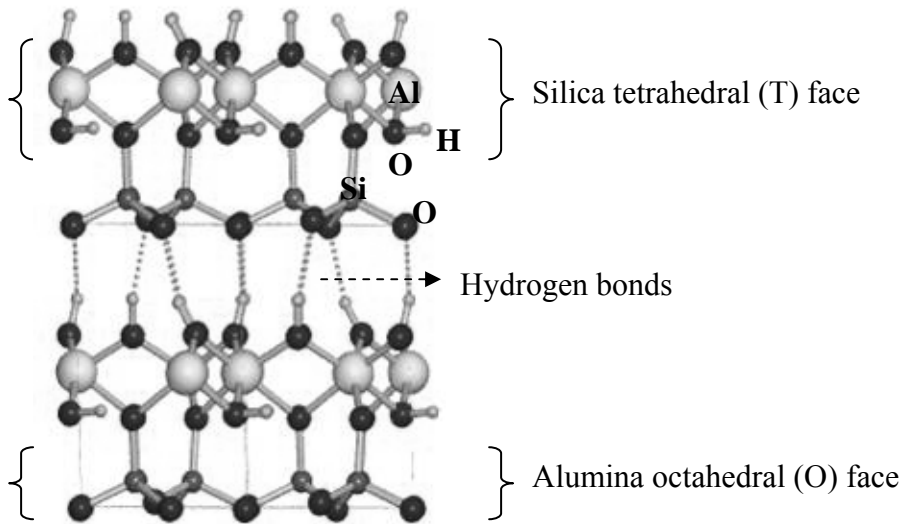


Figure 1.6 Atomic structure of kaolinite clay showing T and O faces. (Modified from Tombacz and Szekeres, 2006).

2008). Figure 1.7 shows a schematic of card-house flocculation structure for kaolinite particles. A fraction of the dispersing medium is trapped inside the void spaces of card-house structures and the free volume of the suspension is reduced. The viscosity of the suspension increases as the free volume is reduced. Hence, viscosity of a flocculating suspension containing void aggregate structures is higher compared with a dispersed suspension containing the same mass fraction of solids (Tombacz and Szekeres, 2006).

At pH values above 6.5, negative charges develop on the O faces and at the edges by direct OH^- transfer from water. Under alkaline conditions, repulsive electrostatic forces between negatively charged edges and faces are dominant over attractive Van der Waals forces, and the particles deflocculate. Also, the addition of negatively charged dispersing agents to kaolinite suspensions favours repulsion among the particles by altering the particle surface charge (Papo et al., 2002). Figure 1.8 depicts deflocculated kaolinite particles.

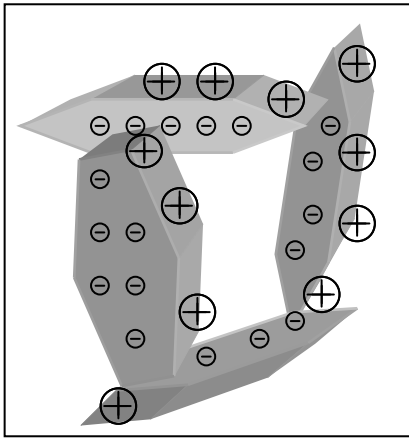


Figure 1.7 Illustration of card-house flocculation structure for kaolinite particles at low pH.

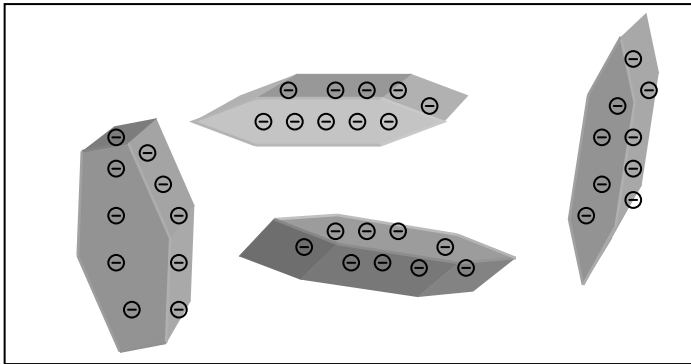


Figure 1.8 Illustration of de-flocculated kaolinite particles.

At high pH and electrolyte concentrations, the electrostatic diffuse layer shrinks and Van der Waals attractive forces between the basal faces dominate the electrostatic repulsion. In this case particles adhere to one another along basal

surfaces, forming “card-pack” structures shown schematically in Figure 1.9. In order to visualize the kaolinite aggregate structures, Zbik et al. (2008) captured SEM images of frozen samples obtained from column sedimentation tests. The fact that the kaolinite particles are highly flocculated in favourable water chemistries is evident from these images. The SEM micrograph by Zbik et al. (2008) in Figure 1.10 clearly shows face–face associations for a 4 wt% kaolinite suspension at pH 8 in presence of 0.01 M NaCl. These packed structures are not able to retain much of the dispersing medium. Hence, viscosity of a flocculating suspension containing dense card-packed aggregate structures is fairly similar to that of a dispersed suspension (Tombacz and Szekeres, 2006).

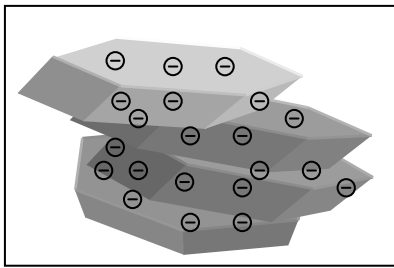


Figure 1.9 Illustration of card-pack flocculation structure for kaolinite particles at high pH in presence of strong electrolytes.

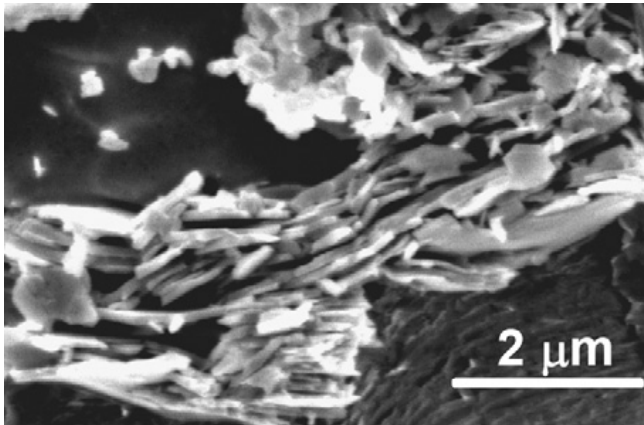


Figure 1.10 SEM micrograph of kaolinite aggregates obtained from Zbik et al. (2008).

In the presence of divalent electrolytes, the negative charges on isomorphous substitution sites on T faces of kaolinite are satisfied by adsorption of

exchangeable cations such as Ca^{+2} . This causes the diffuse layer to shrink and the degree of flocculation increases due to strong particle interactions. Under these conditions, faces and edges of kaolinite particles are attracted strongly to each other and highly expanded void structures are formed (Zbik et al., 2008). Figure 1.11 shows a schematic of the highly expanded flocculated structure for kaolinite particles. Larger aggregate structures are formed as a result of stronger particle interactions. As aggregate structures grow larger, more of the suspending medium is trapped in their void spaces. Viscosity of the flocculating suspension increases as the suspension free volume decreases.

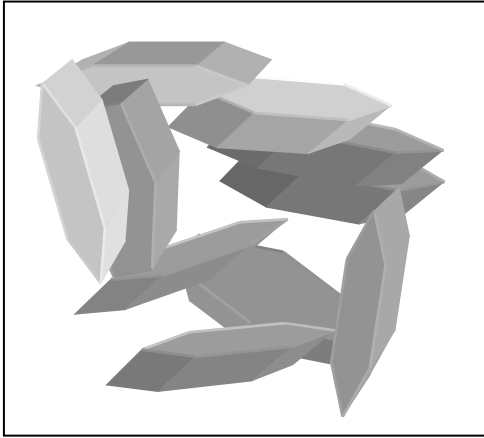


Figure 1.11 Illustration of highly flocculated structure for kaolinite particles.

In summary, kaolinite particle interactions in aqueous suspensions are affected by the crystal structures of particles and the suspension chemistry. For kaolinite-water suspensions that are prepared following similar mixing procedure using the same type of kaolinite, particle interaction depends only on type and number of ions of the dissolved electrolyte in the suspension. In such flocculating suspensions, water chemistry governs the structure of resulting aggregates. Strong particle interactions results in the formation of large aggregate structures. As aggregate structures grow larger, more of the suspending medium is trapped in their void spaces. Viscosity of a flocculating suspension increases as the chemistry of the mixture induces the formation of larger, void aggregates

(Tombacz and Szekeres, 2006). Therefore, it is the structure of the aggregates that govern the viscosity of the flocculating suspensions.

1.7. Modeling of Carrier Fluid Viscosity

Fines mineral solids in the carrier fluid, usually taken as less than 44 μm in sieve type diameter (Masliyah et al., 2009), are a mixture of sand and clay-type particles (Kaminsky et al., 2008). Experimental data found in the literature demonstrate that inert fine sands and flocculating clay-type particles play different roles in determining the carrier fluid viscosity (Sumner et al., 2000; Adeyinka et al., 2009). Particle interaction measurements by Atomic Force Microscopy (AFM) reveal that silica particles repel each other as they are constantly negatively charged in aqueous suspensions (Liu et al., 2003). Because sand particles do not flocculate, they are considered to behave as inert particles in an aqueous suspension. Hence, the viscosity of sand particle suspensions depends only on the volume concentration of the sand. Correlations that predict the viscosity of sand-water suspensions have been presented in Section 1.5. However, clay particles are not inert and they flocculate in favourable mixture chemistries. In such colloidal systems, suspension chemistry influences the mixture viscosity by governing particle interactions (Masliyah and Bhattacharjee, 2006).

There are numerous studies available in the literature that provide qualitative insight to the rheological behaviour of flocculating clay suspensions (Papo and Piani, 2000; Papo et al., 2002; Li et al., 2003; Nasser and James, 2008). However, very few quantitative studies concerning modeling the rheological characterization of flocculating suspensions exist in the scientific literature. Russel (1980) reviewed interparticle force equations to study the rheological characteristics of flocculating suspensions from a theoretical framework. Russel (1980) conducted experimental and theoretical work to define the effects of Brownian motion, steric, and electrostatic forces on the rheology of flocculating suspensions. Rheological characteristics can be related to the suspension

microstructure through analyses of pair interactions between monodisperse hard spheres (Russel, 1980). The developed model suggests that magnitude of the interparticle forces dominates the rheological properties that may vary from exhibiting low Newtonian viscosities to solid like behaviour. However, the level of complication and idealized assumptions associated with the proposed models make them inapplicable to clay suspensions. Scales et al. (1998) derived an expression to relate the shear yield stress of alumina particles to particle concentration and size distribution. The model incorporates the effects of electrostatic and Van der Waals particle interactions into a general equation for yield stress of a polydisperse suspension. The developed model by Scales et al. (1998) is able to describe the effect of the PSD, solid concentration, and pH of the suspension on the rheological behaviour of polydisperse, flocculated suspensions. For successful application of this model, the dependence of zeta potential on mixture ionic strength and pH must be explicitly known. Unfortunately, such explicit equations for clay particle characteristics are not yet available.

A notable study has been conducted by Michaels and Bolger (1962) (b) to theoretically model the rheological properties of kaolinite suspensions. Michaels and Bolger (1962) (b) assume the building blocks of such flocculating mixtures to be a cluster of flocculated particles, which are referred to as “flocs”. It is proposed that at low shear rates the flocs tend to group with each other to form extended networks (Figure 1.12, left). At high shear rates, a network of flocs is assumed to be broken down into individual flocs. The flocs still attract each other as strongly as before, but the shear forces pull the floc couplets apart as quickly as they form (Figure 1.12, right).

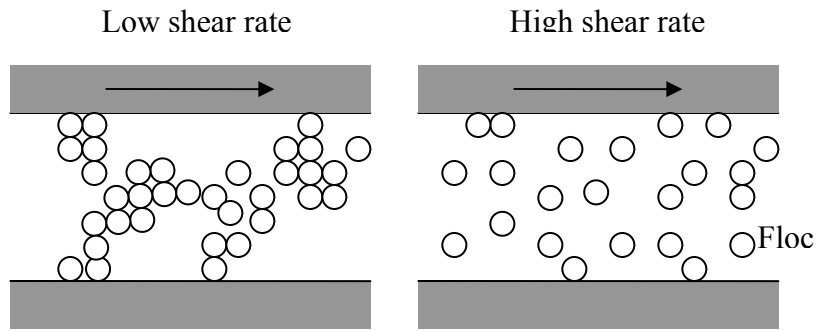


Figure 1.12 Particle structures in a flocculating suspension flowing at low shear rates (right) and high shear rates (left), modified from Michaels and Bolger (1962) (b).

Experimental data of shear stress versus shear rate were obtained by Michaels and Bolger (1962) (b) using a concentric cylinder viscometer. Concentrated suspensions were found to exhibit a finite yield stress at low shear rates. This observation verifies the existence of the proposed network of flocs. At high shear rates, a straight-line relationship was observed between shear stress and shear rate. At very dilute concentrations, the suspension exhibits Newtonian behaviour:

$$\tau = \mu \dot{\gamma} \quad \mathbf{1.6}$$

The slurry behaviour for more concentrated suspensions was found to be reasonably expressed using the Bingham model:

$$\tau = T_0 + \mu \dot{\gamma} \quad \mathbf{1.7}$$

Michaels and Bolger (1962) (b) consider flocs as the basic units in the mixture. They suggest that slurry resistance to deformation is due to the sum of a structural strength of a network of bonds between flocs, plus a viscous resistance to flow that arises from bonds between the flocs and the ambient fluid. The latter viscous energy term accounts for the exact type of energy losses that Einstein equation (Equation 1.3) explains for rigid non-interacting uniform spheres (Thomas, 1965).

Michaels and Bolger (1962) (b) analyze the strength of bonds between flocs to calculate the yield stress of the flocculating kaolinite mixture. Viscosity of the mixture is calculated by placing the volume concentration of flocs into Einstein equation. Therefore, a model is developed to predict the viscosity of kaolinite suspensions. The model proposed by Michaels and Bolger (1962) (b) is not a general model, it is only valid for the data from which constant of the model is derived. The constant of the model is the ratio of volume fraction of kaolinite flocs to that of solid particles, which is obtained from the analysis of the results of sedimentation tests. The value of this constant depends on the chemistry of the suspension. This means that sedimentation experiments should be conducted for each new system to obtain the model constant, which is obviously a major drawback.

Experimental data presented by Michaels and Bolger (1962) (b) show that rheological behaviour of flocculated kaolinite aqueous suspensions can be more accurately modeled if the volume fraction of flocs is used as the primary correlating parameter. Depending on mixture chemistry, kaolinite particles may exist in deflocculated form or may build aggregated structures. Larger aggregate structures are formed as a result of stronger particle interactions. Aggregate structures trap more of the suspending medium as they grow larger. Therefore, the suspension free volume decreases, which means that volume fraction of aggregates increases. Figure 1.13 represents the change in particle volume fraction with aggregate size and structure.

If the volume fraction of solids in the suspension is C_{solid} , then the volume fraction of aggregates in the suspension (C_A) can be expressed as a function of C_{solid} and particle interactions:

$$C_{A,\text{solid}} = \frac{C_A}{C_{\text{solid}}} = f(\text{Particle Interactions}) \quad \mathbf{1.8}$$

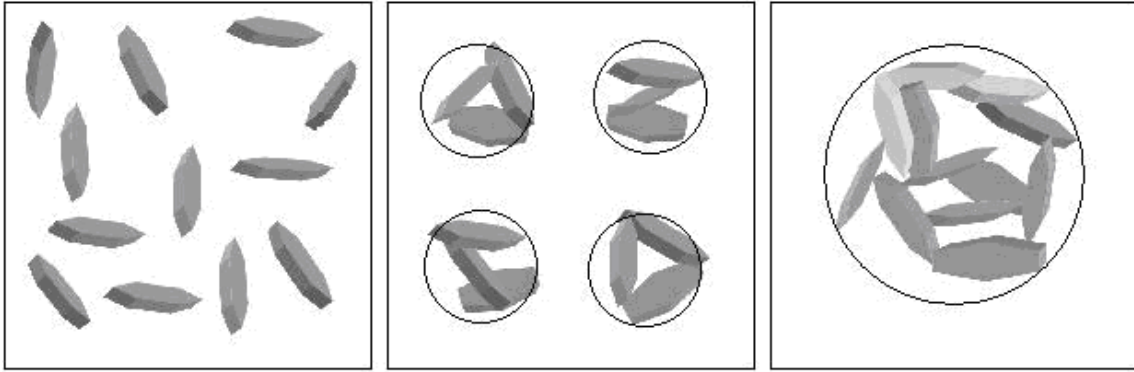


Figure 1.13 Illustration of the effect of particle interactions on volume fraction. Aggregate size and void fraction increases from left to right: $C_{\text{primary particles}} \sim 1/10$, $C_A \sim 1/4$, and $C_A \sim 1/2$

where $C_{A, \text{solid}}$ is the ratio of aggregate volume fraction to solid volume fraction. In this project, the aggregate structures are considered to be the building blocks of the flocculating carrier fluid. It is the concentration of aggregate structures that govern the carrier fluid viscosity. Therefore, it is necessary to measure the size of aggregates rather than the size of the fully dispersed particles. A novel, optical-based particle size measuring device, the Sysmex FPIA-3000, is used to measure the size and concentration of kaolinite clay aggregates in this study.

1.8. Characterization of Particle Suspensions by FPIA

The FPIA is used in this study to measure the size of kaolinite clay aggregates rather than the fully dispersed particle size of the clay in the mixture. This device takes images of clay aggregates without breaking the aggregates down to primary sizes. Concentration of clay aggregates are estimated from statistical analysis of these images. Hence, volume fraction of aggregates, instead of volume fraction of solids, could be measured and used in viscosity correlations.

The Sysmex FPIA-3000 (Flow Particle Image Analyzer) measures the size and morphology of emulsions and suspensions with particle size distribution ranging from 0.5 to 300 μm . The sample is poured into the mixing unit of the FPIA

sample chamber and flows down into a transparent flow cell. “Particle Sheath” liquid is injected parallel to and around the sample flow, pressing it to form a laminar flat flow. Next, the device captures images of the particles in the flat sample flow. These images are automatically analyzed in the image processing unit. Two-dimensional size distribution and particle shape parameters are produced in data processing unit.

1.8.1. Applications of FPIA in Literature

The FPIA has recently been used to study particle shape and size distribution of different suspensions. Arnold et al. (2003) studied the PSD of aqueous suspension of lithium iron phosphate particles by the FPIA. Lithium iron phosphate is used as positive electrode material for lithium batteries. Synthesis of smaller lithium iron phosphate particles improves the performance of available lithium batteries. The FPIA was used to measure the PSD of the newly-synthesized fine lithium iron phosphate particles. Tanaka et al. (2008) studied the shape of toner powder particles by the FPIA. Toner powder particles are in the range of 5.5 to 6.5 μm in diameter and consist of polyester resin, carbon black and wax. The image quality of printers is affected by the fluidity of the toner. Fluidity of the toner depends on the shape and roughness of toner powder particles. Particle shape analysis information of toner particles was successfully provided by the FPIA and was used in the determination of surface roughness of toner particles. Komabayashi and Spangberg (2008) (a, b) used the Sysmex-FPIA3000 to study the particle size and shape distributions of fine mineral trioxide aggregates in water. The particle sizes reported in their study range from 0.5 to 40 μm . Komabayashi and Spangberg (2008) (a, b) choose the FPIA image analysis technology over Scanning Electron Microscopy (SEM), x-ray diffraction and spectroscopy, in order to benefit from the FPIA capability of rapid particle imaging. In their study, the FPIA successfully provided all the necessary size and shape information required for understanding the penetration process of mineral trioxide aggregates

into dental tubules. After their initial success, Komabayashi and Spangberg (2009) used the FPIA to examine the capability of calcium hydroxide powder to function as the dressing in root canal treatment. The FPIA enabled the authors to successfully measure the length, width, perimeter, and aspect ratio of calcium hydroxide powder aggregates in alcohol with particle size diameter of 0.5 to 3.5 μm . Krause et al. (2009) utilised the FPIA to examine carbon nanotube agglomerates in aqueous dispersions, the size of which range from 1.6 μm to 20 μm in diameter. The study of the size and circularity distribution of carbon nanotube agglomerates provided assessments of the dispersity of carbon nanotube particles in aqueous dispersions. The shape analysis results by the FPIA were found to correspond to the observations from cryofractured analysis.

Although the FPIA has been used in the literature to study particle shape and size distribution of numerous suspensions with success, there has not been any research reported on the application of the FPIA in clay suspension analysis.

1.8.2. Advantages of FPIA over Conventional Sizing Techniques

Particle size distribution is one of the most important parameters in characterizing the performance of processes such as settling and dewatering of slurries (Masliyah et al., 2011). In the oil sands industry, the assessment of clay particles in a slurry is mostly based on light scattering particle size analysis (PSA) technique. Light scattering techniques can provide fast and reliable results over a broad particle size range with common cutoff point of 0.4 μm , and cutoff point of 0.05 μm for more advanced instruments (Govoreanu, 2009). However, this technique is susceptible to particle shape effects and produces a broader size distribution for non-spherical particles, such as clays (Govoreanu, 2009). Light scattering is based on the principle that large particles scatter light strongly at low angles while smaller particles scatter light more weakly and at higher angles. This technique requires an infinitely dilute and fully dispersed suspension to eliminate possible multiple scattering. For this purpose, samples are fully dispersed prior to testing

using chemical dispersing agents and sonication technique which would break down the aggregate structures. Franco et al. (2004) studied the effects of sonication on the PSD of kaolinite clay particles. It is shown in their work that sonication directly affects the structure and PSD of the sample by inducing de-aggregation and delamination of the clay particles. In summary, this particle size measurement method involves sample treatments that have a drastic effect on the structure of flocculated suspensions and is not suitable for this project.

Another commonly used technique for the characterization of particles in different industrial suspensions is the Coulter Counter technology. This technique can routinely measure particles in the size range of 0.4 μm to 1200 μm in diameter with an accuracy of 1%. In a Coulter Counter, the volume of individual particles is measured as they are pumped through an aperture with electrical sensing zone. This method requires particles to be adequately suspended in an electrolyte solution (DeBlois and Bean, 1970). Coulter Counter electrolytes (mainly NaCl, KCl and HCl) drastically affect clay aggregate structure by altering the suspension chemistry. Measurement errors could also occur when large aggregates sedimentate at the bottom of the dispersion unit instead of being pumped through the system. This method is slow for large particles and there is a risk of clogging the aperture during the measurement. Therefore, Coulter Counter technique is only suitable for small particle sizes in stable dispersed suspensions. Due to these limitations, this technique is not applicable to the flocculated suspensions of interest in this project.

The sedimentation technique can be used to calculate the equivalent spherical diameter of particles from measured values of particle settling velocity based on Stokes law:

$$u_T = \frac{(\rho_p - \rho_f)g d^2}{18\mu} \quad \mathbf{1.9}$$

Michaels and Bolger (1962) (a) placed sedimentation experimental data into Equation 1.3 to calculate the size of kaolinite aggregates in aqueous suspensions. Settling velocity was recorded by measuring the rate of change of the height of the interfacial plane between the slurry and the supernatant fluid. The two main disadvantages of this method are the requirement of large amount of sample and long measuring time. Therefore, this technique cannot be used with sufficient frequency in this project. Furthermore, plate-like clay particles settle slower than spherical particles of the same volume due to a higher drag force acting on the particles. Hence, sedimentation technique would under-predict the particle size of dispersed clay suspensions.

An excellent technique for direct visual examination of size, shape and structural properties of aggregate structures is optical microscopy. Zbik et al. (2008) used Cryo-SEM analysis method to measure clay aggregate sizes. Their procedure includes freezing the samples and using SEM to look at the preserved aggregate structures in the sample. However, this technique is not suitable for this study as it requires elaborate sample preparation and very few particles are examined during each measurement.

A rapid particle imaging technique that does not break aggregate structures into dispersed particles is desirable for this project. The FPIA is capable of determining not only the particle size but also the particle shape. The particle size and shape information is generated from the analysis of a large number of particles. This device captures images of the sample flow without breaking the aggregated structure down into deflocculated particles. This method allows one to view the aggregate structures in the sample in their natural state. Images of individual particles are stored in the FPIA data base. A display of images of all analyzed particles provides further visual understanding of the measurement data. This feature also enables offline morphological study of particles. Particle images are automatically analyzed in the image processing unit. Aggregate size measurement techniques based on such automated image analysis allow for a

rapid determination of particle size distribution. Measurement time is relatively short, as analysis of each sample takes only 2-5 minutes. Another advantage of the FPIA instrument is that it requires a small sample volume of 1 to 5 ml (Sysmex-FPIA-3000 Operators Manual, 2006). Because of the numerous advantages of the FPIA over the aforementioned sizing techniques, FPIA technology is used to characterize clay and sand suspensions in this project.

1.8.3. Limitations of FPIA

There are a few limitations associated with the use of the FPIA instrument for testing kaolinite suspensions. There is some concern that the FPIA may affect the particle size distribution and the shape of flocculated particles. The FPIA injects “Particle Sheath” liquid parallel to and around the sample flow, pressing it to form a flat flow. Particle sheath liquid contains salts, surfactants and buffers and alters the chemistry of sample as it comes to contact, and possibly mixes with the sample flow. Sample chemistry dominates the aggregate structure of flocculating particles. Any change in the chemistry of sample influences aggregate structures. Aggregate structures are also affected by the sample flow pattern and the shear exerted on the sample inside the FPIA during the testing process. This fact introduces uncertainty in reporting absolute values for the PSD of samples containing aggregates that are sensitive to mixture chemistry.

Another limitation of the FPIA relates to the fact that the sample should be fairly dilute for accurate measurements. The FPIA cannot measure more than 36,000 particles in one μl of the sample. As an example, particle number density for a kaolinite-water mixture ($C_k = 0.25\%$) in a moderately-flocculated state, also for a kaolinite-water mixture ($C_k = 0.1\%$) in dispersed condition, goes over the FPIA acceptable limit. These mixtures need to be diluted prior to testing to ensure an accurate measurement. Dilution alters the chemistry of the sample which affects the clay aggregate structures. Therefore, it is necessary to account for the effect of dilution on PSD of flocculated mixtures. Effect of FPIA on the particle size of

idealized carrier fluid samples through sample dilution and sample mixing process inside the instrument are studied in this project.

Particles in aqueous kaolinite slurries do not grow larger than the FPIA upper size limit without polymer-induced flocculation. However, in completely dispersed forms, kaolinite particles in the sub-micron size range can be found. Particles smaller than 0.25 μm in diameter cannot be measured by the FPIA; hence, a fraction of dispersed kaolinite particles cannot be detected. Corrections for the effect of the FPIA measurement procedure on size and structure of samples are not necessary if PSD is studied from a qualitative or a comparative point of view.

2. Project Objectives

There are numerous difficulties associated with the measurement of carrier fluid viscosity and as a result one has to use correlations to evaluate this important parameter. The accuracy and applicability of the empirical correlations that are typically used to predict carrier fluid viscosity in the oil sands industry are uncertain. The main deficiency of the available correlations is that the viscosity is predicted using the volume fraction of total fines as the primary correlating parameter. This approach neglects the effects of the different particle types in the suspensions. Fine particles in the carrier fluid consist of sand and clay-type particles. Clay particles flocculate in the process water while sands are inert. Flocculating and inert particle types have distinguished effects on the carrier fluid viscosity. The main objective of this project is to provide a more accurate method of predicting carrier fluid viscosity.

In this project, the different roles of “inert fines” and “flocculating fines” in determining the carrier fluid viscosity are demonstrated. Volume fraction and PSD of a flocculating mixture are determined without breaking the aggregate structures down to primary particles. A novel PSD measurement technique, the Sysmex Flow Particle Image Analyzer (FPIA-3000) is introduced to the industry for this purpose. This instrument captures images of particles in the mixture in their natural state. Therefore, it is possible to study the different contributions of flocculating and inert fines to the PSD of a mixture. Next, viscosity measurements are conducted on mixtures containing flocculating and inert fines to study the effect of each fine type on carrier fluid viscosity. This overall project has two main stages. In the first stage of this project, idealized aqueous slurries consisting of kaolinite clay and sand flour ($d \sim 20 \mu\text{m}$) are studied. In the second stage of the project, samples will be obtained from actual hydrotransport and tailings streams. Samples from the oil sands industry contain coarse fractions and finite concentrations of bitumen. Therefore, special procedures should be developed for

testing these complex samples. The second stage of the project is not covered in the present study.

In the present study, the Sysmex FPIA-3000 is used to study the PSD of the idealized slurries. The main objectives of the initial tests are to commission the FPIA and to investigate the capabilities and limitations of the instrument for suspensions of the type used in this project. Next, sand-kaolinite-water suspensions are tested with the FPIA to investigate the different effect of flocculating and inert particles on the PSD of the idealized slurry. Flocculating particles form aggregate structures in the suspension. It is proposed in this project that the aggregate structures are the building blocks of a flocculating mixture, and it is the concentration of aggregate structures that govern the viscosity of the mixture. Hence, volume fraction of aggregates, instead of volume fraction of solids, should be measured and used in viscosity correlations. Concentration of clay aggregates will be estimated from statistical analysis of the images captured by the FPIA. The size and structure of aggregates depend on the mixture chemistry. An analysis of the variability of the volume fraction of aggregates with changes in water chemistry and component volume fraction will be provided in this study.

Finally, viscosity measurements are conducted for idealized slurries at varying component volume fractions and water chemistries. Here, the volume fraction of aggregates will be used to represent the effect of both the flocculating solid concentration and water chemistry on the mixture viscosity. The main objective of this work is to demonstrate that viscosity correlations are improved significantly if the volume fraction of aggregates is used as the primary correlating parameter, rather than the more conventional use of total solids concentration.

2.1. Activities

The Sysmex FPIA-3000 is used in this work to study the PSD of the idealized slurries. Particle size and circularity analysis tests on the performance of the FPIA on the flocculated kaolinite-water mixtures are reported in Section 4.1. The study of the effect of FPIA measuring method on the particle size and structure of samples follows in Section 4.2. Lastly, sand-kaolinite-water suspensions are tested with the FPIA to investigate the different effect of kaolinite and sand particles on the PSD of the idealized slurry. It will be shown in Chapter 4 that the FPIA is an appropriate device to achieve the objective of this project to assess the kaolinite or sand water suspensions in their natural state.

Kaolinite-water suspensions are tested by the FPIA to investigate the change in aggregate size of kaolinite at different water chemistries in the first section of Chapter 5. Measurements were taken at different water chemistries to illustrate suspension behaviour under caustic and acidic process operations. Calcium chloride solution (0.25 M) was added as coagulant to make highly-coagulated mixtures. Tetrasodium pyrophosphate (TSPP) was used as a dispersant to study fully dispersed mixtures. Aggregate volume fraction is determined for kaolinite-water mixtures at pH 4 and pH 9 using the FPIA measurement results in Section 5.2. Table 2.1 presents volume concentrations and water chemistry of kaolinite-water mixtures that were studied by the FPIA in Chapter 5.

Rheological measurements of kaolinite-water and sand-kaolinite-water mixtures were carried out using the concentric cylinder geometry of an AR-G2 viscometer. Low kaolinite concentrations were tested to avoid complication arising from shear-thinning behaviour of concentrated fluids. Measurement of the viscosity of kaolinite-water suspensions at pH 4 and pH 9 is reported in Section 5.3. Kaolinite-water mixtures at pH 4 and pH 9 are shown to have different rheological behaviour. Viscosity data for kaolinite-water mixtures at pH 4 and pH 9 are plotted against aggregate volume fraction in Section 5.4. It is shown that the

Table 2.1 Compositions of idealized carrier fluid for particle size and shape measurements by FPIA.

C_k (%)	C_s (%)	pH	TSPP (wt/wt kaolinite)	Ca^{2+} (M)
0.25	0	4.5	0	0
0.25	0	6.5	0	0
0.25	0	11	0	0.007
0.25	0	11	0.02	0
0.03, 0.07	0	4	0	0
0.03, 0.07	0	9	0	0

viscosity data for these two types of mixtures fall on the same trend line when they are plotted against aggregate volume fraction rather than solid volume fraction. In Section 5.5, sand-kaolinite-water suspensions are tested with the ARG2 rheometer in order to investigate the different effects of sands and clays on the viscosity of the mixture. The viscosity data for the sand-kaolinite-water suspensions is presented in one graph alongside those for the kaolinite-water suspension. It is demonstrated in Chapter 5 that flocculating kaolinite particles increase the mixture viscosity more significantly compared with sand particles for the same amount of solid concentration. Table 2.2 shows the different volume concentrations of kaolinite clay and silica powder in the idealized slurries that were studied in Chapter 5.

Table 2.2 Compositions of idealized carrier fluid for rheology measurements.

C_k (%)	C_s (%)	Suspension pH
0, 1, 2, 3.5, 5, 7, 10	0	9
0, 2, 3.5, 5, 7, 10	0	4
7	0, 10, 15, 20, 25	8

3. Experimental Methods

3.1. Materials

3.1.1. De-ionized Water

De-ionized water was used as the dispersing medium for all the experiments to ensure consistency. The de-ionized water was collected from “Elix Advantage Water Purification System” (Millipore SAS, France). The specifications of the de-ionized water are presented in Table 3.1.

Table 3.1 De-ionized water specifications.

pH	6.02
Conductivity	2.35 $\mu\text{s}/\text{cm}$
Salinity	0.01 psu
TDS	1.6 mg/lit

Acid chloridric (0.1 M) and sodium hydroxide solution (0.25 M) were used to adjust pH. Calcium chloride solution (0.25 M) was added as coagulant to make highly-coagulated mixtures. Tetrasodium pyrophosphate (TSPP) was used as dispersant to study fully dispersed mixtures.

3.1.2. Kaolinite

Idealized clay suspensions were prepared using Pioneer kaolinite. Pioneer kaolinite is a medium plasticity Georgia kaolinite with a chemistry close to that of theoretical kaolinite. Pioneer kaolinite has been a standard for many years in the North American ceramic industry. Table 3.2 presents the characteristics of the Pioneer kaolinite provided by the supplier. Ions present at the surface of kaolinite play an important role in determining the mixture rheological properties. A single bag of kaolinite was used for all experiments to minimize error caused by possible inconsistencies between kaolinite batches.

Table 3.2 Physical properties of Pioneer kaolinite.

Particle size, % < 2 μm	55-65
Mean particle size	1.0-1.2 μm
325 mesh residue	0.75%
Kaolinite mixture pH at 20% solids	4.0-6.5
Particle density	2696 kg/m^3

3.1.3. Silica Flour

Silica flour (Sil 325) was kindly provided by the Saskatchewan Research Council to represent fine inert sand particles in viscosity measurements. Compared with larger sand varieties, silica flour particles are less prone to sedimentation in the viscometer. Table 3.3 presents the specification of this sand. Size distribution information was obtained using Andreasen pipette technique by Gillies (2012).

Table 3.3 Physical properties of Sil 325 fine silica sand.

Particle size, % < 3 μm	6
Particle size, % > 42 μm	34
d_{50}	20 μm
Silica mixture pH at 20% solids	8.0 -8.5
Particle density	2650 kg/m^3

3.2. Apparatus

3.2.1. Mixer

The mixer used for sample preparation is a EUROSTAR power control-visc, by IKA Werke GmbH & Company, Germany. The mixer can operate from 50 to 2000 Revolution Per Minute (RPM). For concentrated kaolinite-water mixtures,

kaolinite volume fraction (C_k) higher than 1%, operating the mixer on low RPM would render inadequate mixing while operating on high RPM causes air entrainment in viscous mixtures (C_k higher than 10%). Air bubbles trapped in a mixture that exhibits yield stress remain inside as they cannot rise up to the surface, which would affect the density and rheology of the mixture. In this project, the Mixer is operated at RPM values which ensures adequate mixing and does not induce the formation of air bubbles in the mixer.

Dimensions of the mixing vessel, the RPM of mixer and the shape and position of propeller affect the flow pattern in the mixer, which in turn, affects the size and structure of aggregates in the mixture. The 45 degree pitched-blade turbine propeller with diameter of 45 mm was used for all mixture preparations. This impeller discharges one half of total flow axially and one half radially and ensures adequate mixing for the mixtures of interest in this project. The ratio of diameters of impeller to mixture vessels used in the experiments falls in the range of 0.4 to 0.6. The impeller was positioned such that the gap between the bottom of the blade and the bottom of the beaker was equal to half of the blade diameter. It is necessary to maintain consistency in mixture preparation procedures. Mixtures were prepared in a 200 cc beaker and the mixer was operated at 400 RPM for all viscosity measurements. Mixtures were prepared in a 400 cc beaker and the mixer was operated at 400 to 700 RPM for all the FPIA measurements.

When kaolinite is mixed with water, the charged ions present on the surface and in between layers of kaolinite particles begin to release into water. Hence, the chemistry of the mixture changes with mixing time until equilibrium is reached between the amount of ions on kaolinite particles and inside water, at which point, pH of the mixture becomes constant. For example, pH of a kaolinite-water mixture ($C_k = 5\%$) prepared by de-ionized water changes from 5.4 at the start of the mixing to 4.7 after 10 minutes of mixing and decreases to 4.4 after 60 minutes of mixing, and then it becomes constant. Samples that contain kaolinite are prepared by 60 minutes of mixing to ensure adequate mixing. Change of mixture

concentration by water evaporation from the mixture surface during mixing time is negligible.

3.2.2. Scale

An FX-3000 electronic balance scale by AND, Japan, was used to weight solids for mixture preparations. This scale can measure maximum weight of 3100 gr with 0.01 gram precision.

3.2.3. Vacuum system

A simple vacuum pump aspirator by Nalge Company (Rochester, New York, USA) was used to facilitate filtration for mixture preparation. The vacuum pump consists of a tee fitting which is attached at the top to a water faucet such that the water flows in the vertical portion of the T. At the intersection part of the T, a tube hose connects the outlet of the T to the vessel that vacuum needs to be applied to. The strength of the vacuum produced by tap water at 25 °C is limited to 3.2 kPa.

3.2.4. Sysmex Flow Particle Image Analyzer-3000 (FPIA)

The Sysmex FPIA-3000 is a Flow Particle Image Analyzer combining flat sheath flow formation technology and image processing technology. This device can be used to measure the size and morphology of emulsions and suspensions with particle size distribution ranging from 0.5 to 300 μm . The FPIA-3000 is built with 10x objective lens as the standard unit. This objective lens can be replaced with other available standard lenses with different magnifications. This option permits the user to measure broad ranges of particle size. Table 3.4 presents particle size measuring ranges for the FPIA-3000 lens units.

The sample is poured into the mixing unit of the FPIA sample chamber and flows down into a transparent flow cell. “Particle Sheath” liquid is ejected parallel and around the sample flow, pressing it to form a laminar flat flow. Next, the device

irradiates pulse light to the flat sample flow every 1/60 second. The duration of the flash is 2 μ s, so that moving particles can be captured in focus as still images.

Table 3.4 FPIA-3000 particle size measuring ranges for 10x, 20x and 5x lens units in High power field (HPF) and Low power field (LPF).

Magnification unit	Particle size, HPF mode (μ m)	Particle size, LPF mode (μ m)
20x	0.25 – 20	0.7 - 80
10x	0.5 – 50	2 - 200
5x	1 – 100	4 - 300

These images are automatically analyzed in the image processing unit. Here, particle images are binarized, dividing the whole image into bright and dark portions. Next, the edge of the particle is traced on the boundaries between light and dark areas. After edge detection, projected area of the particle is calculated and the information is sent to the data processing unit, where statistical analysis is performed. Data processing unit produces two-dimensional size distribution and particle shape parameters (e.g. the circularity) that can be displayed in histograms. After testing is complete, the sample and sheath liquid are rinsed automatically into the waste container. Figure 3.1 shows a schematic of sample flow inside the FPIA.

The required sample volume for testing by the FPIA-3000 is 1 to 5 ml. The sample should be fairly dilute, as the device cannot measure more than 36,000 particles in one μ l of sample. As an example, Table 3.5 presents particle number density,

denoted as particle density (N), calculated by the FPIA for five different kaolinite mixtures. As table 3.5 suggests, particle number density for a kaolinite-water mixture ($C_k = 0.25\%$) in moderately-flocculated state, also for a kaolinite-water mixture ($C_k = 0.1\%$) in dispersed condition, goes over the FPIA acceptable limit. These mixtures need to be diluted prior to testing to ensure an accurate measurement.

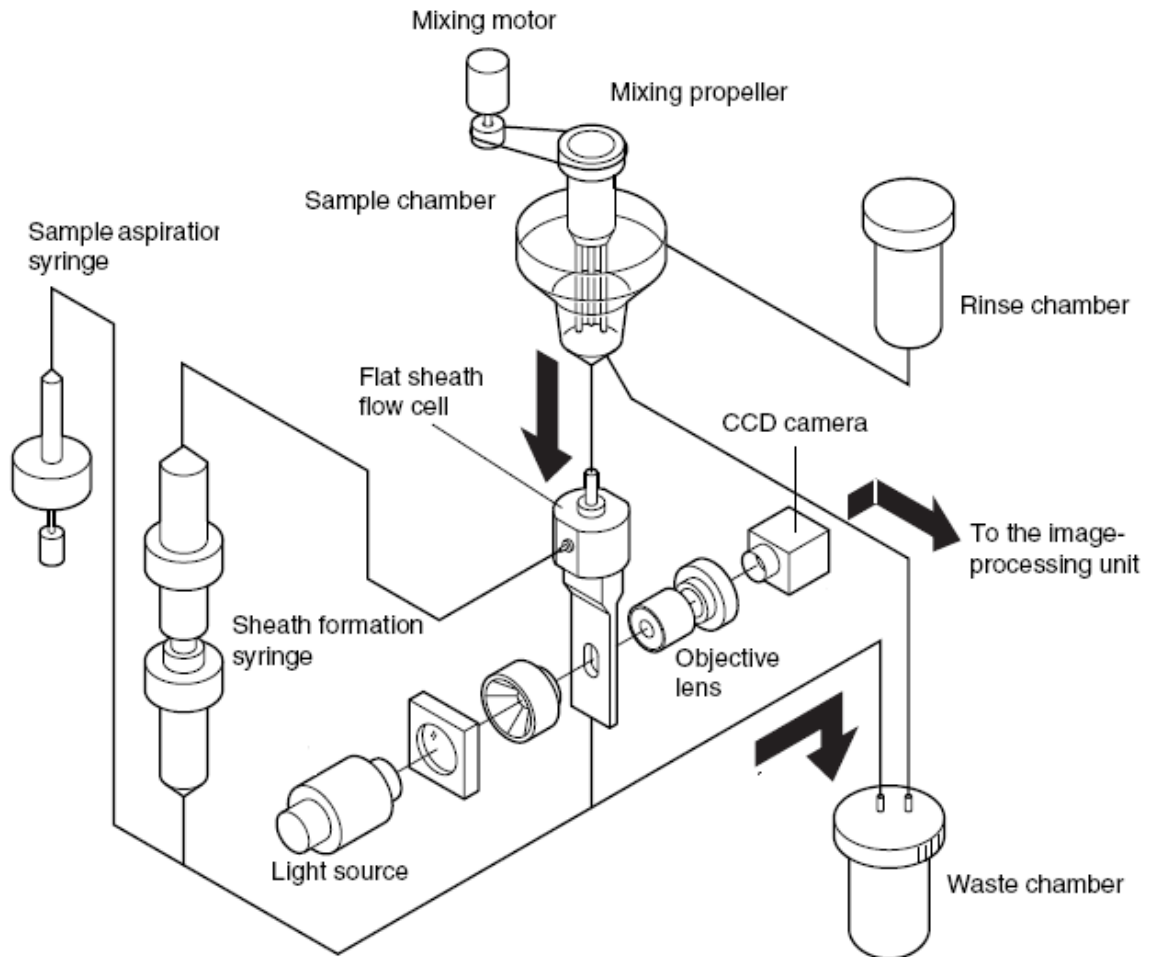


Figure 3.1 Schematics of sample flow inside FPIA (Sysmex FPIA-3000 Operator's Manual, 2006).

Table 3.5 Particle number density measured by FPIA for different kaolinite mixtures using 10x standard lens unit in HPF mode. Mean (N) D_{CE} is the number-based mean circular equivalent diameter of particles.

Kaolinite mixture type	C_k (%)	Mean (N) D_{CE} (μm)	Particle density (N) ($1/\mu\text{l}$)
Highly-flocculated	0.28	9.722	2516
Moderately-flocculated	0.25	5.995	40840
Flocculated	0.1	10.595	5285
Dispersed	0.1	1.516	139302
Dispersed	0.01	1.532	13203

Two mixtures of monodisperse latex spheres ($d = 2.00 \mu\text{m}$) from Malvern Instruments (Worcestershire, UK) in de-ionized water were tested by the FPIA. Particle size and circularity frequency distribution graphs for these measurements are presented in Figure 3.2 to 3.3. The particle mean diameters for these two mixtures are calculated by the FPIA to have a value of 2.07 and 2.09 μm . The error between the measured particle sizes, and the actual value provided by the manufacturer is small and in the acceptable range for this project.

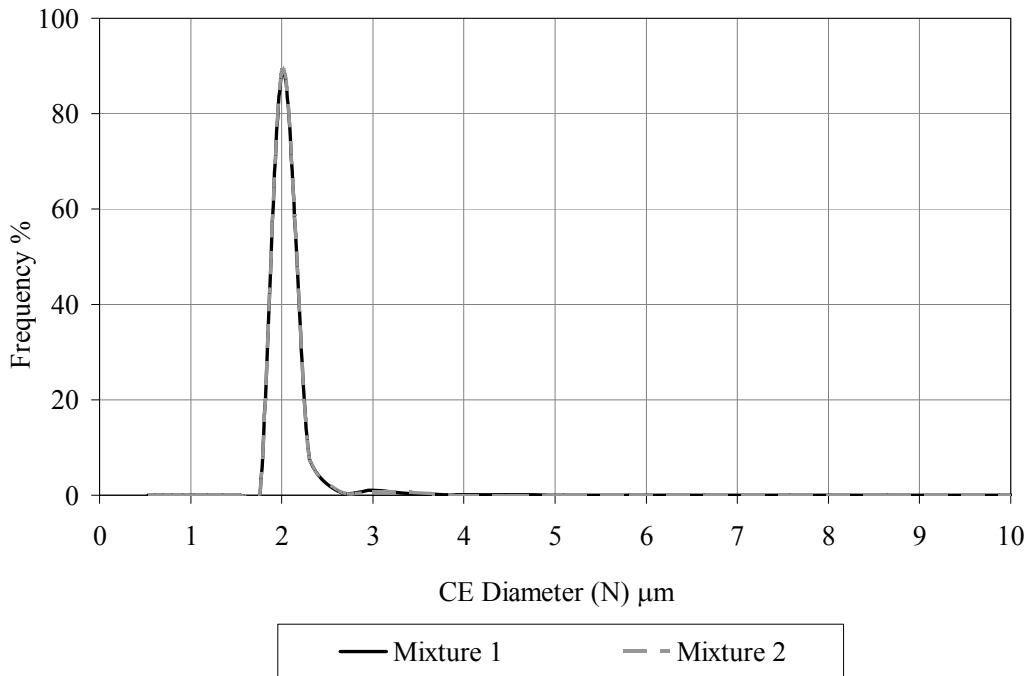


Figure 3.2 PSD results for 2 mixtures of monodisperse latex spheres ($d = 2.00 \mu\text{m}$) in de-ionized water from the FPIA.

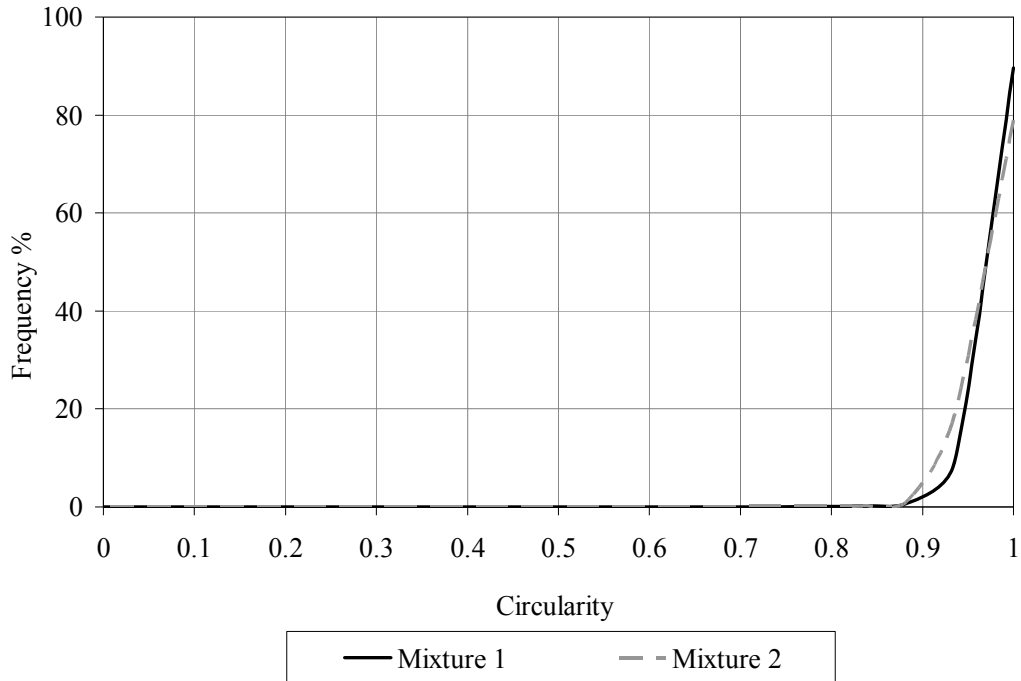


Figure 3.3 Particle shape distribution results for 2 mixtures of monodisperse latex spheres ($d = 2.00 \mu\text{m}$) in de-ionized water from the FPIA.

3.2.5. TA Instrument AR-G2 Rheometer

TA Instruments AR-G2 is a controlled stress/controlled strain/direct rate rheometer featuring combined motor and transducer (CMT) system. AR-G2 is capable of handling many different types of samples. It comes in with four types of measuring systems: the concentric cylinders, cone and plate, parallel plate and rectangular solid sample. Figure 3.4 shows the AR-G2 rheometer without any particular measuring system installed. This rheometer is used for measuring the viscosity of different sand and kaolinite aqueous suspensions.

The concentric cylinder geometry is chosen as the measuring system for this study. This system features nano scale torque and angular velocity control and is capable of characterizing low viscosity materials over broad ranges of shear rate. It needs small sample volume and is suitable for dispersions of limited stability. The sample is loaded into the gap between the outer fixed cylinder (the cup) and the inside rotating cylinder (the spindle). The Standard DIN (conforms to DIN

53019) Aluminum spindle was used with the concentric cylinder system. Figure 3.5 shows a schematic of this geometry.

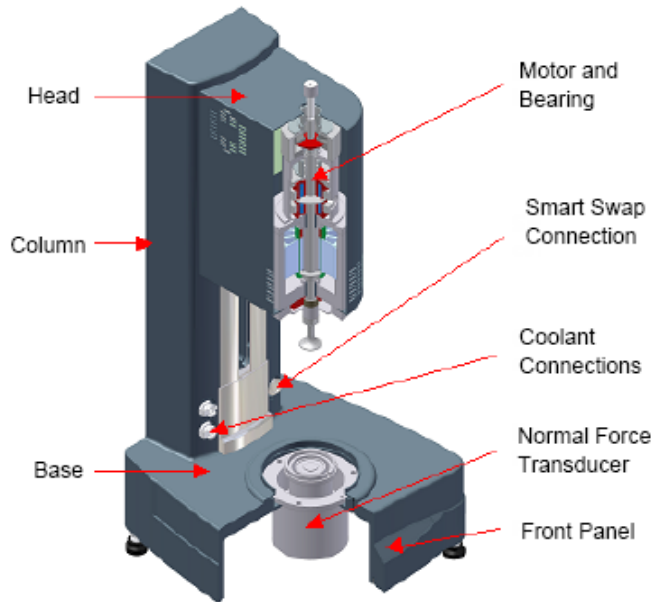


Figure 3.4 The AR-G2 rheometer (AR-G2 Operator's Manual, 2006).

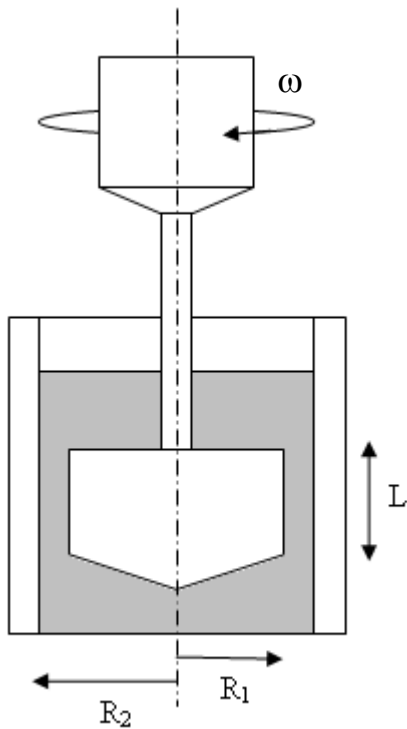


Figure 3.5 Schematic of concentric cylinder system. $R_1 = 14.00$ mm; $R_2 = 15.00$ mm; $L = 42.00$ mm.

The sample is sheared between the spindle and the cup. The cone segment at the bottom of the spindle eliminates “end effects”. The variation of shear rate across the small annulus gap between spindle and cup is negligible for Standard DIN concentric cylinder system. AR-G2 is equipped with a temperature control system; hence the effect of temperature rise due to shear heating is eliminated. In this study, AR-G2 was operated in Steady Controlled Rate (CR) mode where torque is measured over a range of spindle speeds. Table 3.6 presents specifications of this measuring system.

For laminar Couette flow of a Bingham fluid, the equation of the line passing through data of torque versus spindle speed is given by Shook et al. (2002) as Equation 3.1. This equation is used to calculate the value of viscosity. For a Newtonian fluid, a graph of torque against spindle speed is linear through the origin, so that the second term of Equation 3.1 would be zero.

Table 3.6 Specifications of AR-G2 rheometer for concentric cylinders measuring system in controlled rate mode (CR).

Minimum torque	0.01 μ N.m
Maximum torque	200 mili N.m
Torque resolution	0.1 nano N.m
Angular velocity range	1.4 ⁻⁹ to 300 rad/s
Displacement resolution	25 nano rad
Temperature range	-20 to 150 °C
Maximum heating rate	15 °C/min

$$T = \alpha \mu_f \omega + \alpha T_0 \ln \left(\frac{R_2}{R_1} \right) \quad 3.1$$

where α is the measuring system geometry factor:

$$\alpha = 4\pi L \left(\frac{R_1^2 R_2^2}{R_2^2 - R_1^2} \right) \quad 3.2$$

For the standard DIN concentric cylinder system used in this study, α has a value of $80.26 \times 10^{-5} \text{ (m}^3\text{)}$.

In concentric cylinder arrangements, centripetal force drives the fluid near to the spindle outwards more vigorously than the fluid close to the cup, causing local circulations (Taylor vortices) to occur inside the fluid at high spindle speed values (Taylor, 1936). As some of the energy transferred from the spindle into the fluid is dissipated by Taylor vortices, fluid resistance to flow seems to increase, leading to over-estimation of fluid viscosity.

The viscometer must be operated below the spindle speed limit calculated by “Onset of Taylor Vortices” to prevent the error in viscosity calculation due to Taylor vortices (Shook and Roco, 1991):

$$\omega < \frac{45\mu_f}{\rho_f R_m^{0.5} \delta^{1.5}} \quad 3.3$$

where

$$\delta = R_2 - R_1, \quad R_m = \frac{R_1 + R_2}{2}$$

However, operating at low spindle speeds for fluids that exhibit a yield stress can generate a different error. As shear stress decreases from the spindle to the cup, a point might be reached where shear stress exerted on the fluid is less than the fluid yield stress. At this point, part of the fluid region behaves like a solid plug. The spindle speed must be sufficiently high so that the yield value is exceeded everywhere across the gap to prevent incomplete shearing. For a data point to be

meaningful, the torque exerted at the cup must meet the limit set by Equation 3.4 (Shook and Roco, 1991):

$$T > 2\pi L T_0 R_2^2 \quad 3.4$$

where T_0 is the Bingham yield stress and is calculated from the graph of torque versus spindle speed using Equation 3.1.

A sample of the standard oil (S6) from Cannon Instrument (Pennsylvania, USA) and a sample of de-ionized water were tested by the AR-G2 concentric cylinder viscometer. The viscosity values of these two samples are in the lower and higher range of the viscosity values of mixtures in this project. A plot of T/α against spindle speed for these measurements is shown in Figure 3.6. Table 3.7 provides the actual viscosity values of these samples provided by the manufacturer, and the calculated value from AR-G2 measurements. The error between the measured value, and the actual value provided by the manufacturer is in the acceptable range for this project.

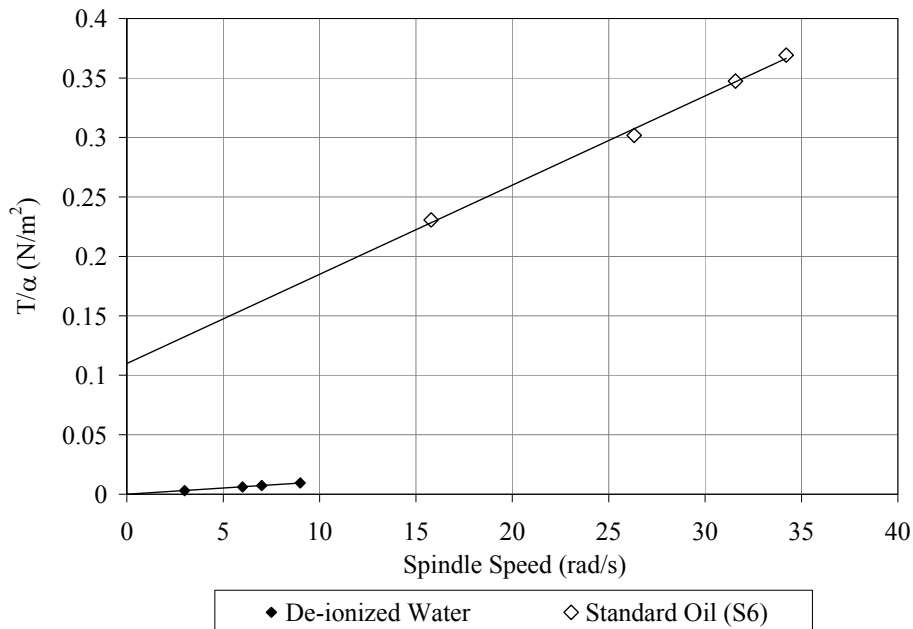


Figure 3.6 Plot of torque divided by α from rheological results for de-ionized water and standard oil (S6).

Table 3.7 Viscosity values of standard oil (S6) and de-ionized water provided by the manufacturer, and the calculated value from AR-G2 measurements.

Material	Temperature (°C)	Actual viscosity (mPa.s)	Measured viscosity (mPa.s)	Error (%)
Standard oil (S6)	20	8.0	8.05	0.6
De-ionized water	22	0.97	1.02	5.1

3.3. Procedures

3.3.1. Mixture Preparation

The mixture preparation procedure steps are listed below.

1. Use the solid density and calculate the weight of solids required to make the desired mixture volume fraction.
2. Put a clean, empty and dry beaker on the scale. Re-zero the scale. Use a stainless steel spatula to add kaolinite powder to the beaker until the desired weight is reached. Wash and dry the spatula, re-zero the scale and use the spatula to add the required amount of sand to the beaker.
3. Calculate the required amount of de-ionized water. If the mixture needs to be dispersed by the addition of TSPP powder, use 50 cc less water than calculated.
4. Remove the beaker from the scale. Use a 100 cc cylinder multiple times to take the required amount of de-ionized water and pour the water into the beaker.
5. Place the beaker under the mixer and adjust the mixer shaft height so that the distance between the bottom of the propeller and the bottom of the beaker is equal to the half of the propeller diameter.
6. Turn the mixer speed knob counter-clock wise to the lowest speed and then turn on the mixer and slowly increase the speed to 400 RPM.
7. Start the stop-watch and mix for 60 minutes. Do NOT turn the mixer off.

8. Measure the pH of the mixture. Adjust the pH to the desired value using either HCl (0.1 M) or NaOH (0.25 M) solution to decrease and increase the pH, respectively. When close to the desired pH, add the solution drop by drop and wait for the pH to become stable before adding more.
9. Add the required amount of calcium chloride solution (0.25 M) for those samples that need to be highly flocculated.
10. For samples that need to be dispersed, weigh the required amount of TSPP in a small beaker and add 50 cc de-ionized water. Put the beaker on a magnetic mixer and heat it to 50 °C. When TSPP powder is completely dissolved in water, stop the mixer and wait for the beaker to reach room temperature. Empty the beaker slowly into the main mixture. Let mix for 10 minutes.

3.3.2. FPIA Tests

As mentioned in Section 3.2.4, the sample introduced into the FPIA should meet a certain concentration limitation. Therefore, samples from concentrated mixtures need to be diluted before testing. It is necessary to ensure that the effect of dilution on the floc size is kept at the minimum. Hence, the water used to dilute the mixture should have similar chemistry to the mixture. For this purpose, the mixture filtrate is used as the diluting medium. However, since the kaolinite particles are charged, their presence affects the pH of the mixture. Hence, a certain mixture and its filtrate may have different pH values. After the sample is diluted by the filtrate, the pH needs to be measured and adjusted to the desired value. The procedure of sample dilution is as follows:

1. Prepare 400 cc mixture with the same properties as the sample that needs to be tested in a 500 cc beaker.
2. Stop the mixer and allow the mixture to rest until the particles sediment.
3. Take a side arm flask and secure the ventilation tube to the vacuum system.

4. Put a grade 5 Whatman filter paper in a clean and dry Büchner funnel and ensemble the funnel on the flask. Grade 5 Whatman filter paper is capable of retaining fine particles larger than 2.5 μm .
5. Wet the whole filter paper area by pouring de-ionized water in the funnel and wait for the water to drain into the flask. This would insure that the paper adheres tightly to the funnel
6. Take the flask out of the ensemble and put a new dry flask under the funnel.
7. Decanter the supernatant into the funnel. After all filtrate accumulates in the flask, dissemble the flask and the funnel. Dispose of the filter paper and the solid cake.
8. Use the filtrate and the main mixture and make the desired sample that meets the FPIA limitations in a 200 cc beaker.
9. Put the beaker under the mixer (RPM = 400).
10. Measure the pH of the sample and adjust it if necessary.

The procedure of testing a sample with the FPIA is as follows:

1. Start the FPIA at least two hours before the testing to ensure the internal temperature of the device reaches room temperature.
2. Consult Table 3.4 to choose the suitable magnification unit. Consult the FPIA operator's manual to install a new lens unit if necessary.
3. The prepared sample should be mixed for at least 5 minutes before starting the tests (rad/s~400).
4. Open the FPIA software and run "Background Check" to look for any particles that might be sticking inside the FPIA channels from previous measurements.
5. Run "Auto Focus" to ensure proper lens placement for optimal image clarity.
6. Create a new folder for the FPIA measurements of the day.

7. Adjust the testing parameters, such as sample name, magnification mode, RPM and sonication power to the desired values.
8. Hit the “Start Test” button of the software. It takes about 10 seconds for the door to the sample chamber to open up. Use this time to take 4 cc of the sample under mixer with a new disposable plastic pipette in a dry and clean 10 cc glass cylinder.
9. Pour the contents of the cylinder into the sample chamber.
10. After the measurement is complete, repeat from step 7 for a new test.

3.3.3. Concentric Cylinders Viscometer Tests

The procedure of testing a sample with AR-G2 rheometer is as follows:

1. Turn on the air supply to the rheometer to 30 psi.
2. Remove the bearing lock and make sure that the spindle rotates freely.
3. Turn on the instrument power switch.
4. Turn on the computer and open the control software. Check Instrument Status Page to make certain that communication has been established between the computer and the instrument.
5. Attach the Concentric Cylinders geometry to the rheometer and open the Standard Size DIN geometry file in the Geometry tab of the software.
6. Perform “Mapping” on the geometry with at least two standard iterations.
7. Perform “Zero Gap” on the geometry and then set the gap distance between the bottom of the spindle and the bottom of the cup to 10-15 μm .
8. Create a new “Procedure”. Include a “Peak Hold” step to condition the sample and two “Steady State Flow” steps: one for ramping up and the other for ramping down. Set the testing parameters according to Table 3.8. Save the procedure on the computer so it can be uploaded for future experiments.
9. For kaolinite mixtures, set the duration of “Peak Hold” step according to table 3.9.

Table 3.8 Testing parameters for AR-G2 viscosity measurements.

Step name	Peak hold step
Controlled variable	Velocity, please consult table 3.8
Duration	Please consult table 3.8
Delay time	0:00:30 hh:mm:ss
Temperature	22.0 °C
Wait for temperature	Yes
Step name	Steady state flow step 1
Start controlled variable	velocity 1.000 rad/s
End controlled variable	velocity 20.00 rad/s
Temperature	22.0 °C
Wait for temperature	Yes
Sample period	0:00:10 hh:mm:ss
Percentage tolerance	10
Consecutive within tolerance	3
Maximum point time	0:01:00 hh:mm:ss
Step name	Steady state flow step 2
Start controlled variable	velocity 20.00 rad/s
End controlled variable	velocity 1.000 rad/s
Temperature	22.0 °C
Wait for temperature	Yes
Sample period	0:00:10 hh:mm:ss
Percentage tolerance	10
Consecutive within tolerance	3
Maximum point time	0:01:00 hh:mm:ss

Table 3.9 Required conditioning time for different mixtures prior to rheological measurements.

C_k (%)	C_s (%)	pH	Conditioning time (s)	Spindle speed (rad/s)
1 – 5	0	4	120	30
7 – 10	0	4	600	40
1 – 5	0	9	60	25
7 – 10	0	9	300	30
7	10, 15, 20, 25	8	60	25

10. For mixtures of SRC sand (silica flour) and kaolinite, reduce the maximum measuring time for recording each data point from the default value of one minute to 15 seconds and condition sample by performing “Peak Hold” step for only one minute to reduce the total measurement time. This would help to minimize the error caused by sand sedimentation that occurs when the sample is loaded into the viscometer.
11. Enter sample information and save it in a new folder created for the batch of experiments run in the same day.
12. The sample should be mixing in a 200 CC beaker under the mixer (RPM = 400). Use a 24 cc Syringe and take 15 cc of sample and load it into the viscometer.
13. Run the test.
14. Once the test is complete, raise the spindle out of the cup, remove both spindle and the cup and wash them with water and soft scrub. Rinse with de-ionized water and dry with a laboratory grade paper napkin, like LintGuard Anti-Stat Polyshield Delicate Task Wipers. Make sure there is no residue left on the surfaces after wiping. Reassemble first the cup and then the spindle back on the rheometer for the next experiment.
15. Start from step 8 to perform a new test. Occasional “Mapping” of the instrument (once every three tests) is recommended (AR-G2 Operator’s Manual, 2006).

4. FPIA Performance Tests Using Suspensions Containing Kaolinite or Sand

The Sysmex FPIA-3000 is used to examine kaolinite aggregates and sand inert particles in this project. In recent literature, the FPIA has been successfully used to study particle shape and size distribution of different aqueous suspensions containing fine particles in the range of 0.5 to 40 μm in diameter (Arnold et al., 2003; Tanaka et al., 2008; and Komabayashi and Spangberg, 2008 (a, b)). However, there has not been any research reported in literature on the application of the FPIA in clay suspension analysis. There are a few limitations associated with the use of this instrument for testing sand and kaolinite suspensions. The main objectives of the initial tests are to commission the FPIA and to investigate the capabilities and limitations of the instrument for suspensions of the type used in this project.

Initial particle size analysis tests targeting the repeatability of the FPIA measurements are conducted using flocculated kaolinite-water mixtures. A flocculated kaolinite-water mixture is sampled 5 times to investigate the repeatability of the FPIA results. A second batch of this mixture is made and tested to investigate human error in mixture preparation and sampling procedures. The results of these tests are presented in Section 4.1. Next, the effect of the FPIA measuring method on the particle size and structure of samples is studied in Section 4.2. The mechanical mixing unit located in the sample chamber of the FPIA is operated between the extremes of the possible values to investigate the effect of the FPIA mixing unit settings on the measured PSD of kaolinite aggregates. The results of these tests are presented in Section 4.2.1. Concentrated samples need to be diluted in respect to the FPIA sample concentration limitations. A dispersed and a flocculated kaolinite-water mixture are tested with the FPIA at different dilution ratios to study the effect of dilution on PSD and the results are shown in Section 4.2.2. Finally, a sand-water and a sand-kaolinite-water suspension are tested with the FPIA to investigate the effect of the addition

of silica flour on the PSD of a kaolinite-water mixture. The PSD curves for the sand-water and the sand-kaolinite-water suspension are presented in Section 4.3.

The effect of mechanical mixing in the sample chamber of the FPIA on the PSD of clay suspensions is found to be negligible when the mixing unit is operated at adequately low values. Results of the FPIA measurements on the flocculated kaolinite-water suspension show that dilution has a visible effect on the PSD of flocculated kaolinite-water mixtures. It was found from the study of the relative contribution of inert fines and flocculating fines to the PSD of sand-kaolinite-water mixtures that the addition of silica flour has only a slight effect on the PSD of a kaolinite-water mixture. It will be shown in this chapter that the FPIA is an appropriate device to achieve the objective of this project to assess the kaolinite or sand water suspensions in their natural state.

Image analysis software provided with the FPIA detects the particle boundary and counts the enclosed pixels to calculate the projected area of the particle. The diameter of a circle that has an area equal to the projected area of the particle is recorded as the “CE” diameter. Statistical analysis has been performed using the Circle Equivalent (CE) diameter in this study. Results of the FPIA measurements support the use of CE diameter to represent particle sizes as clay and sand particles are shown to be fairly circular (please refer to Figures 4.4, 4.6 and 4.11).

In this study, particle size and shape parameters are presented in number based (N) distributions produced by the FPIA data processing unit. In number based (N) distributions, all particles contribute equally to the density of the distribution. The mean particle size for such distribution, signified as “CE Diameter (N) mean” in the FPIA software, is calculated using Equation 4.1:

$$\text{CE Diameter (N) mean} = D [1,0] = \frac{\sum n_i d_i}{\sum n_i} \quad \mathbf{4.1}$$

where n_i is the number of particles with diameter equal to d_i , and $\sum n_i$ gives the total number of particles in the measured volume of sample detected by the FPIA.

Circularity is used to provide a numerical representation of particle shape, where circularity is defined as the ratio of the perimeter of the projected particle image to the circumference of a circle that has an area equal to the projected area of the particle.

4.1. Repeatability of FPIA Measurements

Aggregate structures are more easily altered compared with primary kaolinite or sand particles. Therefore, initial particle size analysis tests targeting the repeatability of the FPIA results were conducted on flocculating kaolinite-water suspensions. Sample concentration limitations imposed by the FPIA do not allow one to test concentrated mixtures. A kaolinite-water mixture containing 0.007 M Ca^{+2} as flocculant was prepared for initial measurements. Kaolinite volume concentration, denoted in this text as C_k , was 0.25%. In order to raise the pH of the mixture to 11, NaOH was added to the mixture. Figure 4.1 shows an image of a kaolinite aggregate in this mixture captured by the FPIA. The ability of the FPIA to capture images of aggregates is clear.

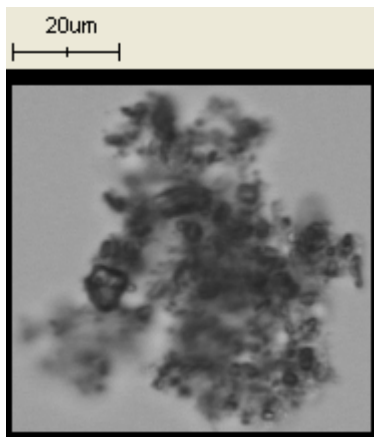


Figure 4.1 Image of a kaolinite aggregate in a kaolinite-water mixture from the FPIA. $C_k = 0.25\%$; pH 11; 0.007 M CaCl_2 .

This mixture was sampled 5 times to investigate the repeatability of the FPIA results. Particle size and shape frequency distribution graphs for these measurements are presented in Figure 4.2 and Figure 4.4, respectively. Alongside the graphs that show results for the 5 samples of this mixture, a curve for a flocculated kaolinite-water suspension ($C_k = 0.25\%$) in absence of flocculant is presented for comparison (Mixture 2). Particle size cumulative distribution results for these measurements are presented in Figure 4.3. This figure shows that although the size frequency of particles does not exceed low values of 6-7%, the distribution does add up to 100%. The obvious difference between the curves of Mixture 1 samples and Mixture 2 highlights the consistency between the results for the 5 samples of the first mixture. It should be noted that PSD results are mainly used in this study to calculate the aggregate volume fraction. It is shown in Section 5.2 that the difference between the PSD results for similar mixtures over certain size ranges does not generate considerable difference in the total volume of aggregates. Furthermore, PSD results are studied in this project from a comparative point of view, i.e. in relation to each other. Therefore, the small difference between the PSD results for the 5 samples of Mixture 1 is negligible relative to the obvious distinct PSD of Mixture 2.

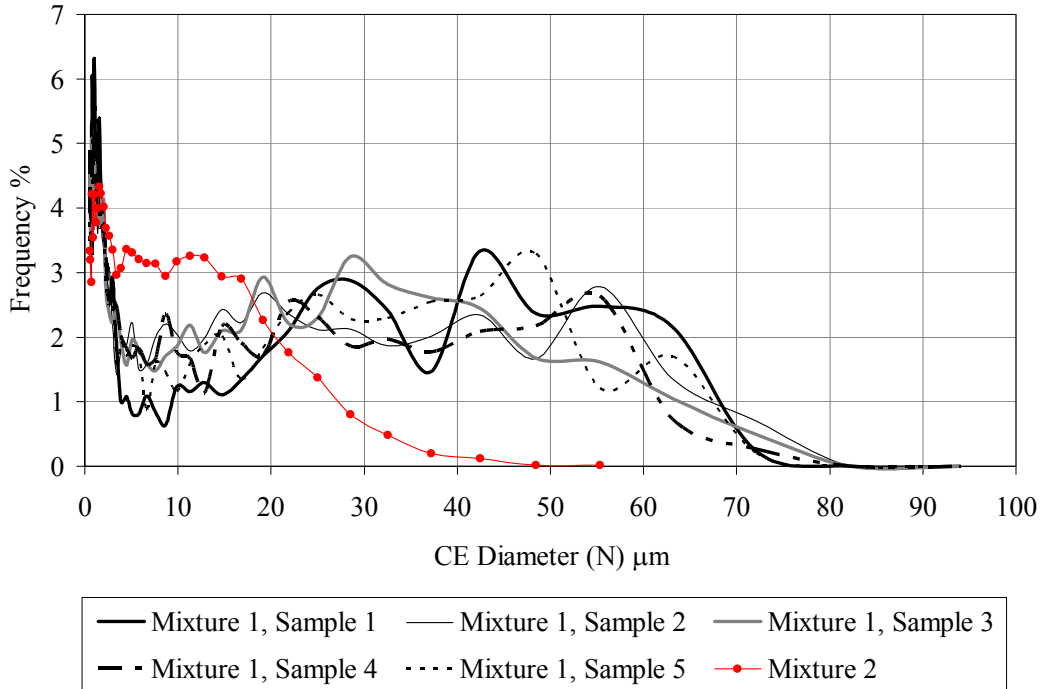


Figure 4.2 PSD results for 5 samples of a highly flocculated kaolinite-water mixture (mixture 1) alongside a PSD curve for a moderately flocculated kaolinite-water mixture (mixture 2) from the FPIA. Mixture 1: $C_k = 0.25\%$; 0.007 M CaCl_2 . Mixture 2: $C_k = 0.25\%$.

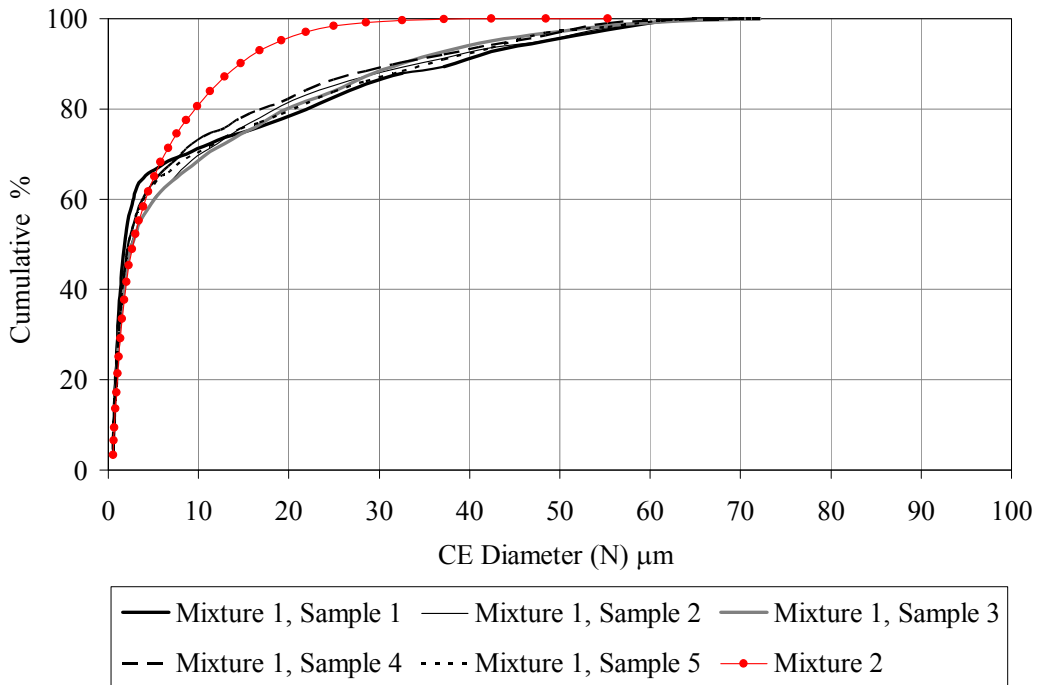


Figure 4.3 Particle size cumulative distribution results for 5 samples of a highly flocculated kaolinite-water mixture (mixture 1) alongside a cumulative distribution curve for a moderately flocculated kaolinite-water mixture (mixture 2) from the FPIA. Mixture 1: $C_k = 0.25\%$; 0.007 M CaCl_2 . Mixture 2: $C_k = 0.25\%$.

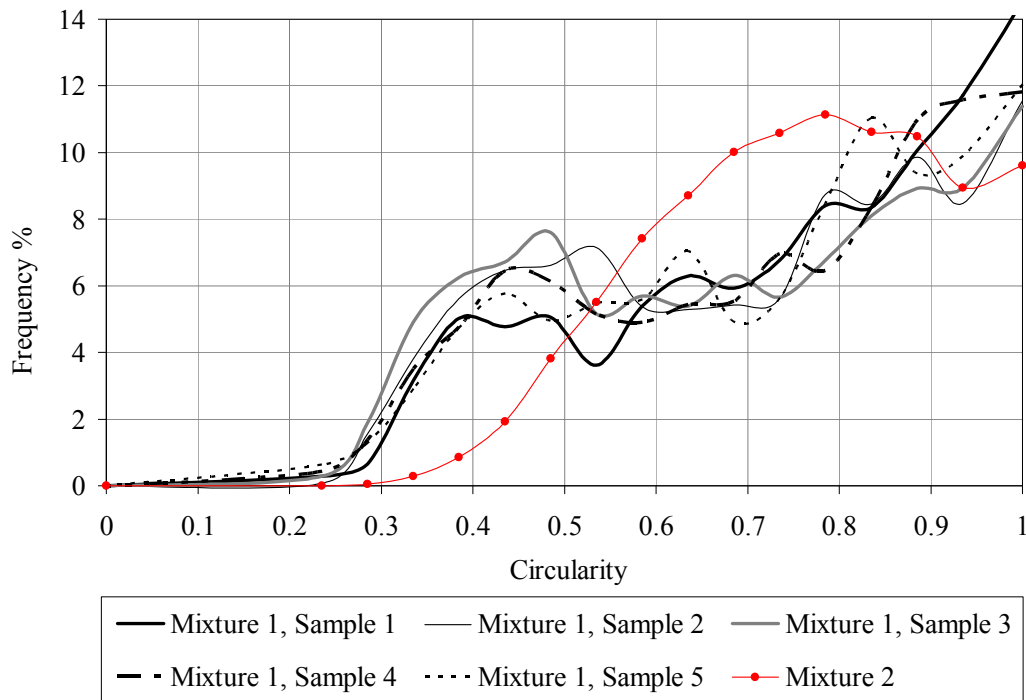


Figure 4.4 Particle shape distribution results for 5 samples of a flocculated kaolinite-water mixture from the FPIA. $C_k = 0.25\%$; 0.007 M CaCl_2 .

Another batch of the highly flocculated kaolinite-water mixture ($C_k = 0.25\%$; 0.007 M CaCl_2) was made and tested with the FPIA. The testing of two identical batches of kaolinite-water mixture allows an assessment of human error in mixture preparation and testing procedures. For comparison, a curve for a second flocculated kaolinite-water suspension ($C_k = 0.25\%$) in absence of flocculant is presented alongside size and shape distributions for the two “identical” batches. Compared with the results for the second mixture, the difference between the size and shape distribution results for the two identical batches is very small. Both systematic and human errors are in the acceptable range for the purpose of this study.

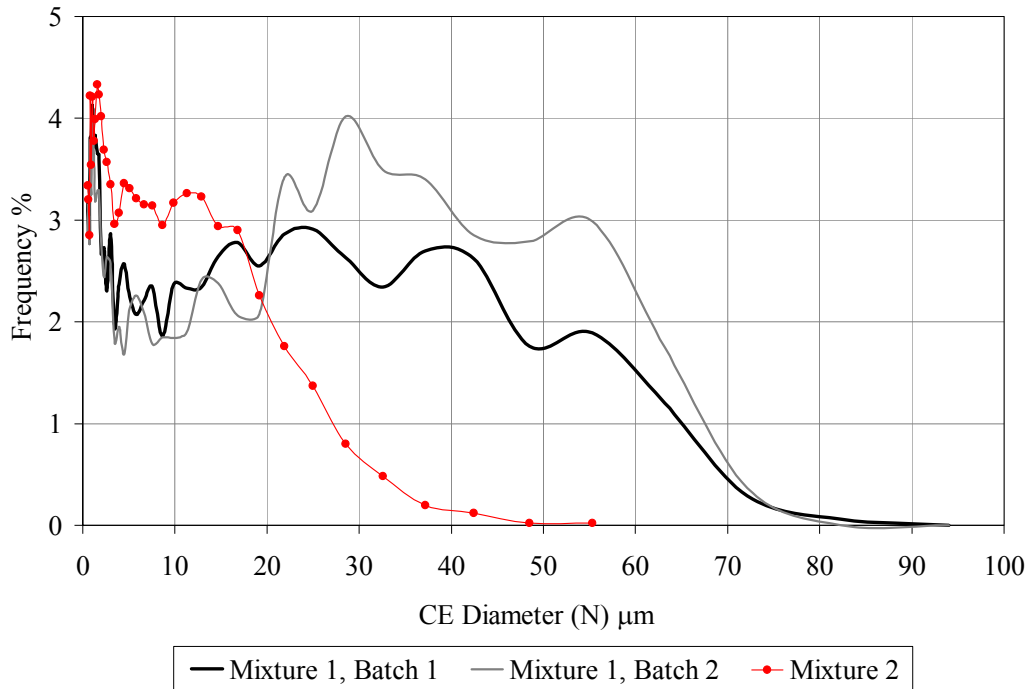


Figure 4.5 PSD results for 2 identical batches of a flocculated kaolinite-water mixture from the FPIA. $C_k = 0.25\%$; 0.007 M CaCl_2 .

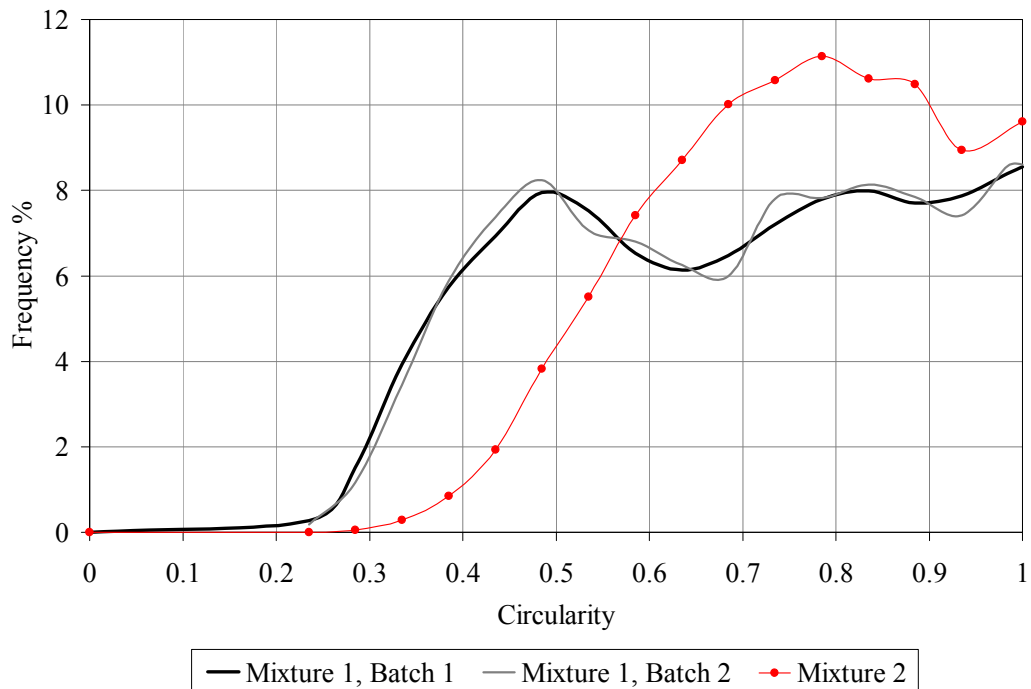


Figure 4.6 Particle shape distribution results for 2 identical batches of a flocculated kaolinite-water mixture from the FPIA. $C_k = 0.25\%$; 0.007 M CaCl_2 .

4.2. Effect of FPIA on Particle Size Distribution

It was explained in Chapter 1 that particle size measuring methods can affect the particle size and structure of samples. Sysmex FPIA-3000 also affects the particle size distribution and the shape of clay aggregates through two main mechanisms: sample dilution and sample dispersion.

4.2.1. Effect of Mixing Unit

The FPIA sample chamber is equipped with “Ultrasonic Dispersion” and “Mixing” units. Both sonication and mechanical mixing influence structure and size distribution of clay suspensions. The effect of sonication can be eliminated by turning off the sonication power. However, the mixing unit cannot be completely turned off as there is the danger of agglomerates formation if the mixing is inadequate.

The controlling parameter here is the mechanical stirring speed. Mechanical stirring speed was changed between the extremes of the possible values to investigate the effect of the agitation intensity on PSD of kaolinite aggregates. A sample of flocculated kaolinite suspension was tested at Revolutions Per Minute speed (RPM) of 50, 400 and 750. Each test was repeated 5 times and the merged PSD results of these measurements are presented in Figure 4.7. Mean particle size of the kaolinite suspension moves from 11.3 μm at 50 RPM to 10.8 μm at 400 RPM, and finally to a value of 8.5 μm at 750 RPM. It can be concluded that the effect of the FPIA mixing unit on the PSD of kaolinite aggregates is negligible when operating at 400 RPM or lower. In this project, the FPIA mixing unit was operated at 400 RPM.

4.2.2. Effect of Sample Dilution

FPIA requires the sample to be fairly dilute as the device cannot measure more than 36,000 particles in one μl of sample. Concentrated mixtures need to be

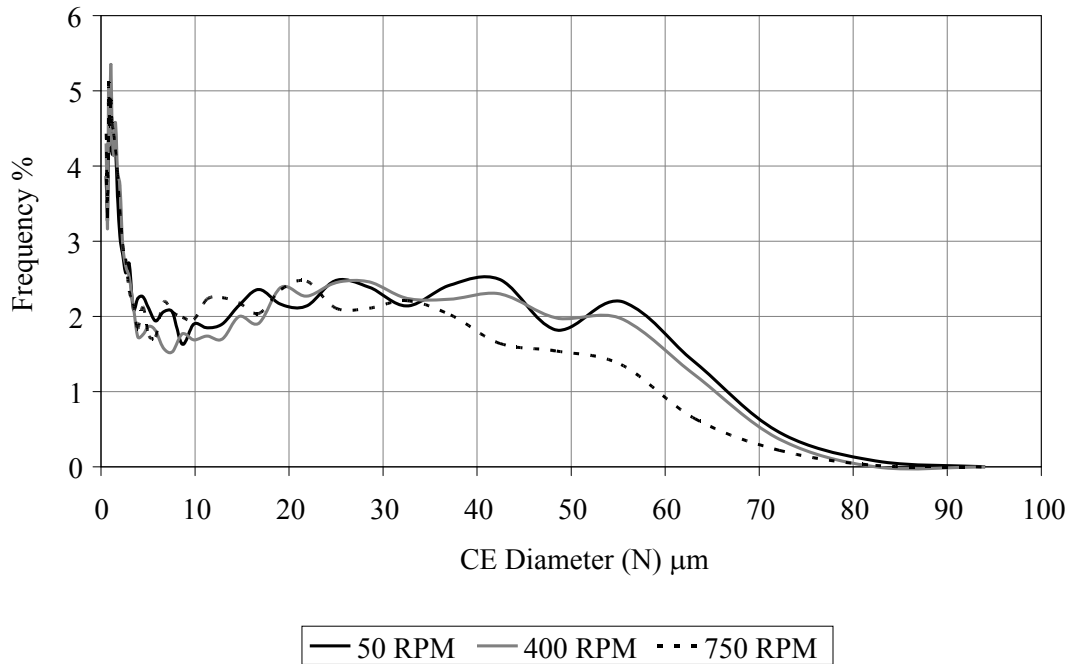


Figure 4.7 PSD results by FPIA for samples of a kaolinite-water mixture from the FPIA. $C_k = 0.25\%$; pH 11; 0.007 M CaCl_2 .

diluted prior to testing to ensure an accurate measurement. Therefore, it is necessary to study the effect of dilution on mixture PSD's. Kaolinite-water mixtures can be dispersed by addition of dispersing agents such as tetrasodium polyphosphate (TSPP). Kaolinite particles in a dispersed mixture are in the form of primary particles. Dilution is expected to have no effect on the size of primary particles in dispersed mixtures. Kaolinite particles in a flocculated mixture are in the form of flocs comprised of a number of primary particles that are attached to each other. Dilution is expected to decrease the size of flocs in flocculated mixtures. In the following measurements the effect of mixture dilution was investigated on both flocculated and dispersed suspensions.

A kaolinite-water mixture $C_k = 5\%$ in presence of dispersant was diluted 5, 10, 20 and 50 times. The size analysis results are presented in Figure 4.8. It is clear from Figure 4.8 that diluting a dispersed kaolinite sample does not affect the PSD.

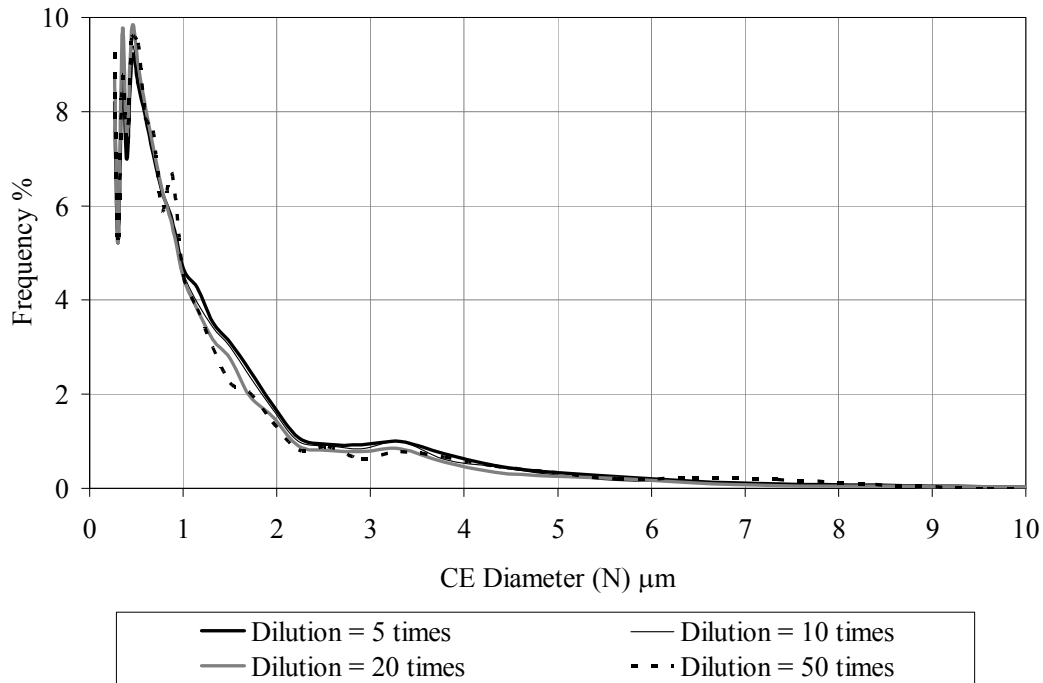


Figure 4.8 PSD results for a dispersed kaolinite-water mixture from FPIA. $C_k = 5\%$; TSPP = 0.002 wt/wt kaolinite.

Addition of dispersant breaks down kaolinite flocculated structures into the primary particles, the size of which cannot be altered by dilution.

In order to investigate the effect of dilution on a flocculated mixture, a kaolinite-water mixture ($C_k = 5\%$) at pH 4 was subjected to 50, 100, 200 and 500 times dilution. Mixture filtrate was used to dilute the flocculated mixture to preserve mixture chemistry. The pH of the resultant diluted mixtures was adjusted to the original pH of 4 by addition of HCl. Each test was repeated 2 times and the two sets of PSD results were merged to create one PSD curve for each mixture. Figure 4.9 presents PSD curves for these mixtures. It can be seen that dilution has a visible effect on the PSD of flocculated kaolinite-water mixtures. Although the chemistry of samples was kept constant, the reduced solid volume fraction causes the formation of smaller flocs. Future work must be conducted to numerically specify the effects of dilution on the PSD results generated by the FPIA.

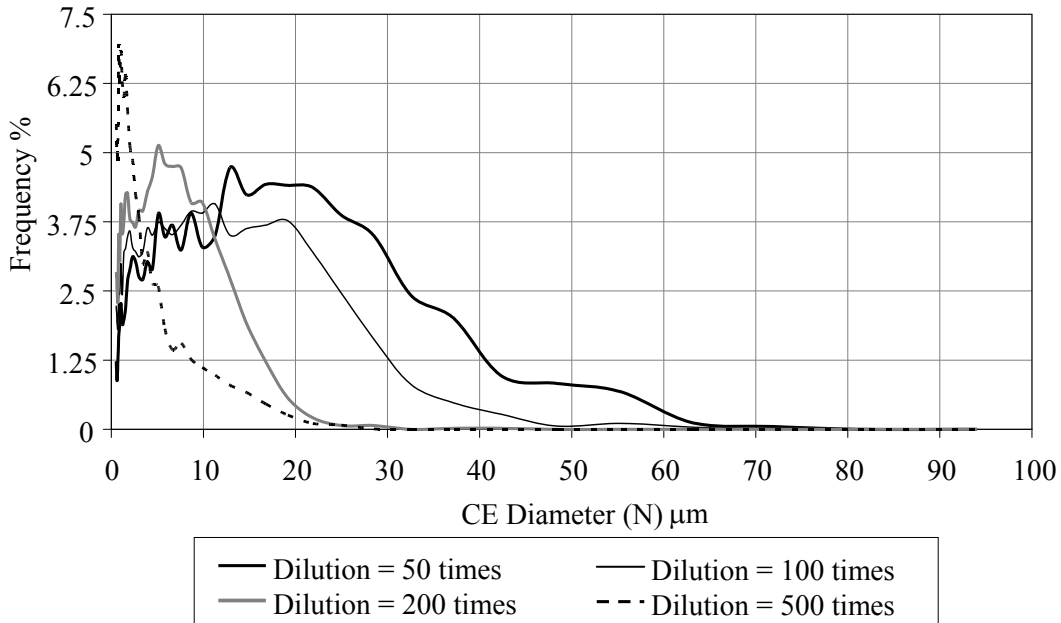


Figure 4.9 PSD results for a kaolinite-water mixture. The mixture was diluted 50, 100, 200 and 500 times. CE mean (N) diameter for each dilution is 11.35, 7.90, 4.66 and 2.57 μm , respectively. $C_k = 5\%$; pH 4.

4.3. Particle Size Distributions of Sand-Kaolinite Suspensions

In the oil sands industry, fine particles suspended in carrier fluid include clay-type and sand-type particles. Flocculating clays and inert sands have very distinct effects on the carrier fluid viscosity. Therefore, it is necessary to study the contribution of each fine type to the PSD of a mixture. In this section, the FPIA has been used to determine the PSD of kaolinite clay and silica flour particles.

Figure 4.10 shows the FPIA image of an inert silica sand particle in an aqueous mixture. A comparison between the image of a sand particle in Figure 4.10 and the image of a kaolinite aggregate in Figure 4.1 demonstrates the flocculating and inert behaviour of these two types of fines in the mixture. Figure 4.11 shows the particle shape distribution for a sand-water mixture. It can be observed that sand particles are fairly circular; therefore, the use of circular equivalent diameter for the statistical analysis of sand-water mixtures is justified.

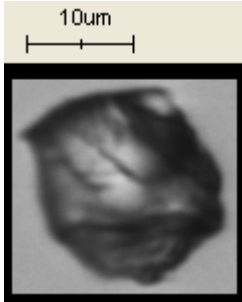


Figure 4.10 FPIA Image of a Silica sand particle in a sand-water mixture.

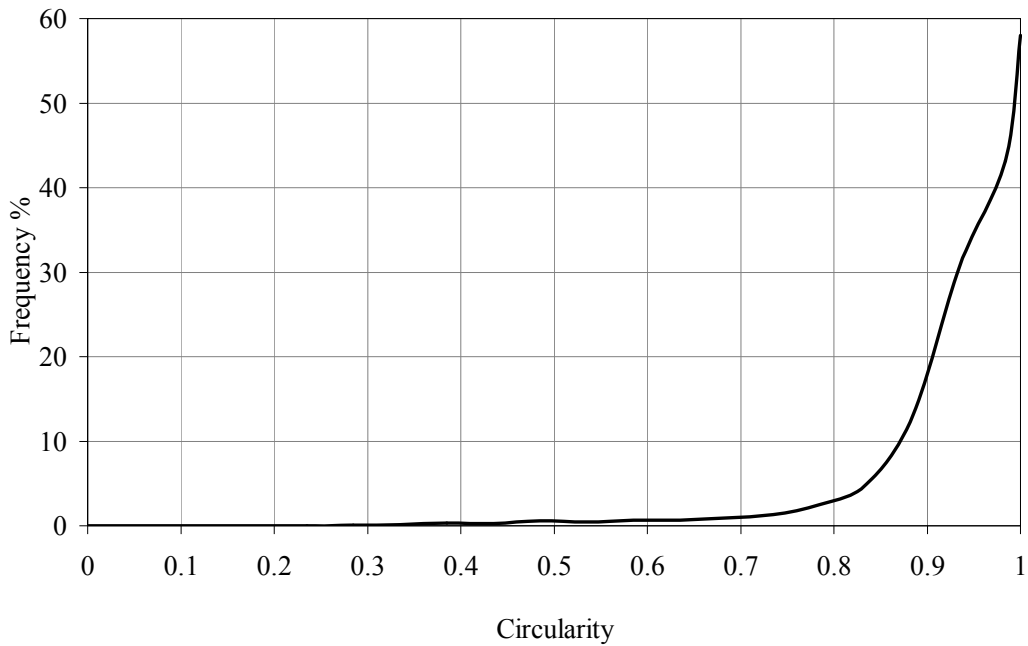


Figure 4.11 Particle shape distribution results for a sand-water mixture from the FPIA. $C_s = 1\%$.

A kaolinite-water mixture ($C_k = 1.7\%$) and a sand-kaolinite-water mixture ($C_k = 1.7\%$; $C_s = 1.7\%$) were tested with the FPIA. Figure 4.12 presents PSD curves for these measurements. Addition of fine sand introduces small non-flocculating particles to the kaolinite-water mixture. Hence, the number of fine particles in the mixture increases but the number of large particles, i.e. kaolinite aggregates, remains unchanged. It can be seen in Figure 4.12 that addition of fine sand flour to a kaolinite-water mixture moves the PSD curve towards smaller particle sizes. According to PSD curves for flocculated kaolinite-water mixture in Figure 4.9,

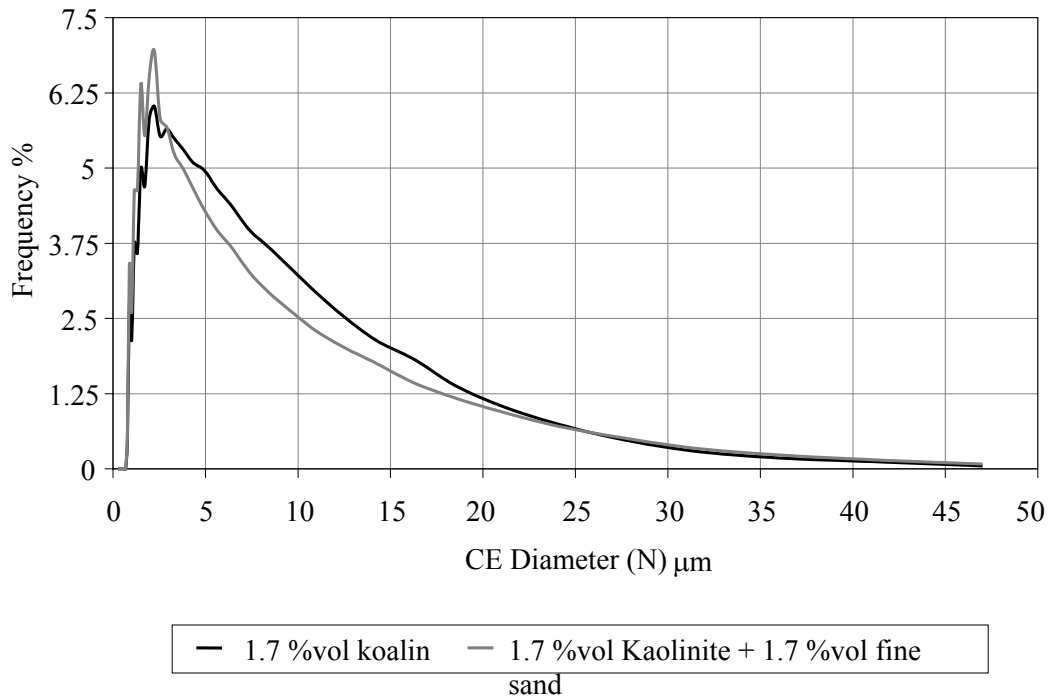


Figure 4.12 PSD results for a kaolinite-water mixture ($C_k = 1.7\%$) and a sand-kaolinite-water mixture ($C_k = 1.7\%$; $C_s = 1.7\%$) from FPIA.

particles grow larger as the solid volume fraction increases. For example, the particle mean (N) diameter increases by 40% as the solids volume fraction doubles from 0.05 to 0.1 for a flocculated kaolinite mixture in Figure 4.9. This shows that when particles sizes are measured in non-dispersed state, inert fines affect the PSD of a mixture in a very different manner compared with the flocculating particles. Addition of silica flour introduces non-flocculating fines into the PSD of the kaolinite-water mixture. The findings in this section would be utilized later in the interpretation of the rheological behaviour of sand-kaolinite-water mixtures in Section 5.5. It is expected that addition of inert sand particles contribute a small amount to the viscosity of a kaolinite-water mixture because the inert sand particles do not engage in aggregate formation.

4.4. Summary

In this chapter, the performance of the FPIA on sand or kaolinite suspensions was tested. The fact that FPIA does not break kaolinite aggregates down to primary sizes is clear from the generated images. Initial particle size analysis tests were conducted on highly-flocculated kaolinite-water suspensions. A flocculated mixture is the most sensitive of all the mixtures of interest in this study. Particle size and shape frequency distribution graphs for measurements on 5 samples of a flocculated kaolinite-water suspension and two identical batches of a flocculated kaolinite-water mixture show that systematic and human error are in the acceptable range for the purpose of this study.

Effect of the FPIA measuring method on the particle size and structure of samples was studied. It was found that the mechanical mixing that occurs in sample chamber of the FPIA slightly influences structure and size distribution of clay suspensions. However, this effect is negligible when the mixing unit is operated at an RPM less or equal to 400. Samples are required to be fairly dilute as the FPIA cannot measure more than 36,000 particles in one μl of sample. For this reason, concentrated mixtures need to be diluted prior to testing by the FPIA. Results of the FPIA measurements on non-flocculating suspensions at different degrees of dilution show that PSD of dispersed particles cannot be altered by dilution. However, it was observed that dilution has a visible effect on the PSD of flocculated kaolinite-water mixtures even when original mixture chemistry is preserved. It can be concluded that although the chemistry of samples was kept constant, the reduced solid volume fraction caused by dilution induces reformation of flocs into smaller particles. Corrections for the effect of the FPIA measurement procedure on size and structure of clay aggregates are not necessary if PSD is studied from a qualitative or a comparative point of view. In summary, the FPIA is found to be an appropriate device to assess the kaolinite or sand water suspensions in their natural state.

The different contribution of kaolinite clay and silica flour particles to the PSD of a sand-kaolinite-water mixture was studied by the FPIA in this section. A comparison between the image of a sand particle and the image of a kaolinite aggregate demonstrates the ability of the FPIA to visually describe the flocculating and inert behaviour of these two types of fines in the mixture. A kaolinite-water mixture and a sand-kaolinite-water mixture were tested with the FPIA. The PSD curves for these measurements shows that the addition of fine sand introduces only small non-flocculating particles to the kaolinite-water mixture. Therefore, the number of kaolinite aggregates does not change in this case. It can be concluded that when particles sizes are measured in non-dispersed state, inert fines affect the PSD of a mixture in a very different fashion compared with the flocculating particles. This observation will be used in Section 5.5 for interpretation of the rheological behaviour of sand-kaolinite-water mixtures. The fact that the inert sand particles do not engage in aggregate formation leads to the expectation that the addition of inert sand particles contribute a small amount to the viscosity of a kaolinite-water mixture

5. Results and Discussion

This main objective of this project includes development of a method of assessing carrier fluid viscosity that is more accurate by employing volume fraction of particle aggregates instead of primary particles. For this purpose, an analysis of the variability of volume fraction of aggregates with changes in water chemistry and component volume fraction should be available. Initially, kaolinite-water suspensions are tested by the FPIA to investigate the change in aggregate size of kaolinite at different water chemistries in this chapter. Next, aggregate volume fraction is determined for kaolinite-water mixtures at pH 4 and pH 9 using the FPIA measurement results. The volume fractions of aggregates would be utilized in Section 5.4 towards a relative study of the viscosity of kaolinite-water mixtures at pH 4 and pH 9.

The AR-G2 rheometer is used in this study to measure the viscosity of kaolinite-water and sand-kaolinite water suspensions. Measurement results for the viscosity of kaolinite-water suspensions at pH 4 and pH 9 is presented in Section 5.3. Kaolinite-water mixtures at pH 4 and pH 9 are shown to have distinguished rheological behaviour. This difference in rheological behaviour is related to the different values of aggregate concentration for these two types of mixtures. The relative volume fraction of aggregates at pH 4 and pH 9 is used to interpret the relative viscosity values for kaolinite-water mixtures. Viscosity data for kaolinite-water mixtures at pH 4 and pH 9 are plotted against aggregates volume fraction in Section 5.4. It is shown in Section 5.4 that the viscosity data for these two types of mixtures fall on the same trend line when they are plotted against aggregate volume fraction rather than solid volume fraction.

In the oil sands industry, the viscosity of carrier fluid is correlated to the volume fraction of total “fines”, neglecting the different effects of the clay-type and sand-type fines present in the suspensions. The findings presented in Chapter 4 indicate that addition of inert sand particles does not affect aggregate concentration in a

sand-kaolinite-water mixture. Hence, it is expected that the viscosity of a kaolinite-water mixture would not be significantly affected by the addition of silica flour. In Section 5.5, sand-kaolinite-water suspensions are tested with the AR-G2 rheometer in order to investigate the different effects of sands and clays on the viscosity of the mixture. A kaolinite-water mixture ($C_k = 7\%$) is used as the dispersing medium to prepare sand-kaolinite-water mixtures at volume concentrations of 10%, 15%, 20% and 25%. The viscosity data for the sand-kaolinite-water suspensions are presented alongside those for the kaolinite-water suspension. A comparison between the change in relative viscosity with solid volume concentration for sand and kaolinite mixtures shows that flocculating particles increase the mixture viscosity more significantly for the same amount of solid concentration.

5.1. Effect of Water Chemistry on PSD of Kaolinite Suspensions

Water chemistry affects aggregate structures by governing interparticle electrostatic interactions as described in Chapter 1. Measurements were conducted on kaolinite-water suspensions to investigate the change in kaolinite aggregate size for different water chemistries. Mixture characteristics are provided in Table 5.1. Mean aggregate diameter obtained from the FPIA measurements are presented in Table 5.2. Particle size distribution curves for Mixture 1, 2, 3 and 4 are presented in Figures 5.1. It can be seen in Figure 5.1 that the degree of flocculation increases from Mixture 1 to Mixture 4.

Kaolinite particles are charged as they are dispersed in aqueous suspensions. Addition of negatively charged dispersing agents to kaolinite suspensions alters the particle surface charge (Papo et al., 2002). Entirely repulsive electrostatic forces between negatively charged edges and faces are dominant over attractive Van der Waals forces and particles deflocculate. It can be seen that the mean particle diameter for dispersed suspensions (e.g. Mixture 1) is very small and near

Table 5.1 Compositions of mixtures for FPIA measurements on the effect of water chemistry for kaolinite suspensions.

Mixture	C _k (%)	pH	TSPP (wt/wt kaolinite)	Ca ²⁺ (M)
1	0.025	11	0.002	0
2	0.25	6	0	0
3	0.25	4.5	0	0
4	0.25	11	0	0.007

Table 5.2 Results of FPIA measurements on the effect of water chemistry for kaolinite suspensions.

Mixture	CE diameter (N) mean (μm)
1	1.46
2	2.42
3	5.88
4	14.34

the diameter of primary kaolinite particles. Figure 5.2 presents the FPIA images of dispersed kaolinite particles in Mixture 1. Kaolinite primary particles flocculate in Mixture 2, in the absence of dispersant and at a decreased pH value of 6. Each formed structure is counted as one particle entity by the FPIA. Mean particle size increases from Mixture 1 to Mixture 2 as kaolinite primary particles attach to each other and form larger particles. These flocculated structures can be viewed in Figure 5.3. As pH is decreased further to a value of 4, electrostatic attraction between positively charged edges and negatively charged faces of kaolinite particles in Mixture 3 causes the formation of large structures. Note that for the same amount of solids, the mean particle size is larger for Mixture 3 compared with Mixture 2. Figure 5.4 shows the expanded flocculated structures of kaolinite particles in Mixture 3. Addition of exchangeable cations such as Ca²⁺ to kaolinite suspensions increases the degree of flocculation. The absorption of Ca²⁺ on

isomorphous substitution sites on T faces of kaolinite gives rise to attractive electrostatic interactions. In Mixture 4, highly expanded structures form as large numbers of primary particles attach to each other to form aggregates. The images of these large aggregates in Mixture 4 are presented in Figure 5.5.

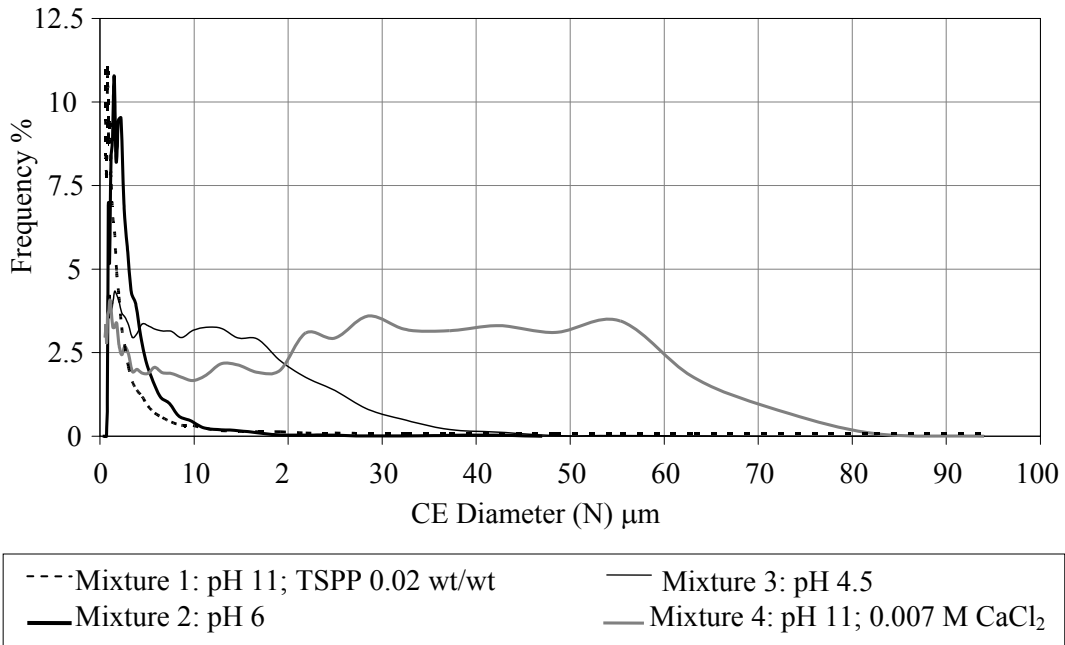


Figure 5.1 PSD results for 4 kaolinite-water mixtures from FPIA at different water chemistries. $C_k = 0.25\%$.

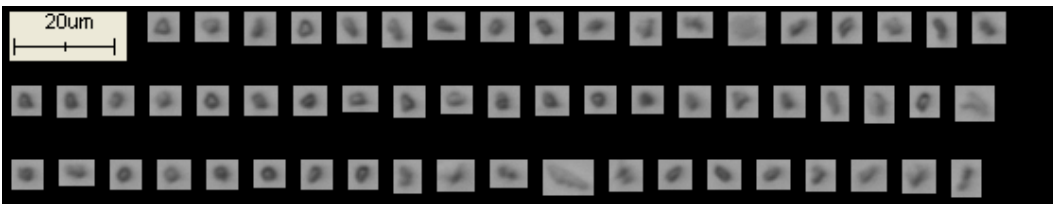


Figure 5.2 FPIA Images of a kaolinite-water mixture from the FPIA. $C_k = 0.25\%$; pH 11; TSPP = 0.02 wt/wt kaolinite.

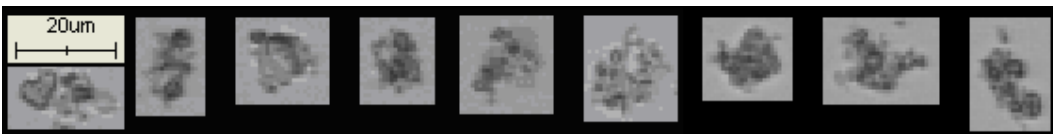


Figure 5.3 FPIA Images of small kaolinite aggregates in a kaolinite-water mixture from the FPIA. $C_k = 0.25\%$; pH 6.

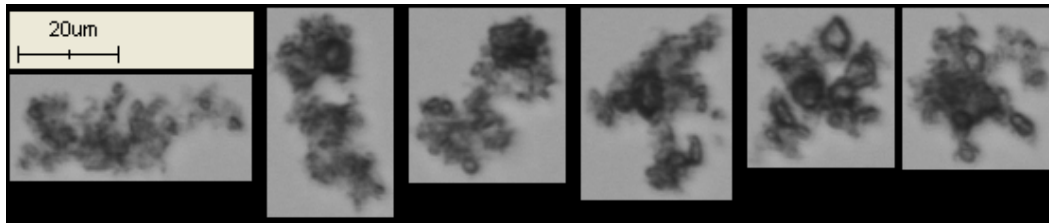


Figure 5.4 FPIA Images of kaolinite aggregates in a kaolinite-water mixture from the FPIA. $C_k = 0.25\%$; pH 5.

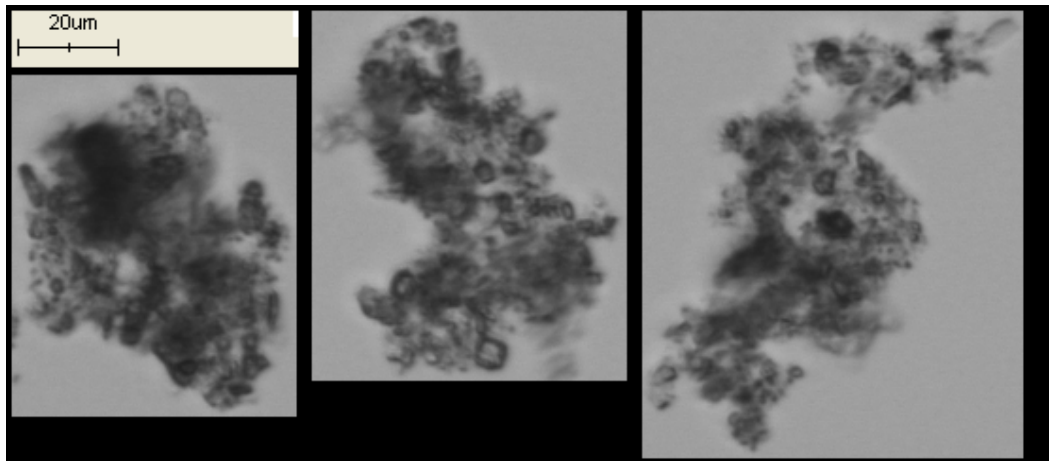


Figure 5.5 FPIA Images of large kaolinite aggregates in a kaolinite-water mixture from the FPIA. $C_k = 0.25\%$; pH 11; 0.007 M CaCl_2 .

A close examination of Table 5.2 reveals that for the same solids concentration, highly flocculated Mixture 4 contains particle entities nearly 6 times larger than poorly flocculated Mixture 2. These observations on the trend of the change in kaolinite aggregate size with suspension chemistry agree with extensive investigations published by Michaels and Bolger (1962) (b), Melton and Rand (1977) (a, b, c), James and Williams (1982), Ohtsubo and Ibaraki (1991), and Litzenger and Sumner (2004). However, very few values have been recorded for kaolinite aggregate size in literature. Michaels and Bolger (1962) (b) report mean diameters of 203, 122 and 99 μm for aggregates in kaolinite-water suspensions at pH 4, 6 and 9, respectively. However, comparison between these values and the FPIA particle size results is avoided because Michaels and Bolger (1962) (b) study different samples of kaolinite-water suspension ($C_k = 0.7\%$). Moreover, their diameter values represent a volume average which is highly skewed to the largest particle sizes as the results are based on the sedimentation

technique. It is difficult to obtain volume-based sizes from two-dimensional images produced by the FPIA.

5.2. Determination of Aggregates Volume Fractions Using FPIA Measurements

Aggregates are void structures that entrain a portion of the dispersing medium. Hence, the volume fraction of aggregated particles in a sample is larger than that of dispersed particles for the similar amount of solids (see Figure 1.13). The volume fraction of aggregates depends on the amount of total solids present in the mixture as well as the degree and structure of flocculation. Consider kaolinite primary particles as Lego bricks. Lego bricks can be connected in many ways to construct different structures. Figure 5.6 depicts loose bricks and two structures constructed by different assemblies of these bricks. The space occupied by the void Structure 3 (space enclosed inside the dashed line) counts to 30 squares. The space occupied by the compact Structure 2 counts to 22 squares. If the constructed structure is taken apart into loose bricks, the occupied space counts to 18 squares. Therefore, in spite of containing the same number of bricks, the space occupied by Structure 2 is the largest.

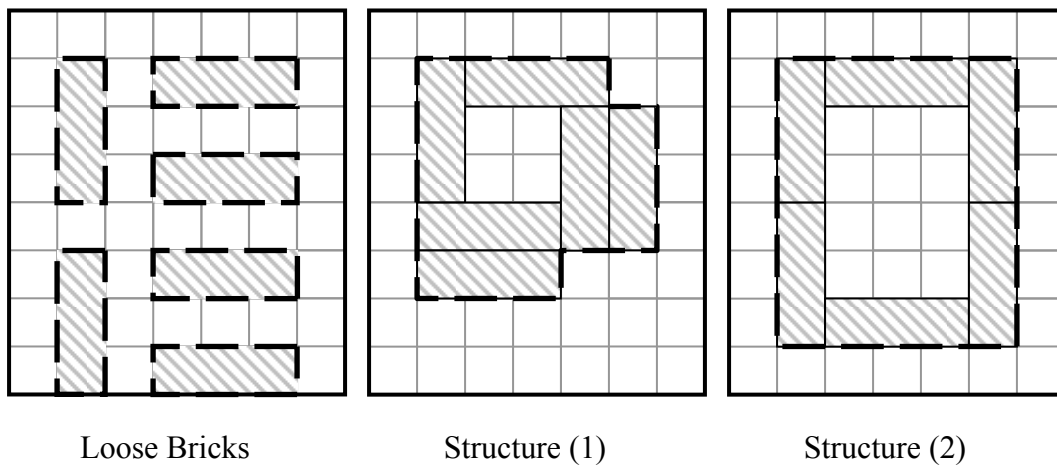


Figure 5.6 Loose bricks and two possible assemblies of the bricks.

If the kaolinite primary particles are Lego bricks, then the brain behind the final structure is particle interaction. Water chemistry affects kaolinite particle interactions. Space occupied by particle structures changes when the water chemistry changes. Therefore, volume fraction of structures depends on the chemistry of the mixture.

Relative volume fractions of aggregates were compared for kaolinite-water mixtures containing a fixed amount of solids at different water chemistries. Mixtures at pH 4 and pH 9 were studied using the FPIA. Tests were conducted on samples with kaolinite volume concentrations of 0.03% and 0.07%. Particle size distribution curves for these measurements are presented in Figures 5.7. It can be observed in Figure 5.7 that kaolinite-water mixtures at pH 4 contain larger aggregates compared with the poorly-flocculated kaolinite-water mixtures at pH 9. Particle shape distribution curves for these tests are presented in Figures 5.8.

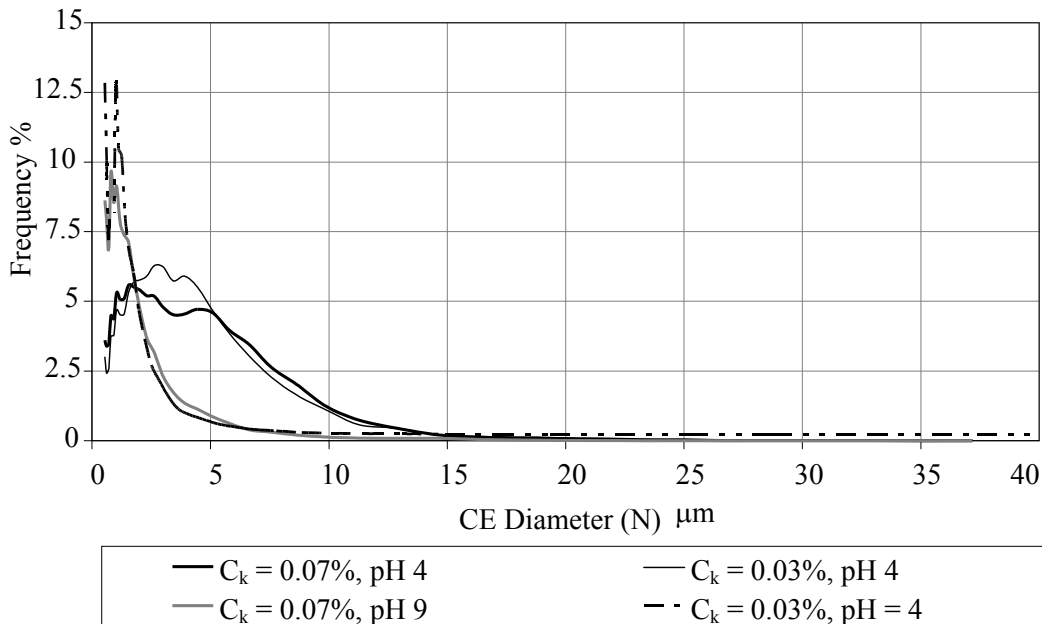


Figure 5.7 PSD results for kaolinite-water mixtures from the FPIA at different water chemistries.

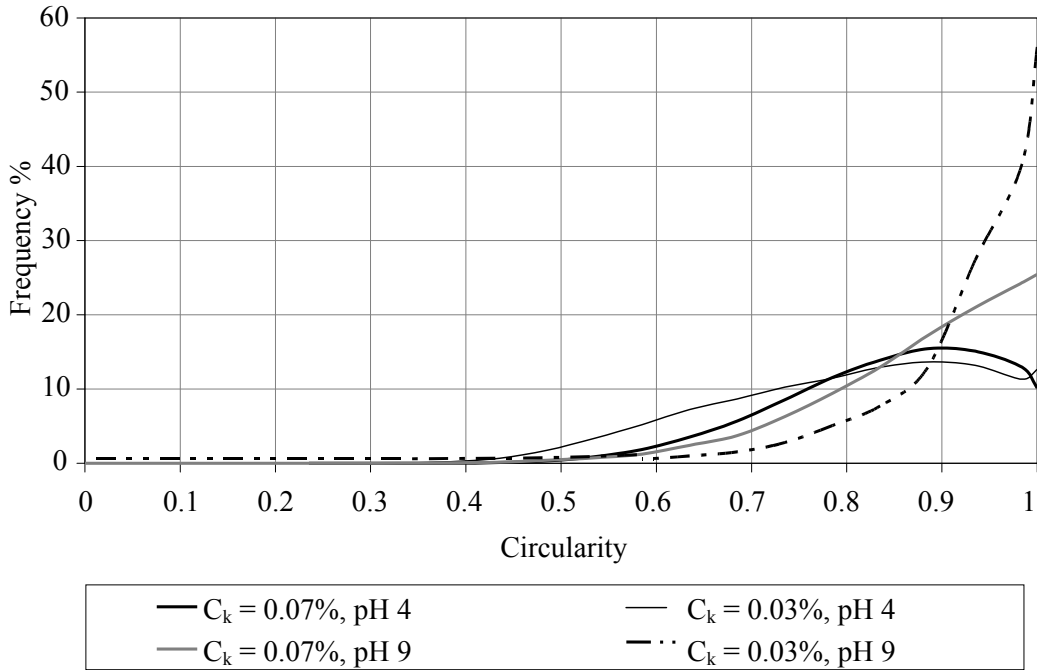


Figure 5.8 Particle shape distribution results for kaolinite-water mixtures at different water chemistries.

It is necessary to determine the volume of each aggregated structure to calculate the total volume fraction of aggregates in the mixture. The volume of each aggregate can be estimated using circular equivalent diameter if aggregates are assumed to be spheres. Particle shape distribution curves in Figure 5.8 reach their maximum values at circularity of 0.9 to 1. Statistical analysis of these curves shows that the mean (N) circularity of particles in these tests is in the range of 0.80 to 0.92. Although it is not possible to measure the sphericity of particles by the FPIA, it can be inferred from the FPIA particle shape analysis results that the projected images of particles in these mixtures are reasonably circular. Kaolinite-water samples are prepared by mixing water and kaolinite in a blender. Therefore, aggregates in the samples are formed under high shear conditions. When exposed to shear for sufficient amount of time, sharp edges of aggregates are smoothed out and aggregates become more spherical. It is assumed here that these aggregates have a certain amount of structural strength and are able to retain their shape though the duration of viscosity measurement. Microscope observation of a sedimentation column by Michaels and Bolger (1962) (a) showed that kaolinite

aggregates settled in roughly spherical shape for dilute suspensions at C_k values below 0.7%.

Hence, it is reasonable to assume that aggregates have a rather spherical shape. Therefore, circular equivalent diameter of each particle can be used to estimate the volume of that particle. Total volume fraction of aggregates in the mixture can be calculated by adding the volume of all detected aggregates. Total volume of particles (V_T) can be calculated from Equation 5.1:

$$V_T = \sum n_i \left(\frac{1}{6} \pi d_i^3 \right) \quad 5.1$$

where n_i is the number of particles with a diameter equal to d_i . For flocculated suspensions, Equation 5.1 gives the total volume of aggregates in the sample. Volume fractions of aggregates would be used in the following sections describing the results of the viscosity measurements conducted for different kaolinite-water mixtures. The absolute value for aggregate volume fractions is not of interest in this work. Here, only the relation between the volume fractions of aggregates at different mixture chemistries is studied. Therefore, a point of reference for calculating the relative volume fraction of aggregates is needed.

Measurements made with a Malvern Mastersizer by Vaezi et al. (2011) shows the mean size of primary particles for the same type of kaolinite used in this project is about 0.64 μm . This means that a large portion of kaolinite particles in dispersed form cannot be measured with the FPIA. Kaolinite particles at pH 9 flocculate slightly and grow large enough to be detected by the FPIA without forming porous structures. Here, the only attractive force is the Van der Waals attraction which causes kaolinite particles to attach to each other mainly face to face. At such conditions, kaolinite particles form small, dense aggregates with card-pack structures that does not immobilize significant amount of the dispersing medium. Hence, it is assumed that volume fraction of aggregates at pH 9 is equal to the

volume fraction of solids. Therefore, mixtures at pH 9, instead of dispersed mixtures, were chosen as a point of reference for calculating the relative volume fraction of aggregates.

Consider a kaolinite-water mixture at two different water chemistries: pH 4 and pH 9. The ratio of volume fraction of aggregates in the mixture at pH 4 to that of the mixture at pH 9 can be calculated from the total volume of aggregates in these two mixtures using Equation 5.2:

$$\lambda = \frac{C_{A,pH4}}{C_{A,pH9}} = \frac{V_{T,pH4}}{V_{T,pH9}} \quad 5.2$$

where $V_{T,pH4}$ and $V_{T,pH9}$ are the total volume of aggregates in the mixture at pH 4 and the mixture at pH 9, respectively. λ is the ratio of volume fraction of aggregates in the two mixtures. Values for λ were calculated from the FPIA results of kaolinite-water mixtures at pH 4 and 9 and are presented in Table 5.3.

Table 5.3 Volume calculations for aggregates using FPIA results for kaolinite-water mixtures.

C_k (%)	Sample	pH	$V_T \times 10^{-13} (\mu\text{m})^3$	λ
0.028	1	4	5.59	3.00
		9	1.86	
	2	4	6.81	3.44
		9	1.98	
0.07	1	4	18.24	3.17
		9	5.76	
	2	4	15.53	2.86
		9	5.44	

It can be concluded from Table 5.3 that for the same total solids in the mixture, the volume fraction of aggregates in a kaolinite-water mixture at pH 4 is, on average, 3.11 times larger than that of mixtures at pH 9.

5.3. Rheological Characterization of Kaolinite Suspensions

5.3.1. Repeatability of AR-G2 Measurements

In order to determine the repeatability of AR-G2 measurements, A kaolinite-water mixture ($C_k = 3.5\%$) at pH 4 was sampled twice. For each sample, torque response was recorded as spindle speed was increased to the end point (ramp up), and as it was decreased to the starting value (ramp down). Figure 5.9 provides the data obtained from these four measurements. It can be seen that there is no significant difference between the results of these tests, which demonstrates reproducibility of AR-G2 results.

Human error associated with preparation and sampling for viscosity measurements was also investigated. Four identical batches of kaolinite-water mixtures ($C_k = 7\%$) at pH 4 were tested. This concentration has been chosen as it was observed that mixture preparation was more prone to error for flocculated suspensions with large solid concentrations. Figure 5.10 provides the torque response data for these four mixtures. It can be seen that the difference between the behaviours of these four batches is very small. As both systematic and human errors are shown to be negligible, the results of one run conducted for each mixture have been included in this work.

5.3.2. Rheological Behaviour of Kaolinite Suspensions at pH 4 and pH 9

Rheological behaviour of kaolinite-water mixtures at pH 9 and pH 4 are tested. Each mixture received a conditioning step at which it was sheared at a constant spindle speed for a certain amount of time following the specifications given in Table 3.9.

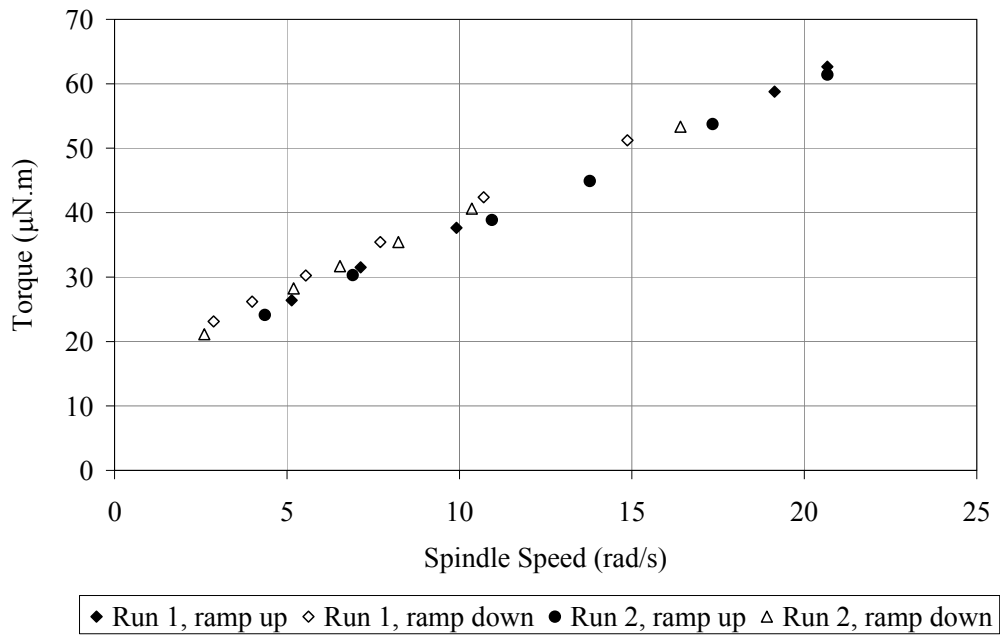


Figure 5.9 Torque response data for two samples of a kaolin-water mixture. $C_k = 3.5\%$; pH 4.

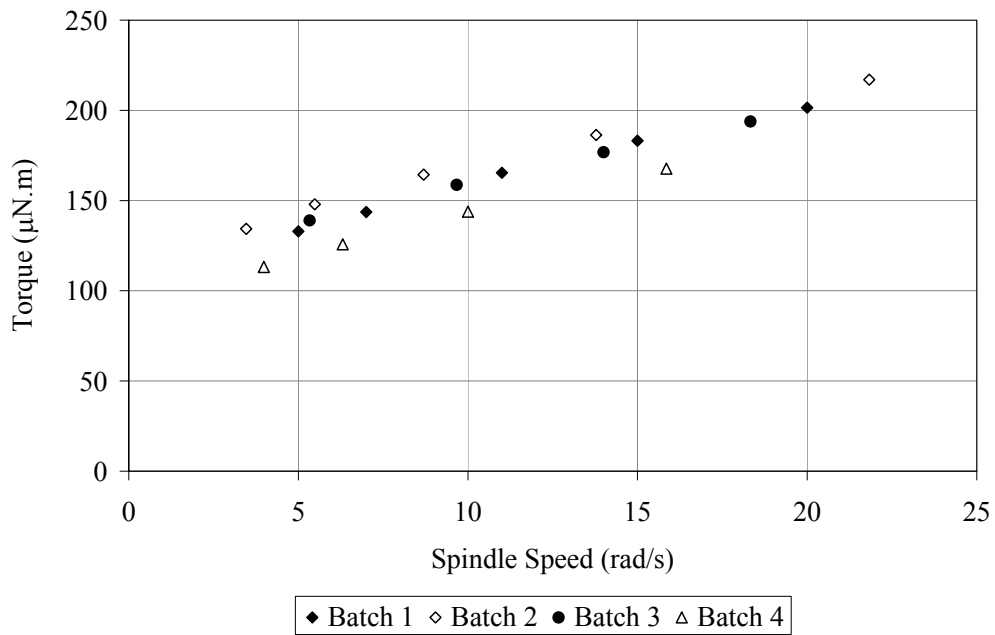


Figure 5.10 Torque response data for 4 identical batches of a kaolin-water mixture. $C_k = 7\%$; pH 4.

Mixtures with $C_k = 10\%$ are the most concentrated ones that were studied in this work. Figure 5.11 presents torque response for the conditioning step performed at

a spindle speed of 30 rad/s on a kaolinite-water mixture ($C_k = 10\%$) at pH 9. Spindle speed is denoted in the figure caption as ω . It can be seen in Figure 5.11 that torque response remains constant with time after 60 seconds of shearing for this mixture. This shows that mixture has received sufficient conditioning.

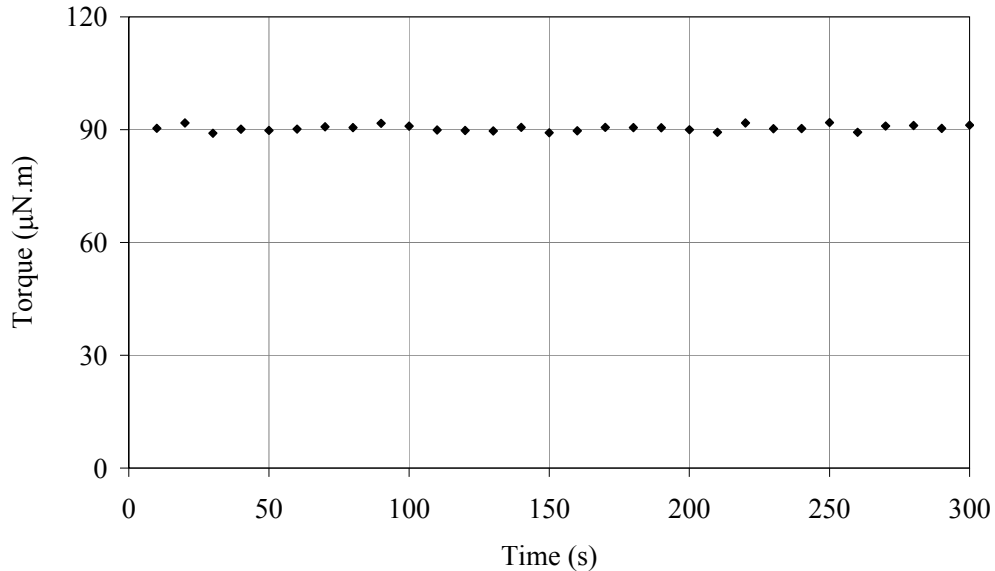


Figure 5.11 Torque response data for conditioning a kaolinite-water mixture. $C_k = 10\%$; $\omega = 30$ rad/s; pH 9.

After the conditioning step is performed successfully, torque response is recorded as the spindle speed is increased in discrete steps (ramp up). At each step, the spindle speed does not vary with time during the measurement time at which one data point for torque value is recorded. Torque response for each data point must become constant with time during the measurement time for that data point to be valid. Figure 5.12 shows torque response for the accepted data points for this measurement. The value at which the torque remains constant is taken as a torque data point and is plotted against the spindle speed value at which it was obtained. Torque response is also recorded as the spindle speed is decreased in discrete steps (ramp down) immediately after the ramp up step is performed. Figure 5.13 presents torque data points plotted against spindle speed for the ramp up and ramp

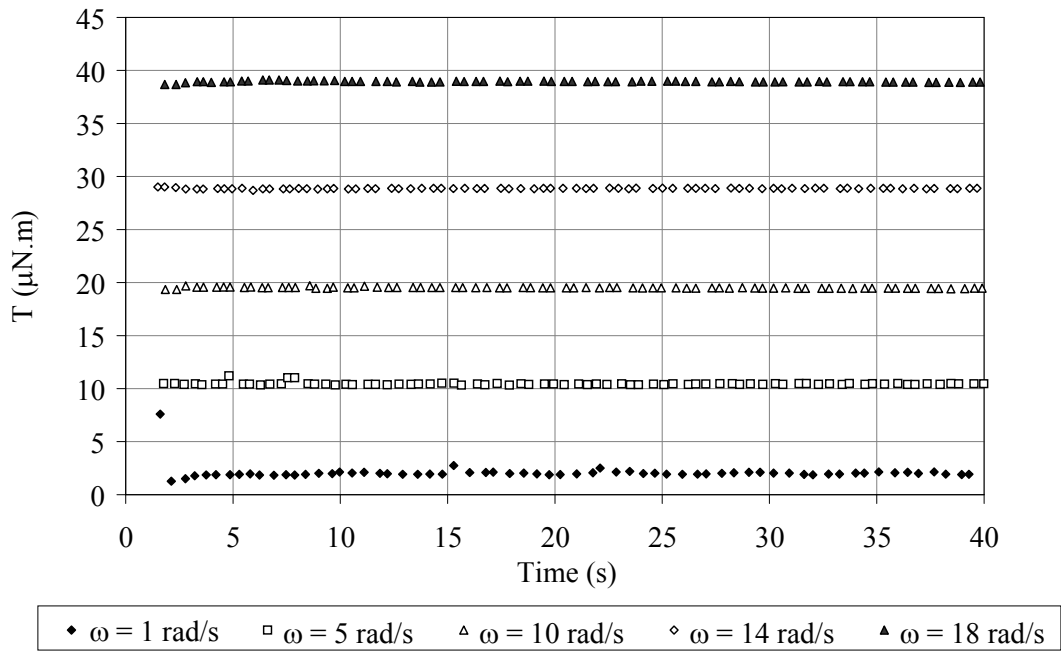


Figure 5.12 Torque response data for the recording of 5 data for a kaolinite-water mixture. $C_k = 10\%$; pH 9.

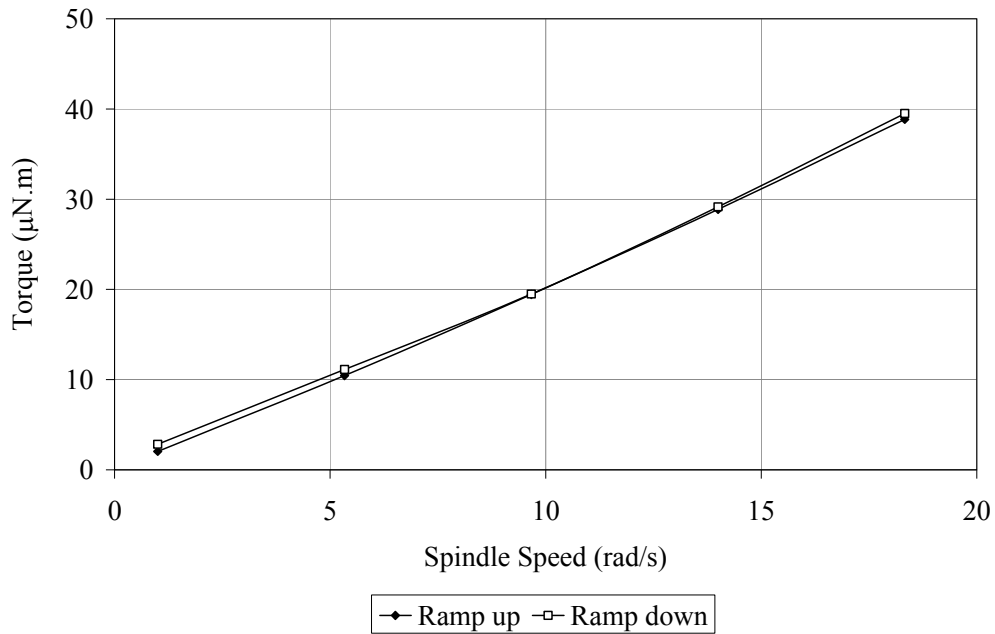


Figure 5.13 Torque response data for ramp up and ramp down steps performed on a kaolinite-water mixture. $C_k = 10\%$; pH 9.

down steps performed on a kaolinite-water mixture ($C_k = 10\%$) at pH 9. It can be observed in Figure 5.13 that the results for ramp up and ramp down measurements are almost identical. It can be concluded that kaolinite-water mixtures at pH 9 that are studied in this work do not exhibit time-dependent flow behaviour.

Viscosity of each suspension can be calculated following Equation 3.1. For this purpose, the values of T/α are plotted against spindle speed, as shown in Figure 5.14. Note that α is the measuring system geometry factor and is calculated, using Equation 3.2, to have a value of $80.26 \times 10^{-5} \text{ m}^3$ for the AR-G2 cylindrical viscometer dimensions. Viscosity is determined from the slope of the straight line that best fits the data points. This fitted line is in the form of Equation 3.1. Standard error of the fit is calculated by the model fitting software of the AR-G2 unit, using Equation 5.3:

$$\text{Standard error} = \frac{\left[\frac{\sum (x_m - x_c)^2}{n - 2} \right]^{1/2}}{\text{Range}} \times 1000 \quad 5.3$$

where x_m is the measured value, x_c is the calculated value of x for each data point, and n is the number of data points. The range is the difference between the maximum and the minimum values of x_m . The lower standard error indicates better fit of the data. According to the AR-G2 manual, a reasonable fit gives a standard error value of less than 20.

Kaolinite-water mixtures at pH 9 with kaolinite volume concentrations of 2%, 3.5%, 5%, 7% and 10% were tested using the AR-G2 rheometer. The conditioning step was performed on each mixture following specifications in Table 3.9. Torque response was recorded as the spindle speed was increased in discrete steps (ramp up). Only data points for which torque response become constant with time during

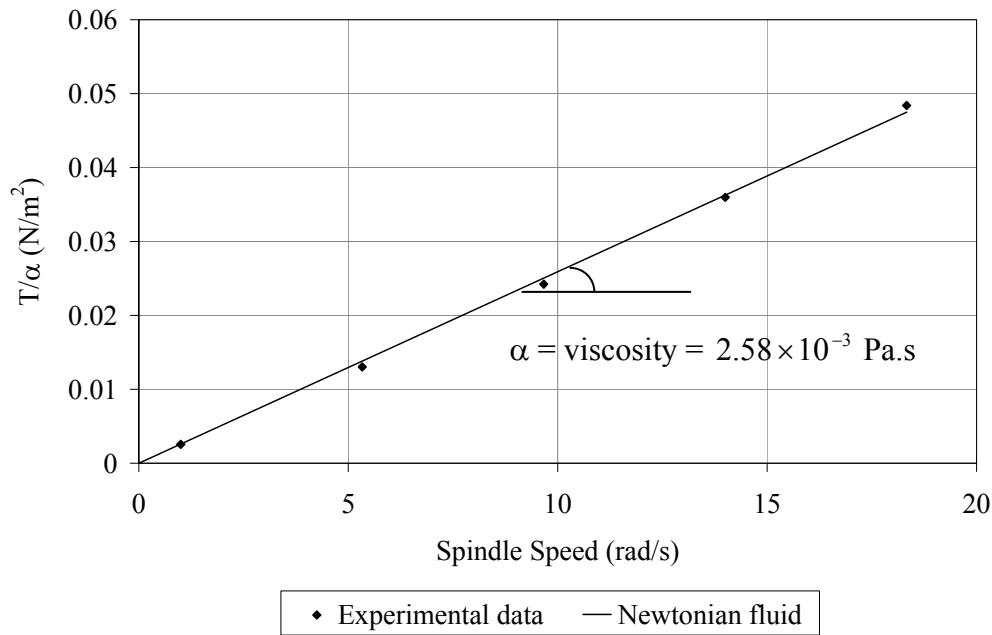


Figure 5.14 Plot of torque divided by α obtained from rheological results for a kaolinite-water mixture. $C_k = 10\%$; pH 9.

the measurement time, i.e. valid data points, were reported. Since mixtures at pH 9 have low viscosity values, there is a risk of formation of Taylor vortices (Shook and Roco, 1991) at high spindle speeds. Therefore, data points that were recorded at spindle speed values that do not satisfy Equation 3.3 were discarded. Figure 5.15 presents valid data points for rheological measurements on these samples. For these mixtures, the second term in Equation 3.1 was found to be zero. Therefore, these mixtures were characterized using the Newtonian fluid model. Table 5.4 provides the error value for the Newtonian model fitting and the calculated value for viscosity of each mixture. It can be seen in Table 5.4 that the standard error is in the acceptable range for a reasonable fit. Therefore, kaolinite-water mixtures at pH 9 that were studied in this work can be characterized by the Newtonian fluid model.

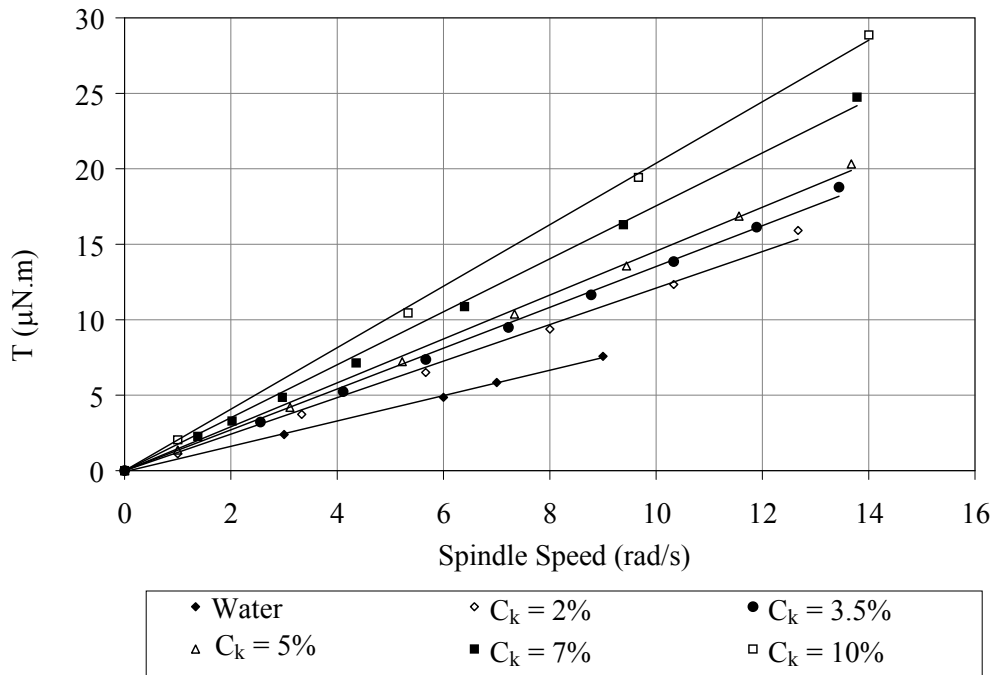


Figure 5.15 Torque response data for kaolinite-water mixtures at pH 9.

Table 5.4 Error value for the Newtonian model fitting and calculated viscosity values for kaolinite-water mixtures at pH 9.

C _k (%)	pH	Standard error	Viscosity (mPa.s)
0	9	21.41	1.02
2	9	28.13	1.49
3.5	9	19.28	1.68
5	9	22.76	1.77
7	9	18.14	2.20
10	9	18.32	2.51

Rheological measurements were repeated for kaolinite-water mixtures at pH 4. The conditioning step was performed on each mixture following the specifications set out in Table 3.9. As an example, Figure 5.16 presents torque response for conditioning step performed at a spindle speed of 40 rad/s on the concentrated kaolinite-water mixture (C_k = 10%) at pH 4. It can be seen in Figure 5.16 that the

measured torque remains constant with time after 300 seconds of shearing for this mixture. This shows that the mixture has received sufficient conditioning and is ready for the main measurement. Figure 5.17 shows torque response for the accepted data points for a steady state ramp up measurement on this mixture. It can be seen in Figure 5.17 that accepted data points are valid as the torque response for each data point becomes constant with time during the measurement.

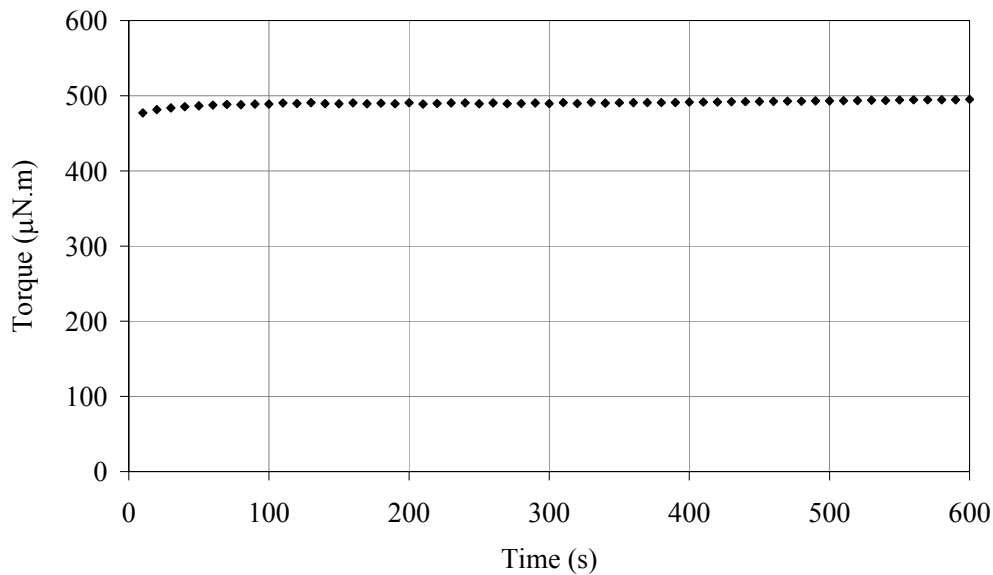


Figure 5.16 Torque response data for conditioning a kaolinite-water mixture. $\omega = 40$ rad/s; $C_k = 10\%$; pH 4.

Figure 5.18 presents torque data points plotted against spindle speed for ramp up and ramp down steps performed on a kaolinite-water mixture ($C_k = 10\%$) at pH 4. It can be observed in Figure 5.18 that the results for ramp up and ramp down measurements are very similar. It can be concluded that kaolinite-water mixtures at pH 4 that are studied in this work do not exhibit time-dependent flow behaviour. Calculation of the viscosity of this mixture from a plot of T/α against spindle speed is shown in Figure 5.19. This mixture exhibited a yield stress. Here, the Bingham fluid model is found to provide a reasonable fit for the torque - spindle speed data.

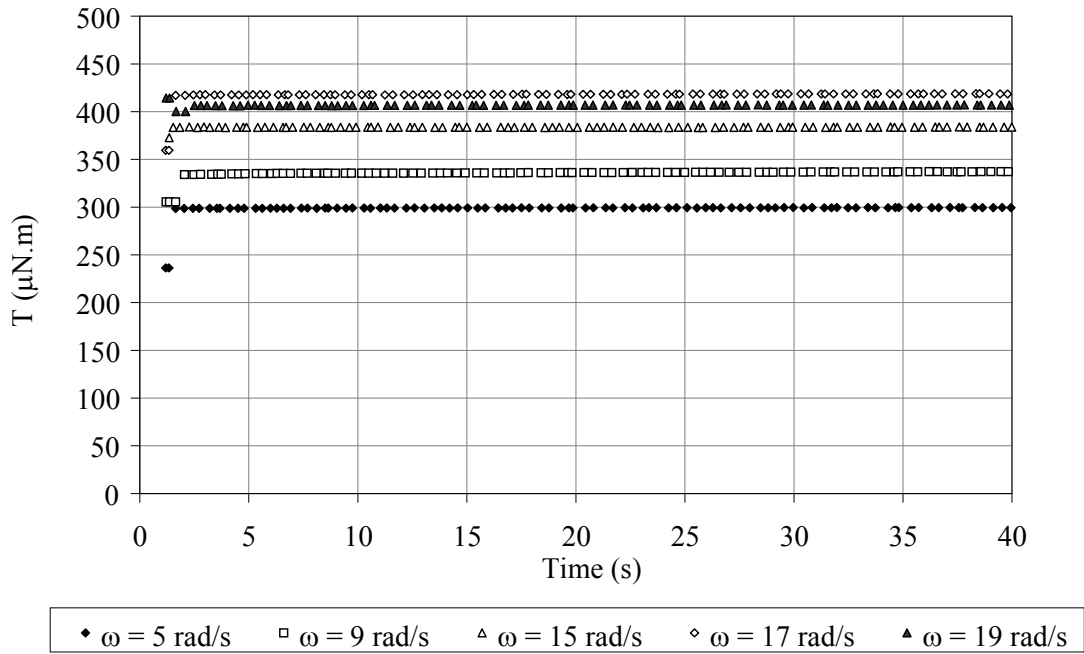


Figure 5.17 Torque response data for the recording of 5 data points for a kaolinite-water mixture. $C_k = 10\%$; pH 4.

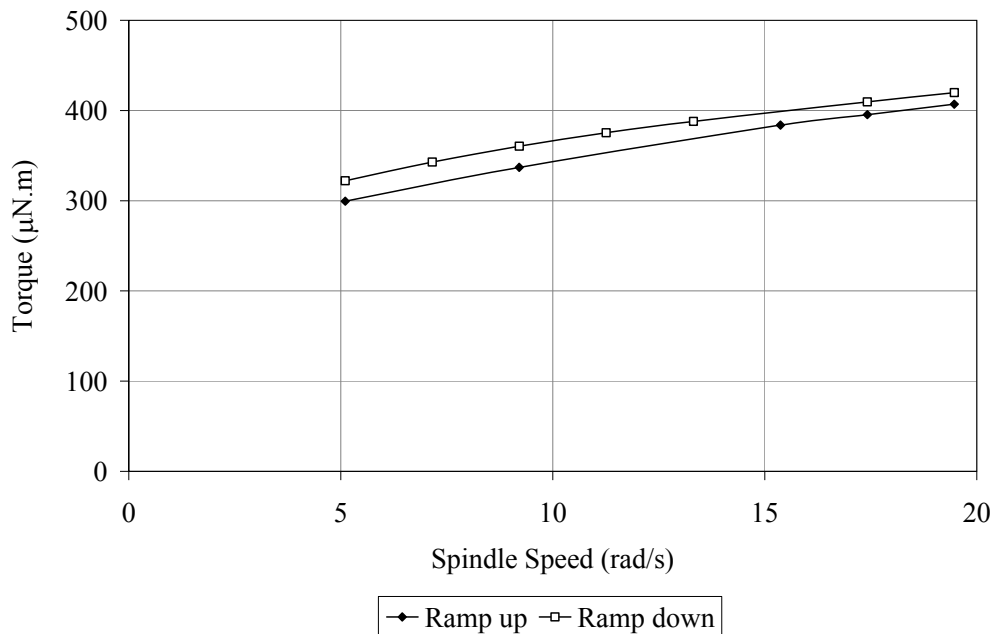


Figure 5.18 Torque response data for ramp up and ramp down steps performed on a kaolinite-water mixture. $C_k = 10\%$; pH 4.

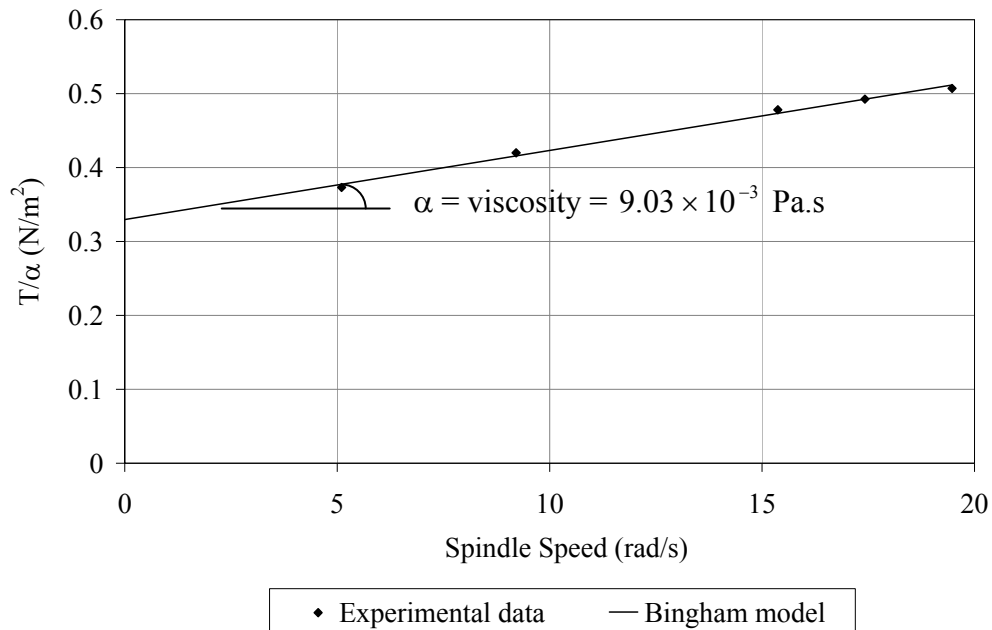


Figure 5.19 Plot of torque divided by α from rheological results for a kaolinite-water mixture. $C_k = 10\%$; pH 4.

Kaolinite-water mixtures at pH 4 with kaolinite volume concentrations of 2%, 3.5%, 5%, 7% and 10% were tested using the AR-G2 rheometer in a similar fashion. The conditioning step was performed on each mixture following specifications in Table 3.9. Torque response was recorded during ramp up steady state steps. Data points for which the torque response did not reach a constant value during the measurement time were discarded. Data points recorded at high spindle speeds that do not satisfy Equation 3.3 were discarded to prevent any errors associated with onset of Taylor vortices. Kaolinite-water mixtures at pH 4 exhibit yield stress, therefore, operating at low spindle speeds might generate errors pertaining to incomplete shearing. Hence, data points recorded at low spindle speed should satisfy the conditions specified by Equation 3.4 to be valid. Valid data points for rheological measurements on kaolinite-water mixtures at pH 4 are presented in Figure 5.20.

For these mixtures, the second term in Equation 3.1 was found to have a non-zero value. Therefore, these mixtures were characterized using the Bingham fluid

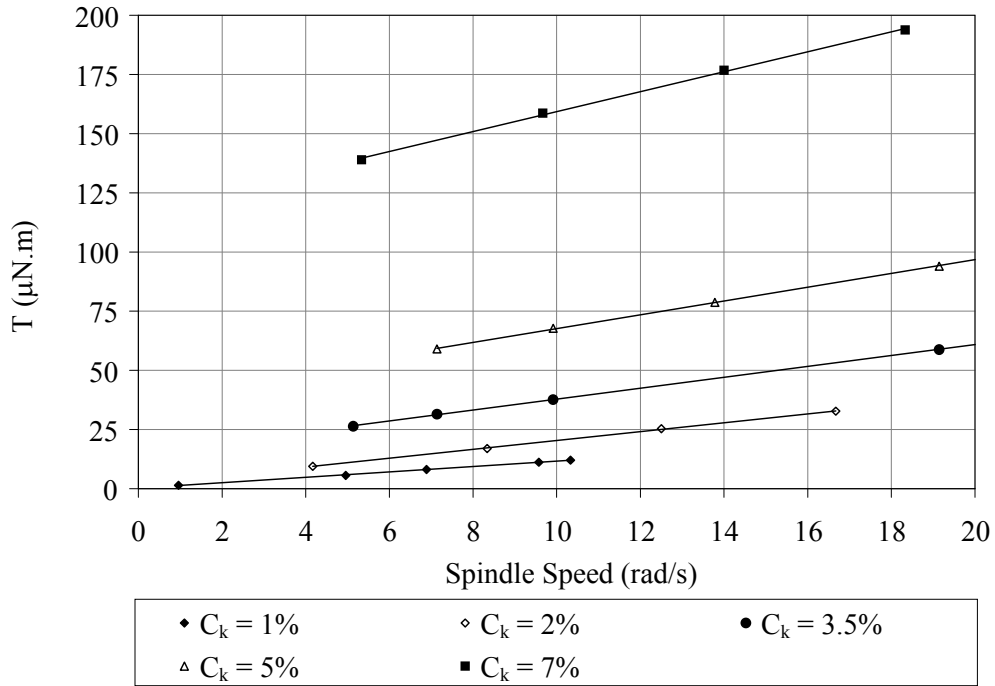


Figure 5.20 Torque response data for kaolinite-water mixtures at pH 4.

model. Table 5.5 provides the error value for the Bingham model fitting and the calculated value for viscosity of mixtures at pH 4. It can be seen in Table 5.5 that the standard error is in the acceptable range for a reasonable fit. Therefore, kaolinite-water mixtures at pH 4 that were studied in this work can be characterized by the Bingham fluid model.

Table 5.5 Error value for the Bingham model fitting and calculated viscosity values for kaolinite-water mixtures at pH 4.

C_k (%)	pH	Standard error	Viscosity (mPa.s)
0	4	21.41	1.02
1	4	14.43	1.40
2	4	8.914	2.32
3.5	4	4.009	2.88
5	4	3.435	3.64
7	4	4.885	5.25
10	4	11.02	9.03

The variation of mixture viscosity with kaolinite solid concentration at pH 4 and 9 is shown in Figure 5.21. The distinct rheological behaviour of mixtures at high and low pH values can be observed in this figure.

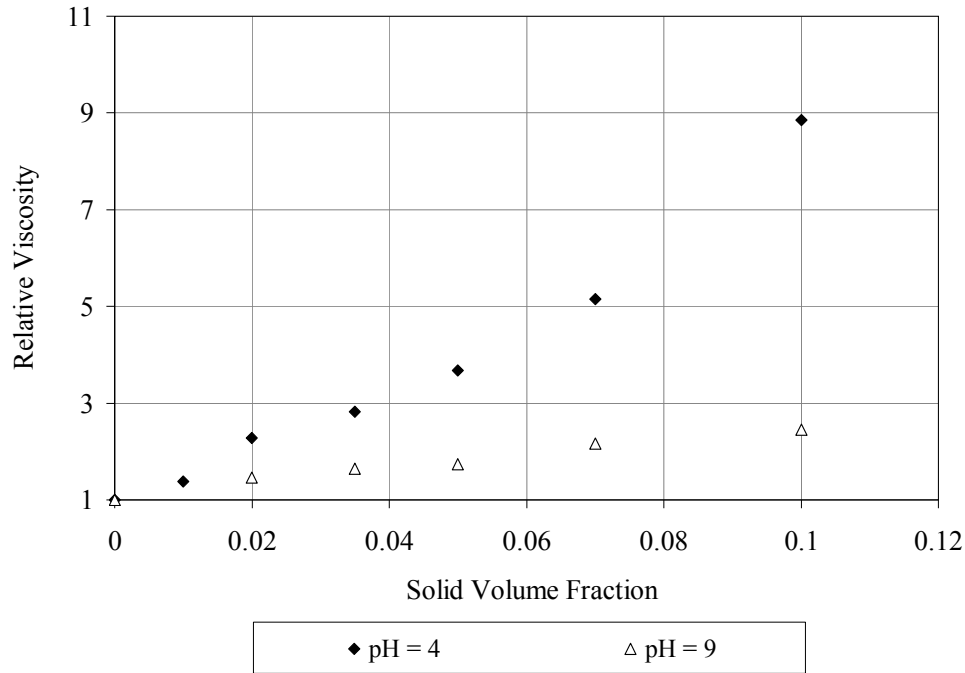


Figure 5.21 Plot of calculated relative viscosity values versus solid volume fraction for kaolinite-water mixtures at pH 4 and 9.

It is clear in Figure 5.21 that for the same solid concentration, the particles in the mixtures at pH 4 have a more pronounced effect on the viscosity compared with those found in mixtures at pH 9. The distinctive rheological behaviour of these two mixtures arises from the difference in the mixture water chemistry between the two. Kaolinite-water mixture at pH 4 has a larger volume fraction of aggregates compared with the poorly-flocculated kaolinite-water mixtures at pH 9. The relative volume fraction of aggregates at pH 4 and pH 9 is used to predict the relative viscosity values for kaolinite-water mixtures in the following section.

5.4. Prediction of Relative Viscosity Using FPIA Measurements

It was observed in the previous section that particles in the kaolinite-water mixtures at pH 4 affect the viscosity more significantly compared with those in the mixtures at pH 9. This distinctive behaviour is attributed to the fact that kaolinite-water mixtures at pH 4 have a larger volume fraction of aggregates compared with the poorly-flocculated kaolinite-water mixtures at pH 9. The relative volume fraction of aggregates at pH 4 and pH 9 were studied in Section 5.1.2. A value of 3.11 was accepted for the ratio of volume fraction of aggregates in kaolinite-water mixtures at pH 4 to that of pH 9 for the same amount of solid concentration. This can be written as:

$$C_{A,pH4} = 3.11 \times C_{A,pH9} = 3.11 \times C_s \quad \mathbf{5.4}$$

Volume fraction of solids was converted to volume fraction of aggregates using Equation 5.4. Viscosity data for mixtures at pH 4 and 9 were plotted as a function of aggregate volume fraction in Figure 5.22. It is clear from Figure 5.22 that experimental data for both pH 4 and pH 9 fall on the same trend line when the viscosity is plotted against aggregate volume fraction. This observation shows that modeling the rheological behaviour of kaolinite suspensions must be based on aggregate volume fraction rather than solid volume fraction. A straight line can clearly pass through data points at dilute aggregate concentrations ($C_k < 0.22$) regardless of water chemistry. The least-square fitting process for this line ($\mu_r = 17.7 C_A + 1$) produces a R-squared value of 0.98. The results of this work demonstrate the possibility of developing superior viscosity correlations when volume fraction of aggregates instead of primary particles is utilized. It should be noted that the carrier fluid correlation obtained in this section is exclusively based on PSD results of the FPIA and only for two certain water chemistries of idealized slurries.

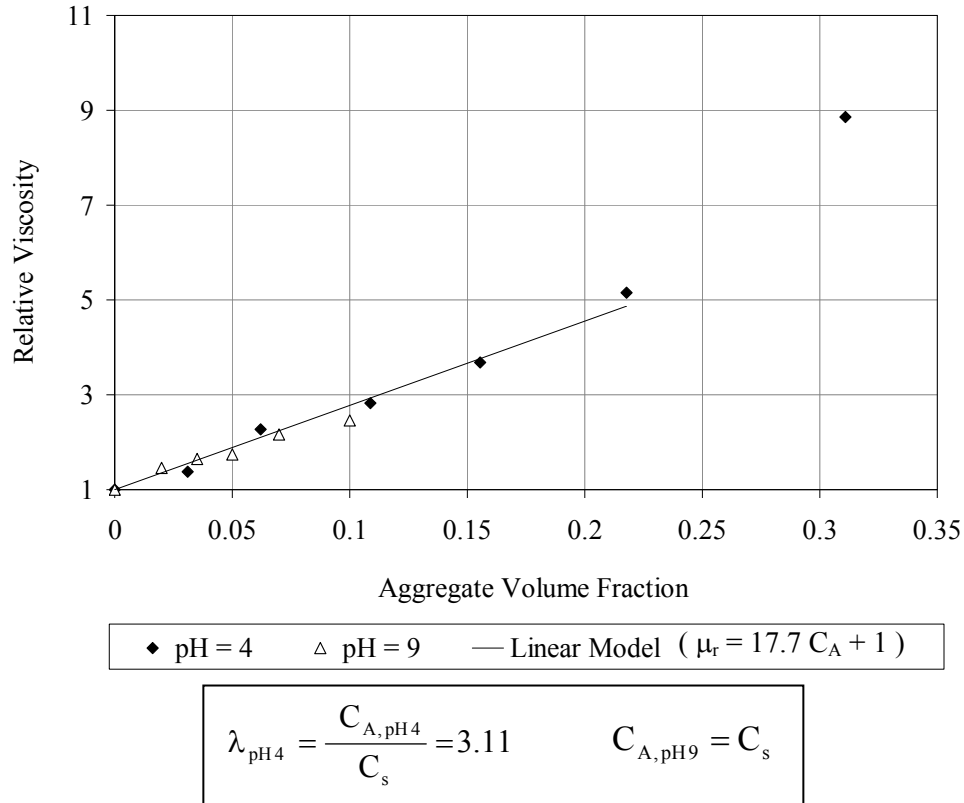


Figure 5.22 Plot of calculated relative viscosity values versus volume fraction of aggregates using value of 3.11 for λ for kaolinite-water mixtures at pH 4 and 9.

5.5. Rheological Characterization of Sand-Kaolinite Suspensions

In the oil sands industry, carrier fluid viscosity is predicted using the empirical correlations. Carrier fluid viscosity is correlated to the volume fraction of total fines, neglecting the different effects of the variety of fines present in the suspensions. Fine particles suspended in carrier fluid include clay-type (flocculating) and sand-type (inert) particles. The flocculating and inert behaviour of these two types of fines were demonstrated in Section 4.3. Particle size distribution curves presented in Figure 4.12 indicate that fine sand particles in a sand-kaolinite-water mixture do not engage in aggregate formation. On the other hand, it is shown in Section 5.3 that the viscosity of a kaolinite-water mixture depends on the concentration of aggregates. Since the addition of inert sand particles does not affect aggregate concentration, it is expected that the viscosity

of a kaolinite-water mixture would not be significantly affected by the addition of silica flour.

In order to investigate the different effects of sands and clays on the viscosity of the mixture, rheology of fine sand-kaolinite-water mixtures was determined at different sand concentrations. For this purpose, a kaolinite-water mixture ($C_k = 7\%$) was used as the base mixture to prepare sand-kaolinite-water mixtures at volume concentrations of 10%, 15%, 20% and 25%. Sand volume concentration is denoted as C_s in this text.

Figure 5.23 presents torque response measured during the conditioning step for a sand-kaolinite-water mixture ($C_s = 20\%$, $C_k = 7\%$). It is observed that torque response starts to increase after 200 seconds of pre-shearing. This is an indicative of continued deposition of sand particles. The gap between the bottom of the rotor and the cup is very narrow ($10\ \mu\text{m}$) and fills up with the settled sand quickly. The sedimentation bed rises up the walls of the viscometer and hinders the movement of the rotor. Sand particles start to settle as the mixture is sheared for adequate period of time (Gillies et al., 1999). Sand-kaolinite-water mixtures received pre-shearing for only 60 seconds. The overall duration of the test was kept shorter than 200 seconds to avoid measurement errors associated with sand deposition in the viscometer. Tests were conducted to investigate if the shortened duration of conditioning could adversely affect the accuracy of the rheological data. The torque response of a mixture after receiving 60 and 600 seconds of pre-shearing was compared.

For this purpose, a sand-kaolinite-water mixture ($C_s = 20\%$, $C_k = 7\%$) was prepared and sampled twice. The first sample was sheared for 600 seconds in the viscometer. Rheological measurement at this stage would be inaccurate due to the large amount of sand deposition in the cup. The content of the cup was removed from the viscometer after conditioning to bypass this problem. The sample received slight agitation and was poured back in the rheometer for rheological

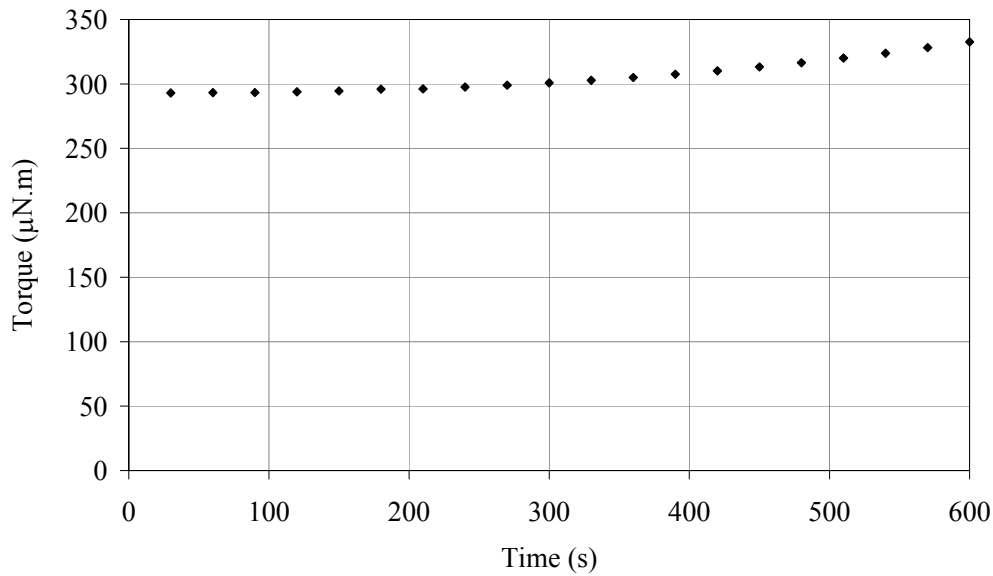


Figure 5.23 Torque response data for conditioning a sand-kaolinite-water mixture. $\omega = 25$ rad/s; $C_s = 20\%$; $C_k = 7\%$.

measurement. Next, the second sample was tested using the rheometer. The second sample received only 60 seconds of pre-shearing prior to rheological measurements. The rheological data for these two samples are presented in Figure 5.24. It was observed that torque response is similar for both mixtures. Hence, sand-kaolinite-water mixtures were conditioned for only 60 seconds at a velocity of 25 rad/s in this work.

Rheological measurements were conducted on sand-kaolinite-water mixtures in the similar fashion as previous measurements on kaolinite-water mixtures at pH 4 and pH 9. As an example, Figure 5.25 presents torque response for the accepted data points for a steady state ramp up measurement on a sand-kaolinite-water mixture ($C_s = 25\%$; $C_k = 7\%$). It can be seen in Figure 5.25 that torque response for each data point for this concentrated mixture becomes constant with time during the measurement.

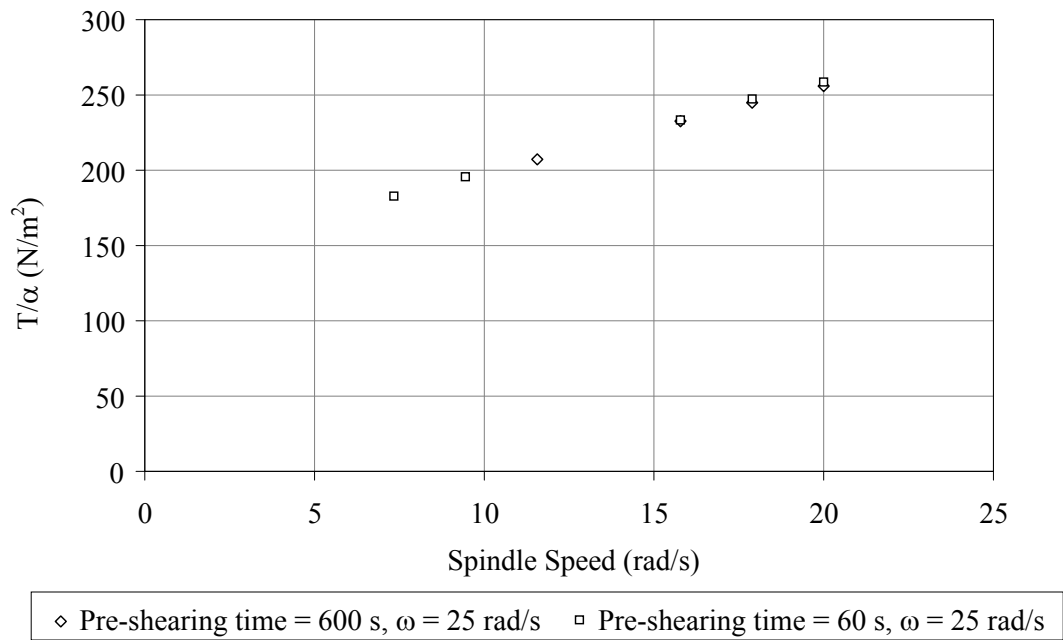


Figure 5.24 Torque response data for 2 samples of a sand-kaolinite-water mixture. $C_s = 20\%$; $C_k = 7\%$.

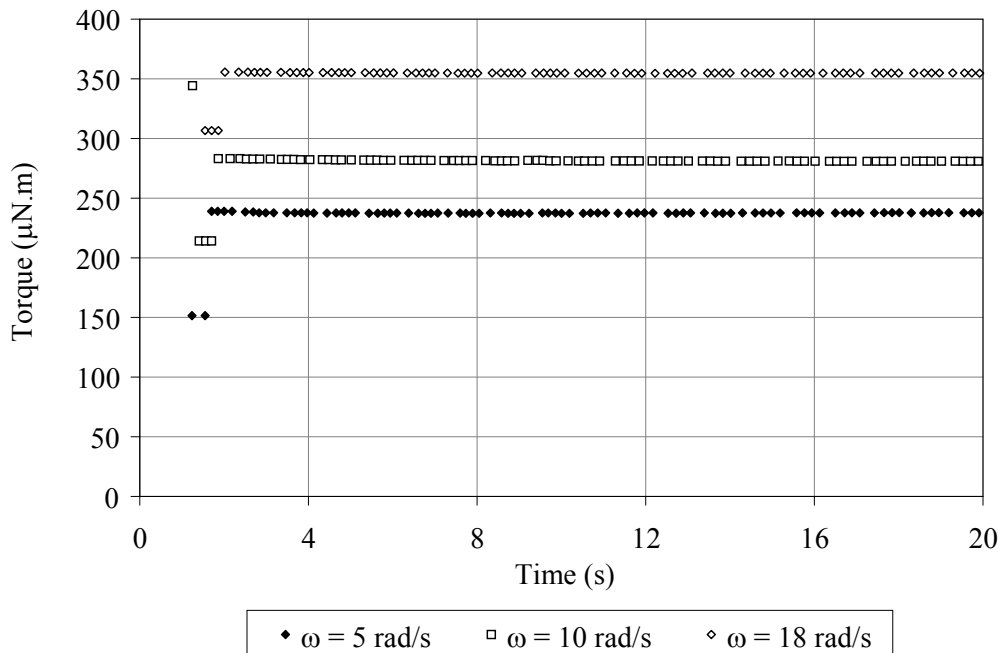


Figure 5.25 Torque response data for the recording of 3 data points for a sand-kaolinite-water mixture. $C_s = 25\%$; $C_k = 7\%$.

Sand-kaolinite-water mixtures ($C_k = 7\%$) with sand volume concentrations of 15%, 20% and 25% were tested. Torque response was recorded during ramp up steady state steps. Data points for which the torque response did not reach a constant value during the measurement time or failed to satisfy Equation 3.3 and 3.4 were discarded. Valid data points for rheological measurements on the sand-kaolinite-water mixtures are presented in Figure 5.26. These mixtures exhibited a yield stress and were characterized using the Bingham fluid model with a reasonable fit. Table 5.6 provides calculated viscosity values and the standard error value for the Bingham model fitting of sand-kaolinite-water mixtures.

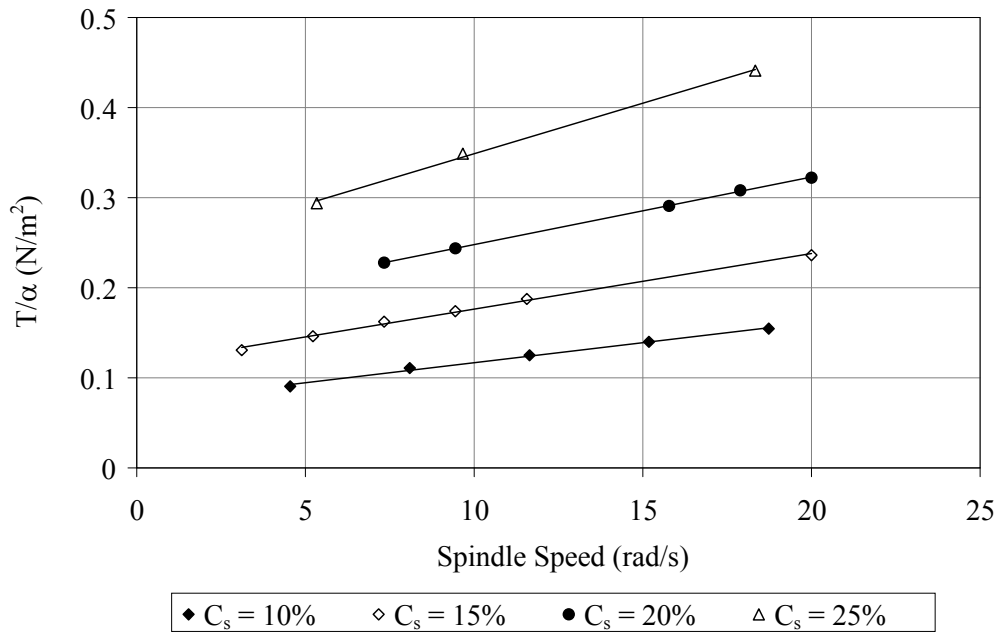


Figure 5.26 Torque response data for sand-kaolinite-water mixtures. $C_k = 7\%$.

The relative viscosities of sand-water mixtures were calculated using the viscosity value of the kaolinite-water mixture in which the sands were dispersed ($C_k = 7\%$ at pH 8) as the reference value. Relative viscosity of sand-water mixtures were plotted against sand concentration in Figure 5.27. It can be observed in Figure 5.27 that Equation 1.5 by Gillies et al. (1999) for predicting viscosity of sand-water mixtures with change in solids volume concentration fits

Table 5.6 Error value for the Bingham model fitting and calculated viscosity values for sand-kaolinite-water mixtures.

C_s (%)	C_k (%)	pH	Standard error	Viscosity (mPa.s)
0	7	8	6.96	4.21
10	7	8	12.92	4.44
15	7	8	10.2	6.17
20	7	8	2.45	7.49
25	7	8	10.71	11.22

the experimental data reasonably well. For comparison, the variation of relative viscosity with solid volume concentration for sand and kaolinite mixtures is presented along side each other in Figure 5.28. It is clear in Figure 5.28 that for the same solid concentration, the contribution of flocculating particles towards an increase in the mixture viscosity is very large, whereas, inert sand particles only slightly affect the rheological behaviour of the suspension. This conclusion highlights the importance of discriminating between fines based on particle-interactions.

Volume fraction of solids was converted to volume fraction of aggregates using conversion value of 3.11 for kaolinite-water mixtures at pH 4 and a value of 1.00 for kaolinite-water mixtures at pH 9, which were obtained from the FPIA results for λ in Section 5.1.2. Because sand particles are inert and do not flocculate, actual solid volume fraction is used. Viscosity data for kaolinite mixtures at pH 4 and 9 as well as that for sand mixtures were plotted as a function of aggregate volume fraction in Figure 5.29. As Figure 5.29 suggests, the relative viscosity of sand mixtures can be modeled by the Equation 1.5 by Gillies et al. (1999). This observation shows that sand particles in a sand-kaolinite-water mixture do not engage in the aggregate formation. These inert particles increase the viscosity by crowding the mixture in proportion to their solid volume fraction as predicted by Equation 1.5. It can be observed in Figure 5.29 that kaolinite aggregates start to diverge from the

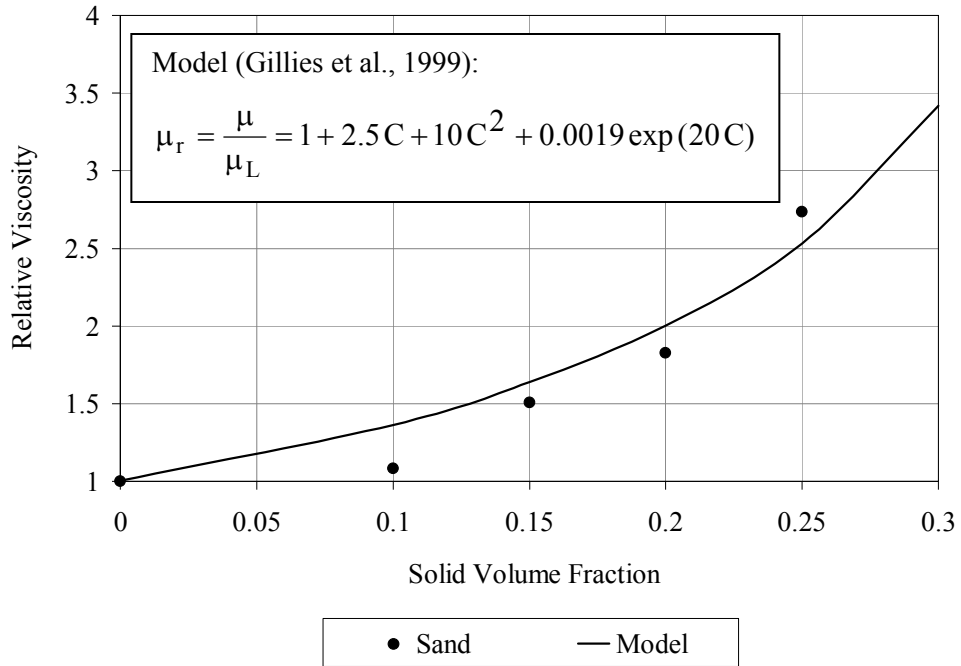


Figure 5.27 Plot of calculated relative viscosity values versus solid volume fraction for sand-kaolinite-water mixtures fitted with Equation 1.5 by Gillies et al. (1999).

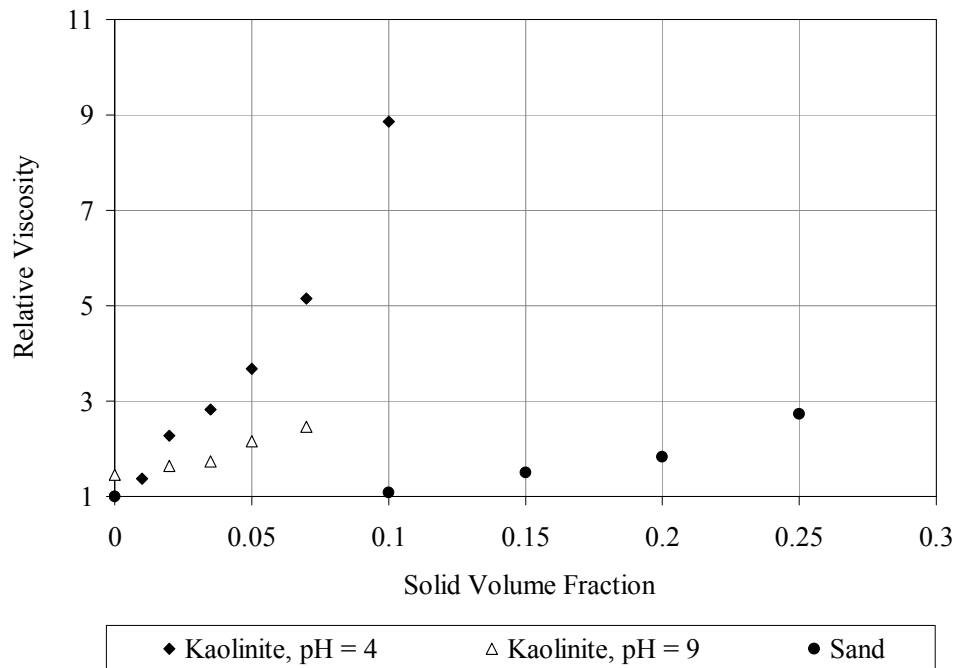


Figure 5.28 Plot of calculated relative viscosity values versus solid volume fraction for kaolinite-water mixtures at pH 4 and 9 and for sand-kaolinite-water mixtures.

behaviour of sand particles from very low volume fractions. It can be interpreted from this divergence that particle interactions exist between kaolinite aggregates. It is clear in Figure 5.29 that when viscosity is plotted as a function of aggregate volume fraction, experimental data for both pH 4 and pH 9 fall on one straight line that passes through the origin. It can also be seen in Figure 5.29 that for the same amount of solid concentration, contribution of flocculating particles towards an increase in the mixture viscosity is larger than inert sand particles. These findings validate the two main arguments of the present study: it is necessary to discriminate between the effect of fines on mixture viscosity based on particle interactions, and that viscosity correlations would be improved if volume fraction of aggregates instead of primary particles is utilized as the correlating parameter.

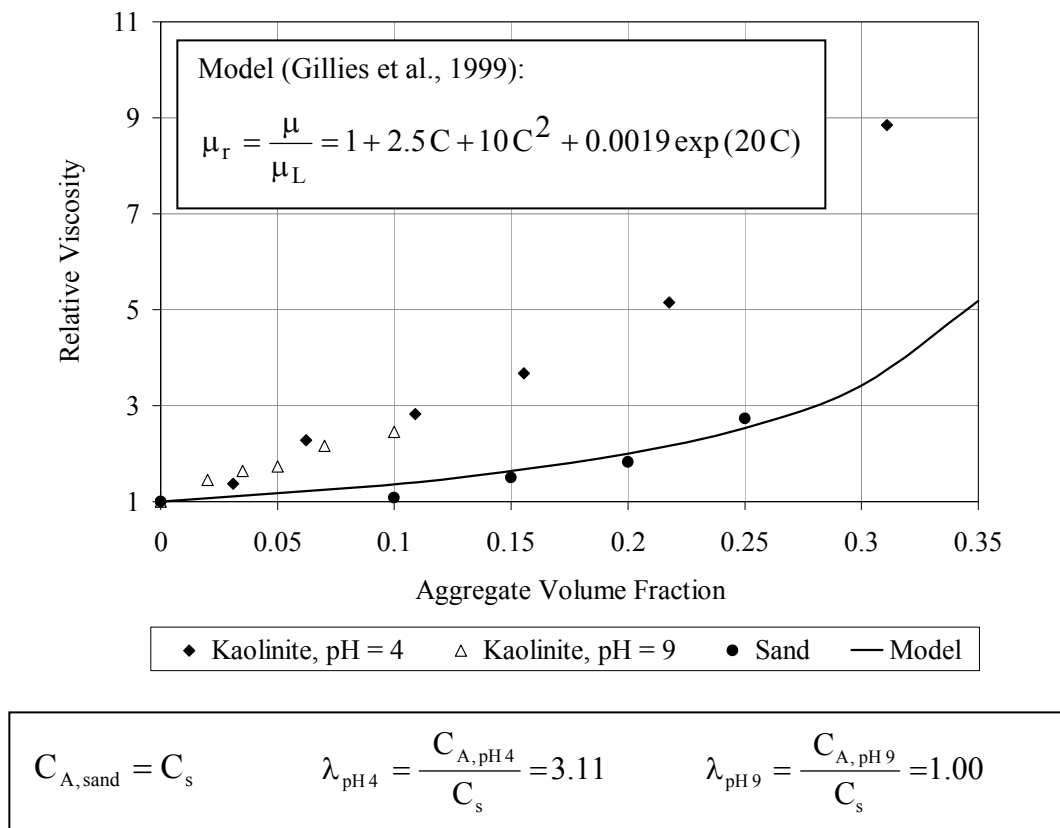


Figure 5.29 Plot of calculated relative viscosity values versus volume fraction of aggregates for kaolinite-water mixtures at pH 4 and 9, and for sand-kaolinite-water mixtures which are fitted with Equation 1.5 by Gillies et al. (1999). A value of 3.11 and 1.00 was used for λ to convert mixture concentration from solid volume fraction to volume fraction of aggregates for kaolinite-water mixtures at pH 4 and 9, respectively.

5.6. Summary

The main objective of this chapter was to assess the variability of carrier fluid viscosity with the volume fraction of particle aggregates instead of solid volume fraction. In the first series of experiments in this chapter, the estimation of the ratio of aggregate volume fraction to solid volume fraction (λ) was conducted from statistical analysis of the FPIA images for kaolinite-water mixtures at pH 4 and pH 9. Aggregates are void structures that entrain a portion of the dispersing medium in between them; hence, the total volume of aggregated particles in a sample is larger than that of dispersed particles for the similar amount of solids. The ratio of volume fraction of aggregates in kaolinite-water mixtures at pH 4 to that of pH 9 was calculated from the FPIA results to have an average value of 3.11. These findings were later utilized towards a relative study of the viscosity of kaolinite-water mixtures at pH 4 and pH 9 in this chapter.

In the second series of experiments, the AR-G2 rheometer was used to measure the viscosity of kaolinite-water suspensions at pH 9 and pH 4. Kaolinite-water mixtures at pH 4 and pH 9 exhibited distinct rheological behaviour. The variation of mixture viscosity with kaolinite solid concentration clearly indicates that for the same amount of solid concentration, particles have a more pronounced effect on the viscosity in mixtures at pH 4 compared with mixtures at pH 9. Volume fraction of solids was converted to volume fraction of aggregates using the calculated λ from the FPIA results. It was observed that when viscosity was plotted as a function of aggregate volume fraction, experimental data for both pH 4 and pH 9 for dilute aggregate concentrations ($C_k < 0.22$) fall on one straight line that passes through the origin ($\mu_r = 17.7 C_A + 1$). This observation is in favour of our argument to model the rheological behaviour of kaolinite suspensions based on aggregate volume fraction, rather than solid volume fraction. However, introduction of a rheological model is avoided in this project since any such model would be exclusively based on PSD results of the FPIA and only for two certain water chemistries.

In the oil sands industry, viscosity of carrier fluid is correlated to the volume fraction of total fines, neglecting the different effects of the clay-type and sand-type fines present in the suspensions. In Section 5.5, idealized sand-kaolinite-water suspensions were tested using the AR-G2 rheometer in order to investigate the different effects of sands and clays on the viscosity of the mixture. Experimental data in this section show that for the same amount of solid concentration, contribution of flocculating kaolinite particles towards an increase in the mixture viscosity is very large, whereas, inert sand particles only slightly affect rheological behaviour of the suspension. This observation highlights the importance of discriminating between fines based on particle interactions.

6. Conclusions and Future Work

6.1. Conclusions

Difficulties associated with the measurement of carrier fluid viscosity leaves us to resort to correlations to evaluate this important pipeline parameter. In the oil sands industry, numerous empirical correlations are typically used to predict carrier fluid viscosity but their applicability and accuracy are suspect. The main deficiency of existing correlations relates to the fact that the viscosity is predicted using the volume fraction of total fines as the primary correlating parameter. This approach neglects the different effects that different types of fines present in the suspensions can have on mixture viscosity. In this project, volume fraction and PSD of flocculating fines were determined in the state in which they exist in a slurry without being broken down into their primary particle sizes. The Sysmex Flow Particle Image Analyzer (FPIA-3000) is utilized in this project for PSD measurements of fine particles.

The FPIA size measurement technique is based on automated image capture of particles in the mixture. The FPIA is a novel technology and there has not been any research reported in literature on the application of the FPIA in clay suspension analysis. Performance of the FPIA on sand or kaolinite suspensions was tested in this project. It was found in this work that the FPIA is an appropriate device to assess the kaolinite or sand water suspensions in their natural state. The images produced by the FPIA shows that this device does not break kaolinite aggregates down to primary sizes. A comparison between the image of a sand particle and the image of kaolinite aggregate demonstrates the ability of the FPIA to visually identify the flocculating and inert behaviour of these two types of fines in the mixture. However, the FPIA cannot properly analyze the particles in a concentrated mixture. Therefore, it is necessary to dilute any sample that contains more than 36,000 particles in one μl of its volume prior to testing with the FPIA. It was found in this work that dilution has a visible effect on the PSD of

flocculated kaolinite-water mixtures even when original mixture chemistry is preserved.

The FPIA successfully captured the change in the PSD of a flocculated mixture at different water chemistries. The FPIA measurement results showing the change in kaolinite aggregate size with suspension chemistry agree with extensive investigations published in literature. Aggregates are void structures and entrain a portion of the dispersing medium depending on their size and structure. Hence, the total volume of aggregated particles in a sample is larger than that of dispersed particles for the similar amount of solids. The ratio of aggregate volume fraction to solid volume fraction was estimated for idealized flocculating slurries at low and high pH values from statistical analysis of the FPIA images. The ratio of volume fraction of aggregates in a kaolinite-water mixture at pH 4 to that of pH 9 was calculated from the FPIA results to have an average value of 3.11.

This main objective of this work is to show that carrier fluid viscosity correlations are improved significantly if the concentration of aggregates is used as the primary correlating parameter, rather than the more conventional use of total solids concentration. The viscosities of the idealized slurries were determined at varying mixture chemistry and component volume fraction in this work. It was found through rheological measurements that kaolinite-water mixtures at pH 4 and pH 9 exhibit distinguished rheological behaviour. The variation of mixture viscosity with kaolinite solid concentration indicates that compared with mixtures at pH 9, particles in mixtures at pH 4 have a more pronounced effect on the viscosity. The distinctive rheological behaviour of these two mixtures can be explained using the FPIA results. For the same amount of solid concentration, volume fraction of aggregates in a kaolinite-water mixture at pH 4 is 3.11 times larger compared with a kaolinite-water mixture at pH 9. When viscosity is plotted as a function of aggregate volume fraction, experimental data for both pH 4 and pH 9 fall on one straight line that passes through the origin. Experimental data presented in this work show that aggregate concentration can be used to represent the effect of both flocculating solid concentration and mixture chemistry on the

mixture viscosity. These observations support the main argument of this project that the rheological behaviour of kaolinite suspensions should be modeled based on aggregate volume fraction, rather than solid volume fraction.

In the oil sands industry, viscosity of carrier fluid is conventionally correlated to the volume fraction of total fines, neglecting the different effects of the clay-type and sand-type fines present in the suspensions. In this project, particles were classified as “inert fines” and “flocculating fines” as they play very different roles in determining the carrier fluid viscosity. The PSD results of the FPIA measurements on sand-kaolinite-water mixtures show that the addition of fine sand introduces non-flocculating particles to the kaolinite-water mixture. The viscosity of a flocculated mixture is governed by the concentration of aggregate structures. Therefore, it is expected that sand particles do not affect the viscosity of a flocculating mixture because they do not engage in aggregate formation.

Rheological measurements on idealized carrier fluids show that addition of fine inert sand to a clay-water suspension could not significantly alter the viscosity of the mixture. It was observed that for the same amount of solid concentration, contribution of clay particles towards an increase in the mixture viscosity is larger than sand particles. Sand particles increase the viscosity by crowding the mixture in proportion to their solid volume fraction as predicted by Gillies et al. (1999). Whereas, clay particles form aggregates and crowd the mixture depending on how dense or how void the resultant structures are. It can be concluded from this study that particles should be classified as “inert fines” and “flocculating fines” as they have distinguished effects on the carrier fluid viscosity. The findings in this project also demonstrate that viscosity correlations would be improved if volume fraction of aggregates instead of primary particles is utilized as the correlating parameter. These findings are expected to improve the industry’s ability to design new hydrotransport and coarse tailings pipeline systems and enhance troubleshooting the operation of existing ones.

6.2. Future Work

The Sysmex FPIA-3000 is used to examine kaolinite aggregates and sand inert particles in this project. In recent literature, the FPIA has been successfully used to study particle shape and size distribution of different aqueous suspensions containing fine particles in the range of 0.5 to 40 μm in diameter (Arnold et al., 2003; Tanaka et al., 2008; Komabayashi and Spangberg, 2008 (a, b)). However, there has not been any research reported in literature on the application of the FPIA in clay suspension analysis. There are a few limitations associated with the use of this instrument for testing sand and kaolinite suspensions. The effect of the FPIA on structure of samples must be explicitly quantified before reporting absolute values for particle size or shape distributions. The flow pattern of the sample inside the device should be studied to identify the effect of shear exerted on the sample inside the FPIA during the testing process. Also, the effect of particle sheath on the chemistry of sample must be investigated. Particle sheath liquid contains salts, surfactants and buffers and has a pH of 7.5. Therefore, particle sheath liquid alters the chemistry of sample as it comes to contact, and possibly mixes with the sample during the measurements. In this project, corrections for such factors were not necessary as the PSDs were studied from a comparative point of view. Here, sample flow pattern and particle sheath liquid were assumed to affect different measurements to the same extent, and hence, were neglected. However, corrections are necessary for quantitative studies reporting absolute values for particle size or shape distributions.

In this project, idealized kaolinite-water and sand-kaolinite-water mixtures were used to represent carrier fluid. Clays are naturally occurring materials and contain not only kaolinite but varying amounts of other types of minerals and some amount of impurities. Moreover, clay surfaces are modified in contact with organic materials including bitumen (Tombacz, 2003). Therefore, future experimental programs should study clays that have been exposed to process

water, bitumen and natural surfactants. Another issue is that water chemistry of process streams is variable in terms of pH and present ions. A comprehensive future work to this study should include samples collected from actual process streams from oil sands industry. Samples from the oil sands industry must be treated prior to testing. Coarse fractions must be separated from the carrier fluid. Also, any possible residue of bitumen must be removed prior to particle characterization by the FPIA as it may foul the device and disturb the clarity of the images.

References

Adeyinka O.B., S. Samiei, Z. Xu and J. H. Masliyah, “Effect of Particle Size on the Rheology of Athabasca Clay Suspensions”, the Canadian Journal of Chemical Engineering, **87**, 422-434 (2009).

AR-G2/AR 2000x Operator’s Manual, TA Instrument, Revision B, Delaware, united States (2006).

Arnold, G., J. Garche, , R. Hemmer, S. Strobele, C. Vogler, M. Wohlfahrt-Mehrens, “Fine-Particle Lithium Iron Phosphate LiFePO Synthesized by a New Low-Cost Aqueous Precipitation”, Journal of Power Source, **119**, 47-251 (2003).

DeBlois, R. W. and C. P. Bean, “Counting and Sizing of Submicron Particles by Resistive Pulse Technique”, Review of Scientific Instruments, **41**, 909–15 (1970).

Franco, F., L.A. Pérez-Maqueda, and J.L. Pérez-Rodríguez, “The Effect of Ultrasound on the Particle Size and Structural Disorder of a Well-Ordered Kaolinite”, Journal of Colloid and Interface Science, **274**, 107-117 (2004).

Gillies, D., “Particle Contributions to Kinematic Friction in Slurry Pipeline Flow”, University of Alberta, MSc Thesis (2012).

Gillies, R.G., K.B. Hill, M. McKibben, and C.A. Shook, “Solids Transport by Laminar Newtonian Flows”, Powder Technology, **104**, 269-277 (1999).

Govoreanu, R., H. Saveyn, P. Van der Meeren, I. Nopens and P.A. Vanrolleghem, “A Methodological Approach for Direct Quantification of the Activated Sludge Floc Size Distribution by Using Different Techniques”, Water Science & Technology, **60**, 1857-1867 (2009).

Hao, T., “Viscosities of Liquids, Colloidal Suspensions and Polymeric Systems Under Zero or Non-zero Electric Field”, Advances in Colloid and Interface Science, **142**, 1-19 (2008).

James A.E., and D.J.A. Williams, “Particle Interactions and Rheological Effects in Kaolinite Suspensions”, *Advances in Colloid and Interface Science*, **17**, 219-232 (1982).

Kaminsky, H.A.W., T.H. Etsell, D.G. Ivey and O.Omotoso, “Characterization of Heavy Minerals in the Athabasca Oil Sands, *Minerals Engineering*, **21**, 264-271 (2008).

Kaminsky, H.A.W., T.H. Etsell, D.G. Ivey and O. Omotoso, “Distribution of Clay Minerals in the Process Streams Produced by the Extraction of Bitumen from Athabasca Oil Sands”, *The Canadian Journal of Chemical Engineering*, **87**, 85-93 (2009).

Komabayashi, T., L.S. Spångberg, “Comparative Analysis of the Particle Size and Shape of Commercially Available Mineral Trioxide Aggregates and Portland Cement: a Study with a Flow Particle Image Analyzer”, *Journal of Endodontics*, **34**, 94-98 (2008) (a).

Komabayashi, T., L.S. Spångberg, “Particle Size and Shape Analysis of MTA Finer Fractions Using Portland Cement”, *Journal of Endodontics*, **34**, 709-711 (2008) (b).

Komabayashi, T., L.S. Spångberg, “Particle Size and Shape of Calcium Hydroxide”, *Journal of Endodontics*, **35**, 284-287 (2009).

Krause, B., G. Petzold, S. Pegel, P. Potschke, “Correlation of Carbon Nanotube Dispersability in Aqueous Surfactant Solutions and Polymers”, *Carbon*, **47**, 602-612 (2009).

Litzenberger C.G, R J Sumner, “Flow Behavior of Kaolinite Clay Slurries”, *BHR Group Hydrotransport*, **16**, 77-91 (2004).

Liu, J., Z. Xu and J. Masliyah, “Studies on Bitumen-Silica Interaction in Aqueous Solutions by Atomic Force Microscopy”, *Langmuir*, **19**, 3911-3920 (2003).

Li Y., É.S. Nagy, M.N. Esmail, Z. Hórvölgyi, “Weak Flocculation of Aqueous Kaolinite Suspensions Initiating by NaCMC with Different Molecular Weights”, *Macromolecular Symposia*, **202**, 307-324 (2003).

Masliyah, J. and S. Bhattacharjee, “Electrokinetic and Colloid Transport Phenomena”, Wiley Interscience, Hoboken, New Jersey (2006).

Masliyah, J., Z. Xu, M. Gray, “Physics in the Oil Sands of Alberta”, *American Institute of Physics*, **62**, 31-35 (2009).

Masliyah, J., J. Czarnecki, Z. Xu, “Handbook on Theory and Practice of Bitumen Recovery from Athabasca Oil Sands, Volume 1: Theoretical Basis”, Calgary, Kingsley (2011).

Melton, I.E. and B. Rand, “Particle Interactions in Aqueous Kaolinite Suspensions I. Effect of pH and Electrolyte upon the Mode of Particle Interaction in Homoionic Sodium Kaolinite Suspensions”, *Journal of Colloid and Interface Science*, **60**, 308-320 (1977) (a).

Melton, I.E. and B. Rand, “Particle Interactions in Aqueous Kaolinite Suspensions II. Comparison of Some Laboratory and Commercial Kaolinite Samples”, *Journal of Colloid and Interface Science*, **60**, 321-330 (1977) (b).

Melton, I.E. and B. Rand, “Particle Interactions in Aqueous Kaolinite Suspensions III. Sedimentation Volumes”, *Journal of Colloid and Interface Science*, **69**, 331-336 (1977) (c).

Mercier, P. H. J., Y. Le Page, Y. Tu and L. S. Kotlyar, “Powder X-Ray Diffraction Determination of Phyllosilicate Mass and Area Versus Particle Thickness Distributions for Clays from the Athabasca Oil Sands,” *Petroleum Science Technology*, **26**, 307-321 (2008).

Michaels, A.S. and J.C. Bolger, “Settling Rates and Sediment Volumes of Flocculated Kaolinite Suspensions”, *Industrial Engineering Chemical Fundamental*, **1**, 24-33 (1962) (a).

Michaels, A.S. and J.C. Bolger, "The Plastic Flow Behavior of Flocculated Kaolinite Suspensions", *Industrial Engineering Chemical Fundamental*, **1**, 153-162 (1962) (b).

Nasser M.S., A.E. James, "Degree of Flocculation and Viscoelastic Behavior of Kaolinite-Sodium Chloride Dispersions", *Colloids and Surfaces*, **315**, 165-175 (2008).

Ohtsubo, M. and M. Ibaraki, "Particle-Size Characterization of Flocs and Sedimentation Volume in Electrolyte Clay Suspensions", *Applied Clay Science*, **6**, 181-194 (1991).

Omotoso, O., R. Mikula, S. Urquhart, H. Sulimma and P. Stephens, "Characterization of Clays from Poorly Processing Oil Sands Using Synchrotron Techniques," *Clay Science*, **12**, 88-93 (2006).

Papo A., L. Piani, "Rheology of Concentrated Aqueous Kaolinite Suspensions", *Silicates Industrials* **65**, 27-32 (2000).

Papo A., L. Piani, R. Ricceri, "Sodium Tripolyphosphate and Polyphosphate as Dispersing Agents for Kaolinite Suspensions: Rheological Characterization", *Colloids and Surfaces*, **201**, 219-230 (2002).

Russel, W.B., "Review of the Role of Colloidal Forces in the Rheology of Suspensions", *Journal of Rheology*, **24**, 287-317 (1980).

Sanders, R.S., J. Schaan, R. Hughes and C.A. Shook, "Performance of Sand Slurry Pipelines in the Oil Sands Industry", *Canadian Journal of Chemical Engineering*, **82**, 850-857 (2004).

Scales, P.J., S.B. Johnson, and T.W. Healy, "Shear Yield Stress of Partially Flocculated Colloidal Suspensions", *American Institute of Chemical Engineers*, **44**, 538-544 (1998).

Schaan J., R.J. Sumner, R.G. Gillies and C.A. Shook, "The Effect of Particle Shape on Pipeline Friction for Newtonian Slurries of Fine Particles", *The Canadian Journal of Chemical Engineering*, **78**, 717-725 (2000).

Schroth, B.K., G. Sposito, "Surface Charge Properties of Kaolinite Clays", *Clay Miner.* **45**, 85-90 (1997).

Shook, C.A., C. Roco, "Slurry Flow: Principles and Practice", Butterworth-Heinemann Series in Chemical Engineering (1991).

Shook, C.A., R.G. Gillies and R.S. Sanders, "Pipeline Hydrotransport with Applications in the Oil Sands Industry", SRC Publication (2002).

Sumner, J.J. Munkler, S.M. Carriere and C.A. Shook, "Rheology of Kaolinite Slurries Containing Large Silica Particles" *Journal of Hydrology and Hydromechanics*, **48**, 110-124 (2000).

Systemex FPIA-3000/FPIA-3000S Operator's Manual, Systemex Corporation, Kobe, Japan (2006).

Taylor, G.I., "Stability of a viscous liquid contained between two rotating cylinders", *Philosophical Transactions of the Royal Society of London*, **223**, 289-343 (1936).

Tanaka M., M. Komagata, M. Tsukada, H. Kamiya, "Fractal Analysis of the Influence of Surface Roughness of Toner Particles on Their Flow Properties and Adhesion Behavior", *Powder Technology*, **186**, 1-8 (2008).

Thomas, D.G., "Transport Characteristics of Suspension; a Note on the Viscosity of Newtonian Suspensions of Uniform Spherical Particles", *Journal of Colloid Science*, **20**, 267-277 (1965).

Tombacz E., "Effect of Environmental Relevant Organic Complexants on the Surface Charge and the Interaction of Clay Mineral and Metal Oxide Particles", *Earth and Environmental Sciences*, **24**, 97-424 (2003).

Tombacz E., Márta Szekeres, "Surface Charge Heterogeneity of Kaolinite in Aqueous Suspension in Comparison with Montmorillonite", *Applied Clay Science*, **34**, 105-124 (2006).

Van Olphen, H., "Introduction to Clay Colloid Chemistry", Interscience, New York (1963).

Wallwork, V., Z. Xu, J. Masliya, “Processibility of Athabasca Oil Sand Using a Laboratory Hydrotransport Extraction System” *The Canadian Journal of Chemical Engineering*, **82**, 687-695 (2008).

Wilson, K. C., G.R. Addie, A. Sellgren, R. Clift, “Slurry Transport Using Centrifugal Pumps”, 3rd Ed., Springer, New York, USA (2006).

Zbik M., R.S.C. Smart, H. Kodama, A.R. Mermut, J.K. Torrance, “Clays for Our Future”, *Proceedings of the 11th International Clay Conference*, Pub. ICC97 Ottawa, Canada, 361-366 (1999).

Zbik M.S., R.S.C. Smart, G.E. Morris, “Kaolinite Flocculation Structure”, *Journal of Colloid and Interface Science*, **328**, 73-80 (2008).

Appendices

Appendix 1: Rheological Measurements of De-ionized Water

For all measurements reported in Appendix 1:

Instrument type	AR-G2
Geometry name	Standard DIN or conical concentric cylinders
Geometry material	Aluminum
Cup inner radius	15.00 mm
Rotor outer radius	14.00 mm
Cylinder immersed height	42.00 mm
Gap	10 μm
Gap tolerance	4 μm
Approximate sample volume	15.42 ml
Controlled variable	Velocity
Velocity tolerance	0.1000 rad/s
Temperature	22.0 $^{\circ}\text{C}$
Wait for temperature	Yes
Temperature tolerance	0.1 $^{\circ}\text{C}$
Instrument inertia	19.09 $\mu\text{N}\cdot\text{m}\cdot\text{s}^2$
Flow torque limit	2000.00 $\mu\text{N}\cdot\text{m}$
Flow velocity limit	1.000×10^{-5} rad/s

Density (kg/m ³)	998
Newtonian viscosity (mPa.s)	1.02

Step name	Conditioning
Pre-shear variable	27.55 rad/s
Pre-shear duration	0:05:00 hh:mm:ss

Step name	Steady state flow step 1
Start controlled variable	Velocity 1.000 rad/s
End controlled variable	Velocity 10.00 rad/s
Temperature	22.0 °C
Sample period	0:00:10 hh:mm:ss
Percentage tolerance	10
Consecutive within tolerance	3
Maximum point time	0:01:00 hh:mm:ss

Velocity (rad.s)	Torque (μN.m)
3.000	2.3990
6.000	4.8590
7.000	5.8462
9.000	7.5777

Step name	Steady state flow step 2
Start controlled variable	Velocity 10.00 rad/s
End controlled variable	Velocity 1.000 rad/s
Sample period	0:00:10 hh:mm:ss
Percentage tolerance	10
Consecutive within tolerance	3
Maximum point time	0:00:15 hh:mm:ss

Velocity (rad.s)	Torque (μ N.m)
7.75	7.7612
5.5	6.5377
3.25	3.3631
1	1.0959

Appendix 2: Rheological Measurements of Kaolinite-Water Mixtures at pH 9

For all measurements reported in Appendix 2:

Instrument type	AR-G2
Geometry name	Standard DIN or conical concentric cylinders
Geometry material	Aluminum
Cup inner radius	15.00 mm
Rotor outer radius	14.00 mm
Cylinder immersed height	42.00 mm
Gap	15 μm
Gap tolerance	4 μm
Approximate sample volume	15.42 ml
Controlled variable	Velocity
Velocity tolerance	0.1000 rad/s
Temperature	22.0 $^{\circ}\text{C}$
Wait for temperature	Yes
Temperature tolerance	0.1 $^{\circ}\text{C}$
Instrument inertia	19.09 $\mu\text{N}\cdot\text{m}\cdot\text{s}^2$
Flow torque limit	2000.00 $\mu\text{N}\cdot\text{m}$
Flow velocity limit	1.000×10^{-5} rad/s

Concentration: $C_k = 2\%$

Mixture Specification:

Density (kg/m ³)	1.06
C_k (%)	2
Mixture pH	9
Newtonian viscosity (mPa.s)	1.49

Measurement Specification:

Step name	Peak hold step
Controlled variable	Velocity 15.00 rad/s
Duration	0:03:00 hh:mm:ss
Delay time	0:00:10 hh:mm:ss

Results:

Time (s)	Velocity (rad/s)	Torque (μ N.m)
10.008	15	22.485
20.016	15	22.219
30.032	15	22.259
40.016	15	22.223
50.02	15	22.282
60	15	22.129
70.016	15	22.207
80.02	15	22.228
90	15	22.202
100.02	15	22.235
110.02	15	22.206

Time (s)	Velocity (rad/s)	Torque ($\mu\text{N.m}$)
120.02	15	22.048
130.02	15	22.15
140	15	22.289
150	15	22.285
160	15	22.1
170.01	15	22.136
180.01	15	22.385

Measurement Specification:

Step name	Steady state flow step 1
Start controlled variable	velocity 1.000 rad/s
End controlled variable	velocity 15.00 rad/s
Temperature	22.0 °C
Sample period	0:00:10 hh:mm:ss
Percentage tolerance	10
Consecutive within tolerance	3
Maximum point time	0:01:00 hh:mm:ss

Results:

Velocity (rad.s)	Torque (μ N.m)
1	1.1273
3.333	3.7322
5.667	6.5064
8	9.3756
10.33	12.335
12.67	15.925

Measurement Specification:

Step name	Steady state flow step 2
Start controlled variable	velocity 15.00 rad/s
End controlled variable	velocity 1.000 rad/s
Sample period	0:00:10 hh:mm:ss
Percentage tolerance	10
Consecutive within tolerance	3
Maximum point time	0:00:15 hh:mm:ss

Results:

Velocity (rad.s)	Torque (μ N.m)
12.67	15.928
10.33	12.267
8	9.3053
5.667	6.448
3.333	3.7198

Concentration: C_k = 3.5%

Mixture Specification:

Density (kg/m ³)	1.17
C _k (%)	3.5
Mixture pH	9
Newtonian viscosity (mPa.s)	1.68

Measurement Specification:

Step name	Peak hold step
Controlled variable	velocity 20.00 rad/s
Duration	0:05:00 hh:mm:ss
Delay time	0:00:10 hh:mm:ss

Results:

Time (s)	Velocity (rad/s)	Torque (μN.m)
10.004	20	38.401
20.012	20	37.837
30	20	37.794
40.04	20	37.991
50.004	20	38.052
60.04	20	38.321
69.992	20	38.033
80.008	20	37.677
90	20	38.206
100.01	20	37.942
110.01	20	37.761

Time (s)	Velocity (rad/s)	Torque ($\mu\text{N.m}$)
120	20	37.871
130.01	20	37.859
140	20	38.176
150	20	38.09
160.02	20	37.893
170	20	38.171
180.08	20	37.8
190.01	20	38.361
200.03	20	38.239
210.03	20	38.123
220	20	38.135
230	20	38.401
240	20	38.117
250.03	20	38.003
260.01	20	38.203
270.02	20	38.239
279.99	20	38.33
290.02	20	38.439
300.01	20	38.107

Measurement Specification:

Step name	Steady state flow step 1
Start controlled variable	velocity 1.000 rad/s
End controlled variable	velocity 15.00 rad/s
Temperature	22.0 °C
Sample period	0:00:10 hh:mm:ss
Percentage tolerance	10
Consecutive within tolerance	3
Maximum point time	0:01:00 hh:mm:ss

Results:

Velocity (rad.s)	Torque (μ N.m)
1	1.3658
4.111	5.6071
5.667	7.8587
7.222	10.122
8.778	12.379
10.33	14.708
11.89	17.119
13.44	19.583

Measurement Specification:

Step name	Steady state flow step 2
Start controlled variable	velocity 15.00 rad/s
End controlled variable	velocity 1.000 rad/s
Sample period	0:00:10 hh:mm:ss
Percentage tolerance	10
Consecutive within tolerance	3
Maximum point time	0:00:15 hh:mm:ss

Results:

Velocity (rad.s)	Torque (μ N.m)
13.44	19.628
11.89	17.2
10.33	14.811
8.778	12.456
7.222	10.162
5.667	7.9197
4.111	5.7331
2.556	3.5696

Concentration: $C_k = 5\%$

Mixture Specification:

Density (kg/m ³)	1083
C_k (%)	5
Mixture pH	9
Newtonian viscosity (mPa.s)	1.77

Measurement Specification:

Step name	Peak hold step
Controlled variable	velocity 25.00 rad/s
Duration	0:05:00 hh:mm:ss
Delay time	0:00:10 hh:mm:ss

Results:

Time (s)	Velocity (rad/s)	Torque (μ N.m)
10.000	25.00	56.848
20.020	25.00	56.236
30.000	25.00	56.729
40.016	25.00	56.334
50.000	25.00	56.587
59.996	25.00	56.223
70.012	25.00	56.747
79.996	25.00	56.720
89.996	25.00	56.657
99.996	25.00	55.882
110.02	25.00	56.540

Time (s)	Velocity (rad/s)	Torque ($\mu\text{N}\cdot\text{m}$)
120.00	25.00	56.873
130.00	25.00	56.875
140.01	25.00	56.243
150.00	25.00	55.786
160.01	25.00	56.349
170.01	25.00	56.549
180.01	25.00	56.241
190.00	25.00	56.924
200.01	25.00	56.906
209.99	25.00	56.150
219.99	25.00	56.318
230.01	25.00	55.927
240.01	25.00	56.474
250.01	25.00	56.606
259.99	25.00	55.994
269.99	25.00	56.404
280.01	25.00	56.323
289.99	25.00	55.835
299.99	25.00	56.124

Measurement Specification:

Step name	Steady state flow step 1
Start controlled variable	velocity 1.000 rad/s
End controlled variable	velocity 20.00 rad/s
Temperature	22.0 °C
Sample period	0:00:10 hh:mm:ss
Percentage tolerance	10
Consecutive within tolerance	3
Maximum point time	0:01:00 hh:mm:ss

Results:

Velocity (rad.s)	Torque (μ N.m)
17.89	32.810
15.78	25.665
11.56	16.918
9.444	13.612
7.333	10.378
5.222	7.2630

Measurement Specification:

Step name	Steady state flow step 2
Start controlled variable	velocity 20.00 rad/s
End controlled variable	velocity 1.000 rad/s
Sample period	0:00:10 hh:mm:ss
Percentage tolerance	10
Consecutive within tolerance	3
Maximum point time	0:00:15 hh:mm:ss

Results:

Velocity (rad.s)	Torque (μ N.m)
13.44	19.628
11.89	17.2
10.33	14.811
8.778	12.456
7.222	10.162
5.667	7.9197
4.111	5.7331
2.556	3.5696

Concentration: $C_k = 7\%$

Mixture Specification:

Density (kg/m ³)	1167
C_k (%)	7
Mixture pH	9
Newtonian viscosity (mPa.s)	2.20

Measurement Specification:

Step name	Peak hold step
Controlled variable	velocity 40.00 rad/s
Duration	0:5:00 hh:mm:ss
Delay time	0:00:10 hh:mm:ss

Measurement Specification:

Step name	Steady state flow step 1
Start controlled variable	velocity 1.000 rad/s
End controlled variable	velocity 20.00 rad/s
Temperature	22.0 °C
Sample period	0:00:10 hh:mm:ss
Percentage tolerance	10
Consecutive within tolerance	3
Maximum point time	0:01:00 hh:mm:ss

Results:

Velocity (rad.s)	Torque (N.m)
1.378	2.2722
2.022	3.2871
2.968	4.8638
4.357	7.1398
6.395	10.868
9.386	16.300
13.78	24.752

Measurement Specification:

Step name	Steady state flow step 2
Start controlled variable	velocity 20.00 rad/s
End controlled variable	velocity 1.000 rad/s
Sample period	0:00:10 hh:mm:ss
Percentage tolerance	10
Consecutive within tolerance	3
Maximum point time	0:00:15 hh:mm:ss

Results:

Velocity (rad.s)	Torque ($\mu\text{N.m}$)
15.99	29.733
10.89	19.462
7.420	12.974
5.055	8.5321
3.444	5.7682
1.378	2.2863

Concentration: $C_k = 10\%$

Mixture Specification:

Density (kg/m ³)	1167
C_k (%)	10
Mixture pH	9
Newtonian viscosity (mPa.s)	2.51

Measurement Specification:

Step name	Peak hold step
Controlled variable	velocity 30.00 rad/s
Duration	0:05:00 hh:mm:ss
Delay time	0:00:10 hh:mm:ss

Results:

Time (s)	Velocity (rad/s)	Torque (μ N.m)
10.008	30.00	90.356
20.024	30.00	91.778
30.008	30.00	89.052
40.024	30.00	90.126
50.012	30.00	89.801
60.024	30.00	90.159
70.008	30.00	90.759
80.008	30.00	90.560
90.024	30.00	91.678
100.01	30.00	90.932
110.02	30.00	89.909

Time (s)	Velocity (rad/s)	Torque ($\mu\text{N}\cdot\text{m}$)
120.03	30.00	89.783
130.02	30.00	89.652
140.02	30.00	90.596
150.01	30.00	89.186
160.02	30.00	89.700
170.00	30.00	90.610
180.02	30.00	90.554
190.02	30.00	90.503
200.02	30.00	89.985
210.00	30.00	89.312
220.02	30.00	91.792
230.00	30.00	90.266
240.02	30.00	90.312
250.02	30.00	91.892
260.02	30.00	89.306
270.02	30.00	90.960
280.00	30.00	91.101
290.02	30.00	90.321
300.00	30.00	91.211

Measurement Specification:

Step name	Steady state flow step 1
Start controlled variable	velocity 1.000 rad/s
End controlled variable	velocity 40.00 rad/s
Temperature	22.0 °C
Sample period	0:00:10 hh:mm:ss
Percentage tolerance	50
Consecutive within tolerance	3
Maximum point time	0:01:00 hh:mm:ss

Results:

Velocity (rad.s)	Torque (μ N.m)
1.000	2.0460
5.333	10.454
9.667	19.435
14.00	28.871

Measurement Specification:

Step name	Steady state flow step 2
Start controlled variable	velocity 40.00 rad/s
End controlled variable	velocity 1.000 rad/s
Sample period	0:00:10 hh:mm:ss
Percentage tolerance	5
Consecutive within tolerance	3
Maximum point time	0:00:15 hh:mm:ss

Results:

Velocity (rad.s)	Torque ($\mu\text{N.m}$)
27.00	76.665
22.67	57.284
18.33	39.501
14.00	29.156
9.667	19.493

Appendix 3: Rheological Measurements of Kaolin-Water Mixtures at pH 4

For all measurements reported in Appendix 3:

Instrument type	AR-G2
Geometry name	Standard DIN or conical concentric cylinders
Geometry material	Aluminum
Cup inner radius	15.00 mm
Rotor outer radius	14.00 mm
Cylinder immersed height	42.00 mm
Gap	10 μm
Gap tolerance	4 μm
Approximate sample volume	15.42 ml
Controlled variable	Velocity
Velocity tolerance	0.1000 rad/s
Temperature	22.0 $^{\circ}\text{C}$
Wait for temperature	Yes
Temperature tolerance	0.1 $^{\circ}\text{C}$
Instrument inertia	19.09 $\mu\text{N}\cdot\text{m}\cdot\text{s}^2$
Flow torque limit	2000.00 $\mu\text{N}\cdot\text{m}$
Flow velocity limit	1.000×10^{-5} rad/s

Concentration: $C_k = 1\%$

Mixture Specification:

Density (kg/m ³)	1015
C_k (%)	1
Mixture pH	4
Newtonian viscosity (mPa.s)	1.40

Measurement Specification:

Step name	Peak hold step
Controlled variable	Velocity 30.00 rad/s
Duration	0:05:00 hh:mm:ss
Delay time	0:00:10 hh:mm:ss

Step name	Steady state flow step 1
Start controlled variable	velocity 1.000 rad/s
End controlled variable	velocity 15.00 rad/s
Temperature	22.0 °C
Sample period	0:00:10 hh:mm:ss
Percentage tolerance	10
Consecutive within tolerance	3
Maximum point time	0:01:00 hh:mm:ss

Results:

Velocity (rad.s)	Torque (μ N.m)
0.9571	1.4902
4.957	5.6239
6.888	8.1258
9.571	11.227
10.33	12.072

Measurement Specification:

Step name	Steady state flow step 2
Start controlled variable	velocity 15.00 rad/s
End controlled variable	velocity 1.000 rad/s
Sample period	0:00:10 hh:mm:ss
Percentage tolerance	10
Consecutive within tolerance	3
Maximum point time	0:01:00 hh:mm:ss

Results:

Velocity (rad.s)	Torque (μ N.m)
7.436	8.4320
5.352	5.9141
3.852	4.1392
1.995	2.1760
1.436	1.5673

Concentration: $C_k = 2\%$

Mixture Specification:

Density (kg/m ³)	1032
C_k (%)	2
Mixture pH	4
Newtonian viscosity (mPa.s)	2.32

Measurement Specification:

Step name	Peak hold step
Controlled variable	Velocity 30.00 rad/s
Duration	0:05:00 hh:mm:ss
Delay time	0:00:10 hh:mm:ss

Results:

Time (s)	Velocity (rad/s)	Torque (μ N.m)
10.000	30.00	79.382
19.996	30.00	79.822
30.000	30.00	79.941
39.996	30.00	79.952
50.000	30.00	80.138
60.000	30.00	80.181
69.996	30.00	80.147
79.996	30.00	80.052
89.996	30.00	80.032
99.996	30.00	79.925
110.01	30.00	79.904

Time (s)	Velocity (rad/s)	Torque ($\mu\text{N}\cdot\text{m}$)
120.00	30.00	79.876
130.00	30.00	79.697
140.01	30.00	79.626
150.00	30.00	79.606
160.01	30.00	79.583
170.00	30.00	79.427
179.99	30.00	79.324
190.00	30.00	79.247
199.99	30.00	79.276
209.99	30.00	79.130
219.99	30.00	78.972
230.01	30.00	78.933
239.99	30.00	78.982
250.01	30.00	78.913
259.99	30.00	78.843
269.99	30.00	78.725
279.99	30.00	78.727
290.01	30.00	78.789
299.99	30.00	78.727

Measurement Specification:

Step name	Steady state flow step 1
Start controlled variable	velocity 1.000 rad/s
End controlled variable	velocity 25.00 rad/s
Temperature	22.0 °C
Sample period	0:00:10 hh:mm:ss
Percentage tolerance	5
Consecutive within tolerance	3
Maximum point time	0:01:00 hh:mm:ss

Results:

Velocity (rad.s)	Torque (μ N.m)
4.167	9.5141
8.333	17.011
12.50	25.353
16.67	32.758

Measurement Specification:

Step name	Steady state flow step 2
Start controlled variable	velocity 25.00 rad/s
End controlled variable	velocity 1.000 rad/s
Sample period	0:00:10 hh:mm:ss
Percentage tolerance	5
Consecutive within tolerance	3
Maximum point time	0:01:00 hh:mm:ss

Results:

Velocity (rad.s)	Torque ($\mu\text{N.m}$)
20.83	44.784
16.67	33.136
12.50	24.929
8.333	18.205
4.167	10.754

Concentration: $C_k = 3.5\%$

Mixture Specification:

Density (kg/m ³)	1057
C_k (%)	3.5
Mixture pH	4
Newtonian viscosity (mPa.s)	2.88

Measurement Specification:

Step name	Peak hold step
Controlled variable	Velocity 30.00 rad/s
Duration	0:05:00 hh:mm:ss
Delay time	0:00:10 hh:mm:ss

Measurement Specification:

Step name	Steady state flow step 1
Start controlled variable	velocity 1.000 rad/s
End controlled variable	velocity 20.00 rad/s
Temperature	22.0 °C
Sample period	0:00:10 hh:mm:ss
Percentage tolerance	5
Consecutive within tolerance	3
Maximum point time	0:01:00 hh:mm:ss

Results:

Velocity (rad.s)	Torque (μ N.m)
5.135	26.386
7.136	31.511
9.915	37.636
19.14	58.783
20.67	62.647

Measurement Specification:

Step name	Steady state flow step 2
Start controlled variable	velocity 20.00 rad/s
End controlled variable	velocity 1.000 rad/s
Sample period	0:00:10 hh:mm:ss
Percentage tolerance	5
Consecutive within tolerance	3
Maximum point time	0:01:00 hh:mm:ss

Results:

Velocity (rad.s)	Torque (μ N.m)
14.87	51.225
10.70	42.392
7.703	35.437
5.544	30.236
3.990	26.189

Concentration: $C_k = 5\%$

Mixture Specification:

Density (kg/m ³)	1083
C_k (%)	5
Mixture pH	4
Newtonian viscosity (mPa.s)	3.64

Measurement Specification:

Step name	Peak hold step
Controlled variable	velocity 35.00 rad/s
Duration	0:05:00 hh:mm:ss
Delay time	0:00:10 hh:mm:ss

Measurement Specification:

Step name	Steady state flow step 1
Start controlled variable	velocity 1.000 rad/s
End controlled variable	velocity 20.00 rad/s
Temperature	22.0 °C
Sample period	0:00:10 hh:mm:ss
Percentage tolerance	5
Consecutive within tolerance	3
Maximum point time	0:01:00 hh:mm:ss

Results:

Velocity (rad.s)	Torque (μ N.m)
7.136	59.042
9.915	67.778
13.78	78.693
19.14	94.025
20.67	98.997

Measurement Specification:

Step name	Steady state flow step 2
Start controlled variable	velocity 20.00 rad/s
End controlled variable	velocity 1.000 rad/s
Sample period	0:00:10 hh:mm:ss
Percentage tolerance	5
Consecutive within tolerance	3
Maximum point time	0:01:00 hh:mm:ss

Results:

Velocity (rad.s)	Torque (μ N.m)
14.08	82.152
9.592	69.860
6.535	60.624
4.452	53.365
3.033	47.650
2.067	43.012

Concentration: $C_k = 7\%$

Mixture Specification:

Density (kg/m ³)	1167
C_k (%)	7
Mixture pH	4
Newtonian viscosity (mPa.s)	5.25

Measurement Specification:

Step name	Peak hold step
Controlled variable	velocity 45.00 rad/s
Duration	0:07:00 hh:mm:ss
Delay time	0:00:10 hh:mm:ss

Results:

Time (s)	Velocity (rad/s)	Torque (μ N.m)
10	45.00	256.30
20	45.00	258.97
30	45.00	261.50
40	45.00	263.53
50	45.00	266.51
60	45.00	268.61
70	45.00	270.00
80	45.00	271.16
90	45.00	273.05
100	45	274.87
110	45	275.91

Time (s)	Velocity (rad/s)	Torque ($\mu\text{N.m}$)
120	45	276.15
130	45	277.81
140	45	279.16
150	45	280.25
160	45	280.71
170	45	281.41
180	45	282.51
190	45	283.08
200	45	284.32
210	45	284.1
220	45	284.89
230	45	285.65
240	45	286.09
250	45	286.46
260	45	286.57
270	45	287.23
280	45	287.8
290	45	288.3
300	45	288.08
310	45	288.56
320	45	288.97
330	45	289.77
340	45	289.87
350	45	289.49
360	45	289.99
370	45	290.56
380	45	291.09
390	45	290.69

Time (s)	Velocity (rad/s)	Torque ($\mu\text{N.m}$)
400	45	290.44
410	45	291.17
420	45	291.85

Measurement Specification:

Step name	Steady state flow step 1
Start controlled variable	velocity 1.000 rad/s
End controlled variable	velocity 40.00 rad/s
Temperature	22.0 °C
Sample period	0:00:10 hh:mm:ss
Percentage tolerance	5
Consecutive within tolerance	3
Maximum point time	0:01:00 hh:mm:ss

Results:

Velocity (rad.s)	Torque ($\mu\text{N.m}$)
5.333	139.00
9.667	158.70
14.00	176.81
18.33	193.84

Measurement Specification:

Step name	Steady state flow step 2
Start controlled variable	velocity 40.00 rad/s
End controlled variable	velocity 1.000 rad/s
Sample period	0:00:10 hh:mm:ss
Percentage tolerance	10
Consecutive within tolerance	3
Maximum point time	0:01:00 hh:mm:ss

Results:

Velocity (rad.s)	Torque (μ N.m)
36	265.17
32	252.75
28	237.95
21	209.01
17	195.46
13	178.4
9	164.5
5	141.83

Concentration: $C_k = 10\%$

Mixture Specification:

Density (kg/m ³)	1167
C_k (%)	10
Mixture pH	4
Newtonian viscosity (mPa.s)	9.03

Measurement Specification:

Step name	Peak hold step
Controlled variable	velocity 40.00 rad/s
Duration	0:10:00 hh:mm:ss
Delay time	0:00:10 hh:mm:ss

Results:

Time (s)	Velocity (rad/s)	Torque (μ N.m)
10	40	477.17
20	40	481.48
30	40	483.78
40	40	485.34
50	40	486.5
60	40	487.48
70	40	488.34
80	40	488.08
90	40	488.9
100	40	488.88
110	40	490.23

Time (s)	Velocity (rad/s)	Torque ($\mu\text{N}\cdot\text{m}$)
120	40	489.66
130	40	490.77
140	40	489.49
150	40	489.29
160	40	490.49
170	40	489.29
180	40	490.01
190	40	489.4
200	40	490.67
210	40	488.93
220	40	489.69
230	40	490.4
240	40	490.54
250	40	489.25
260	40	490.36
270	40	489.35
280	40	489.61
290	40	490.4
300	40	489.55
310	40	490.96
320	40	489.63
330	40	491.19
340	40	490.2
350	40	490.65
360	40	490.79
370	40	490.94
380	40	490.9
390	40	490.98

Time (s)	Velocity (rad/s)	Torque ($\mu\text{N.m}$)
400	40	491.55
410	40	491.56
420	40	491.62
430	40	492
440	40	492.17
450	40	492.24
460	40	492.53
470	40	492.77
480	40	492.69
490	40	493.2
500	40	493.2
510	40	493.44
520	40	493.49
530	40	494.09
540	40	493.72
550	40	494.32
560	40	494.49
570	40	494.53
580	40	494.69
590	40	494.67
600	40	495.21

Measurement Specification:

Step name	Steady state flow step 1
Start controlled variable	velocity 1.000 rad/s
End controlled variable	velocity 40.00 rad/s
Temperature	22.0 °C
Sample period	0:00:10 hh:mm:ss
Percentage tolerance	5
Consecutive within tolerance	3
Maximum point time	0:01:00 hh:mm:ss

Results:

Velocity (rad.s)	Torque (μ N.m)
5.105	299.47
15.37	383.81
17.42	395.39
19.47	406.99
21.53	418.68

Measurement Specification:

Step name	Steady state flow step 2
Start controlled variable	velocity 40.00 rad/s
End controlled variable	velocity 1.000 rad/s
Sample period	0:00:10 hh:mm:ss
Percentage tolerance	5
Consecutive within tolerance	3
Maximum point time	0:01:00 hh:mm:ss

Results:

Velocity (rad.s)	Torque ($\mu\text{N.m}$)
38	504.44
36	494.94
34	485.88
32	476.89
28	458.15
26	449.26
22	430.17
19	419.89
11	375.32
9	360.35

Appendix 4: Rheological Measurements of Sand-Kaolin-Water Mixtures

For all measurements reported in Appendix 4:

Instrument type	AR-G2
Geometry name	Standard DIN or conical concentric cylinders
Geometry material	Aluminum
Cup inner radius	15.00 mm
Rotor outer radius	14.00 mm
Cylinder immersed height	42.00 mm
Gap	10 μm
Gap tolerance	4 μm
Approximate sample volume	15.42 ml
Controlled variable	Velocity
Velocity tolerance	0.1000 rad/s
Temperature	22.0 $^{\circ}\text{C}$
Wait for temperature	Yes
Temperature tolerance	0.1 $^{\circ}\text{C}$
Instrument inertia	19.09 $\mu\text{N}\cdot\text{m}\cdot\text{s}^2$
Flow torque limit	2000.00 $\mu\text{N}\cdot\text{m}$
Flow velocity limit	1.000×10^{-5} rad/s

Concentration: $C_s = 10\%$

Mixture Specification:

Density (kg/m ³)	1270
C_s (%)	10
Mixture pH	8
Newtonian viscosity (mPa.s)	4.44

Measurement Specification:

Step name	Peak hold step
Controlled variable	Velocity 45.00 rad/s
Duration	0:02:00 hh:mm:ss
Delay time	0:00:10 hh:mm:ss

Results:

Time (s)	Velocity (rad/s)	Torque (μ N.m)
10.004	45.00	240.31
20.004	45.00	242.81
30.016	45.00	241.84
40.004	45.00	241.47
50.020	45.00	241.30
60.016	45.00	241.78
70.000	45.00	241.83
80.020	45.00	243.02
90.000	45.00	244.40
100.00	45.00	245.95
110.00	45.00	245.81

Time (s)	Velocity (rad/s)	Torque ($\mu\text{N.m}$)
120.00	45.00	245.60

Measurement Specification:

Step name	Steady state flow step 1
Start controlled variable	velocity 1.000 rad/s
End controlled variable	velocity 40.00 rad/s
Temperature	22.0 °C
Sample period	0:00:10 hh:mm:ss
Percentage tolerance	10
Consecutive within tolerance	3
Maximum point time	0:00:15 hh:mm:ss

Results:

Velocity (rad.s)	Torque ($\mu\text{N.m}$)
4.545	72.698
8.091	88.918
11.64	100.44
15.18	112.46
18.73	124.12
22.27	133.16

Concentration: $C_s = 15\%$

Mixture Specification:

Density (kg/m ³)	1347
C_s (%)	15
Mixture pH	8
Newtonian viscosity (mPa.s)	6.17

Measurement Specification:

Step name	Peak hold step
Controlled variable	velocity 25.00 rad/s
Duration	0:01:00 hh:mm:ss
Delay time	0:00:30 hh:mm:ss

Results:

Time (s)	Velocity (rad/s)	Torque (μ N.m)
30.008	25	216.03
60.024	25	217.39

Measurement Specification:

Step name	Steady state flow step 1
Start controlled variable	velocity 1.000 rad/s
End controlled variable	velocity 20.00 rad/s
Temperature	22.0 °C
Sample period	0:00:10 hh:mm:ss
Percentage tolerance	10
Consecutive within tolerance	3
Maximum point time	0:00:15 hh:mm:ss

Results:

Velocity (rad.s)	Torque (μ N.m)
3.111	105
5.222	117.39
7.333	130.32
9.444	139.66
11.56	150.63
20	189.58

Concentration: $C_s = 20\%$

Mixture Specification:

Density (kg/m ³)	1423
C_s (%)	20
Mixture pH	8
Newtonian viscosity (mPa.s)	7.49

Measurement Specification:

Step name	Peak hold step
Controlled variable	velocity 25.00 rad/s
Duration	0:01:00 hh:mm:ss
Delay time	0:00:15 hh:mm:ss

Results:

Time (s)	Velocity (rad/s)	Torque (μ N.m)
30.016	25	291.77
60.008	25	291.96

Measurement Specification:

Step name	Steady state flow step 1
Start controlled variable	velocity 1.000 rad/s
End controlled variable	velocity 20.00 rad/s
Temperature	22.0 °C
Sample period	0:00:10 hh:mm:ss
Percentage tolerance	10
Consecutive within tolerance	3
Maximum point time	0:00:15 hh:mm:ss

Results:

Velocity (rad.s)	Torque (μ N.m)
7.333	182.87
9.444	195.69
15.78	233.41
17.89	247.34
20	258.61

Concentration: $C_s = 25\%$

Mixture Specification:

Density (kg/m ³)	1500
C_s (%)	25
Mixture pH	8
Newtonian viscosity (mPa.s)	11.22

Measurement Specification:

Step name	Peak hold step
Controlled variable	velocity 45.00 rad/s
Duration	0:01:00 hh:mm:ss
Delay time	0:00:10 hh:mm:ss

Results:

Time (s)	Velocity (rad/s)	Torque (μ N.m)
10.004	45	452.57
20	45	455.57
30	45	459.88
40.016	45	464.47
50.02	45	469.1
60	45	472.98

Measurement Specification:

Step name	Steady state flow step 1
Start controlled variable	velocity 1.000 rad/s
End controlled variable	velocity 40.00 rad/s
Temperature	22.0 °C
Sample period	0:00:10 hh:mm:ss
Percentage tolerance	10
Consecutive within tolerance	3
Maximum point time	0:00:15 hh:mm:ss

Results:

Velocity (rad.s)	Torque (μ N.m)
5.333	191.17
9.667	228
14	257.59
18.33	286.91
22.67	314.18